Transverse Asymmetry in Nucleon Deuteron Scattering in Pionless Effective Field Theory

by

Arman Margaryan

Department of Physics
Duke University

Date: ____________________________
Approved:

Roxanne Springer, Supervisor

Thomas Mehen

Ronen Plesser

Stephen Teitsworth

Kate Scholberg

Dissertation submitted in partial fulfillment of the requirements for the degree of
Doctor of Philosophy in the Department of Physics
in the Graduate School of Duke University
2017

Abstract

Transverse Asymmetry in Nucleon Deuteron Scattering in Pionless Effective Field Theory

by

Arman Margaryan

Department of Physics
Duke University

Date: __________________________
Approved:

____
Roxanne Springer, Supervisor

____
Thomas Mehen

____
Ronen Plesser

____
Stephen Teitsworth

____
Kate Scholberg

An abstract of a dissertation submitted in partial fulfillment of the requirements for
the degree of Doctor of Philosophy in the Department of Physics
in the Graduate School of Duke University
2017

Abstract

In this dissertation we apply the pionless effective field theory ($\mathrm{EFT}_{\not\pi}$) to low energy neutron deuteron elastic scattering process. We calculated some of the polarization observables in neutron deuteron scattering to next-to-next-to-next-to-leading-order, in particular the transverse asymmetry A_y. All of the previous calculations have the same characteristic feature of under-predicting this observable, this is known as the A_y-puzzle. At this order of the $\mathrm{EFT}_{\not\pi}$ new two-body P-wave interaction terms enter into the Lagrangian. This interaction terms give crucial contributions to the A_y observable. By varying the interaction coefficients within the allowed error estimates of the $\mathrm{EFT}_{\not\pi}$ we find results that at this order are consistent with the experimental data. Our conclusion is that the A_y-puzzle is likely to be solved within the next few orders of the $\mathrm{EFT}_{\not\pi}$. Other observables in neutron-deuteron scattering process are also calculated and are in good agreement with the experimental data.

To my brother David Margaryan.

Contents

List of Figures

List of Abbreviations and Symbols

Symbols

Abbreviations

EFT	Effective Field Theory
EFT$_{\not\pi}$	Pionless Effective Field Theory
QFT	Quantum Field Theory
QCD	Quantum Chromodynamics
QED	Quantum Electrodynamics
χPT	Chiral perturbation theory
HQET	Heavy Quark Effective Theory
HHχPT	Heavy Hadron Chiral Perturbation Theory
X-EFT	Effective Field Theory for the $X(3872)$
SCET	Soft-Collinear Effective Theory
PDS	Power Divergence Subtraction
ERE	Effective Range Expansion
LO	Leading Order
NLO	Next to Leading Order
NDA	Naive Dimensional Analysis
CM	Center of Mass
RG	Renormalization Group

Acknowledgements

I would like to thank Roxanne Springer for being a great advisor. I would also like to thank Jared Vanasse for all the discussions during the course of this work.

This material is based upon work supported by the U.S. Department of Energy, Office of Science, Office of Nuclear Physics, under Award Number DE-FG02-05ER41368 and Award Number DE-FG02-93ER40756 (JV).

1

Introduction

1.1 Strong interactions at low energies

In quantum field theories (QFTs) in general the coupling constants are renormalized at some renormalization energy scale μ. This scale is arbitrary and the coupling constants change their values depending on μ. This is called the renormalization group (RG) flow or the running of the coupling constants. The equation that describes the running of the coupling constant depending on the renormalization scale μ is called the renormalization group equation. It relates the derivative of the coupling constant to a function of the coupling constant Eq. (1.1).

$$\mu \frac{d}{d\mu} g_\mu = \beta(g_\mu), \tag{1.1}$$

where g_μ is the renormalized coupling at the renormalization scale μ. The right hand side of this equation is called the beta-function and is calculated perturbatively. Usually by requiring that the Lagrangian is real and the action of the theory has a minimum it is possible to restrict the values of the coupling g_μ to be non-negative. From Eq. (1.1) we see that if the beta-function is positive then the coupling constant increases with increasing μ. This is the case for example for a scalar field theory for the field ϕ with a ϕ^4 interaction and quantum electrodynamics (QED). But if the beta-function is negative then the coupling constant decreases with increasing μ. This is called the asymptotic freedom. An example theory that has this feature is quantum chromodynamics (QCD). In the regions of μ where the coupling constants are small we can use perturbation theory to calculate matrix elements and scattering amplitudes as sums of Feynman diagrams. But when μ is such that the coupling constants are large perturbation theory is impossible. This is called the non-perturbative regime of the theory. The non-perturbative regime of QCD is at low energies where the nuclear reactions happen.

The atomic nucleus is composed of neutrons and protons, also called nucleons. Nucleons themselves are composite particles, composed of quarks, which carry color and electromagnetic charge. Quarks interact by strong interactions carried by gluons and by electromagnetic forces carried by photons. The fundamental theory that describes strong interactions is QCD, which is asymptotically free at high energies. This means that the beta-function for the QCD coupling α_s is negative, making the coupling decrease with increasing renormalization scale (see Fig. 1.1). Solving the RG flow equation Eq. (1.1) for α_s at the lowest order in perturbation theory at which the beta-function gets a non-zero contribution, gives the asymptotic behavior of $\alpha_s(Q) \sim \frac{1}{\log Q}$ [1, 2], which is the behavior that we see in Fig. 1.1. It follows that at high energies α_s approaches to zero and QCD is perturbative, but at low energies the interaction coefficient is large. The behavior of α_s shown in Fig. 1.1 is derived based on the assumption that the coupling α_s is small, so the part of the Fig. 1.1 where α_s is large cannot be trusted. But the fact that α_s decreases with increasing energy scale means that it increases when the energy scale is small. So before reaching the region where α_s is large in Fig. 1.1 the perturbation theory breaks down precisely because α_s becomes large.

To describe processes involving strongly interacting particles at high energies we can use perturbation theory and calculate Feynman diagrams contributing to the scattering amplitudes. But at lower energies α_s is larger and perturbation theory is not applicable anymore. The low energy few-nucleon systems fall into this energy regime where α_s is large, hence are governed by non-perturbative QCD. Since non-perturbative QCD is extremely difficult and is not yet solved we have to look for other ways to overcome this difficulty and to be able to give quantitative predictions about the low energy few-nucleon systems. I'll describe some of them briefly.

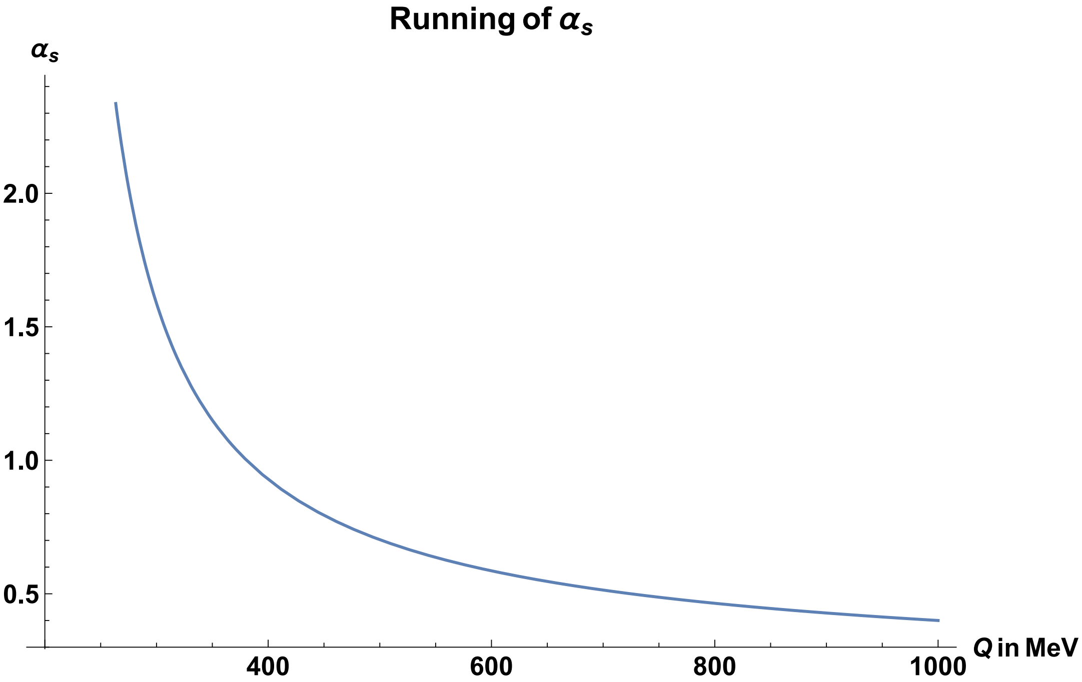

Figure 1.1: The RG running of the QCD coupling constant.

One of the approaches is the lattice QCD [3]. The idea is to discretize the space-time dimensions making it into a lattice. This makes the path integral for the observables into summations over many particle configurations on the lattice. These sums are then calculated numerically and predictions are extracted. Then the lattice spacing is taken to zero and the lattice volume is taken to infinity. The predictions become independent of lattice spacing and this is the continuum limit of lattice QCD. The advantage of this approach is that it gives a non-perturbative result for the observables, but the disadvantage is that it becomes extremely complicated when the number of nucleons increases; a certain class of complications arise called the sign problems. Also it is hard to deal with bound states in lattice QCD.

Another class of approaches is called potential models [4, 5, 6, 7, 8]. The idea is to construct two-nucleon and three-nucleon interaction potentials based on the known symmetries, then to write the Schrödinger equation and determine the energy levels and wave functions by solving the Schrödinger equation numerically. The potentials will have some adjustable parameters which are fit to the few nucleon experimental data. The different potential models usually differ on the short range part of the interaction and the long range part is usually taken to be a one-pion exchange Yukawa potential: $\sim \frac{e^{-m_\pi r}}{r}$ [4]. The disadvantage of potential models is that they do not give a natural way of estimating the theoretical error associated with a particular model and they are not systematically improvable. Also they don't have a way of making a connection to QCD as opposed to effective field theories (EFTs), which are constructed with the symmetries of the underlying fundamental theory.

Our approach is the non-relativistic pionless effective field theory (EFT$_{\not\pi}$) [9, 10, 11, 12, 13, 14, 15, 16, 17, 18]. The EFT$_{\not\pi}$ is constructed to describe nucleons and their interactions at low energies, such that pions are not explicit degrees of freedom and the appropriate degrees of freedom are the nucleon fields coupled with external electromagnetic fields and weak currents.

1.2 Effective Field Theories

EFTs are quantum field theories that approximate an underlying "true" field theory such as QED, QCD, the standard model, etc.. [19]. To describe a given physical process there might be some physical argument why some of the information contained in the underlying theory is irrelevant. For example those processes might be at a certain energy regime, which defines an energy scale in the problem, and in the underlying theory there might exist particles that are much heavier than this scale and hence the dynamics of those particles are irrelevant for the description of those processes to some order. Another example of how an EFT can approximate an underlying theory might be the following: say again we are trying to describe a process at a certain energy and the underlying theory contains particles that are, this time, much lighter than this scale, then, by neglecting the mass of those particles one might obtain more symmetries in the theory which can be useful in the description of the process.

There are two ways to construct an EFT: top to bottom and bottom to top. In a certain sense the top to bottom approach can serve as a justification for the bottom to top approach, so I'll describe both of these.

Here are the steps in the top to bottom approach. Start with the underlying "true" theory and write the path integral for the scattering amplitude of a given process. Then figure out the irrelevant particles (degrees of freedom). Start integrating them out of the path-integral. The last step is an order-by-order process, which gives an expansion in powers of a parameter called the power counting parameter. This parameter can be, for example the ratio of the energy scale existing in the problem over the mass of the particles that are being integrated out. At each order the derived theory is equivalent to a theory given by a particular Lagrangian, which is called the "effective Lagrangian." At every order the effective Lagrangian is the same as at the previous order, along with more terms of higher order in the power counting parameter. Those extra terms are constrained only by the symmetries of the original theory. All the parameters appearing at each order, such as masses or coupling constants in the interaction terms, are fixed by the original parameters of the underlying theory and the relevant energy scales. All of these new parameters encode the information contained in the original theory. As a result one gets a list of effective Lagrangians which can describe the process under consideration in simpler terms than the original theory, because these Lagrangians only contain the relevant degrees of freedom. One hopes that at each order the description gets better, because at each subsequent order the new contributions to the Lagrangian are of higher power in power counting parameter.

In the bottom to top approach the steps are as follows. First figure out and postulate what the symmetries of the underlying "true" theory are. Then take all the degrees of freedom which are the fields of the particles relevant to the process under consideration. Figure out what the power counting parameter is. Then write down a completely general Lagrangian in which the terms go up to a certain order in the power counting parameter, respecting all the symmetries of the original theory. Again at each order we may get several new terms in the Lagrangian. For practical purposes the parameters in the Lagrangian are not fixed by matching to the underlying theory. To fix the parameters in the effective Lagrangian at each order experimental data may be used (position of the poles corresponding to bound states, residues around the poles, scattering lengths, scattering cross-sections, etc...). Again the expectation is that at each order the description of a process under consideration gets more accurate.

QFTs which are constructed to be fundamental theories valid for all energy scales, are required to be renormalizable. This means that all the divergencies at any order can be absorbed into a finite set of interaction parameters. EFTs do not have to satisfy this requirement, because at each order we get new terms in the Lagrangian which can absorb the divergencies. This is called order by order renormalizability.

Here are some examples of EFTs:

1) Chiral perturbation theory (χPT) [20, 21, 22, 23, 24, 25, 26, 27, 28, 29, 30, 31]. In processes where the masses of the light quarks are negligible we can neglect the mass terms for those quarks in the QCD Lagrangian. Then the four component Dirac spinors representing those quarks can be broken into two two-component spinors, which are called left-handed and right-handed Weyl spinors. After doing so it becomes apparent that there are two $SU(2)$ symmetry groups, one acting on left- and the other on right-handed spinors, leaving the Lagrangian invariant. So the total symmetry group is an $\mathrm{SU}(2)_L\times$ $\mathrm{SU}(2)_R$ which is called the chiral symmetry group. In constructing the χPT Lagrangian the terms have to respect all the QCD symmetries and an additional chiral symmetry at leading order (LO). At next-to-leading order (NLO) we should have explicit symmetry breaking for the chiral symmetry as it is broken in QCD by the mass terms of the light quarks. The inclusion of the mass terms, although being NLO in the power counting of the χPT, may give the LO (first non-zero) contribution for certain observables. We will see the same kind of effect in

pionless EFT too, where certain spin-polarization observables get their LO contribution from the N^{2}LO interaction terms in the EFT power counting. The power counting parameters in χPT are the ratio of the pion masse m_π over Λ_{QCD}, and the momentum transfer in a process over Λ_{QCD}. There is a simultaneous expansion in powers of both of these parameters.

2) Heavy quark effective theory (HQET) [32, 33]. This seems to be the opposite situation of the χPT; here the masses of the heavy quarks are taken to infinity. The heavy quarks are treated as classical, stationary sources. At LO no interaction will rotate their spin, hence no interaction can depend on their spin and we get an additional spin-symmetry, which is the heavy quark spin symmetry. Here the power counting parameter is the ratio of Λ_{QCD} over the heavy quark masses.

3) Heavy hadron chiral perturbation theory (HHχPT) [34, 35, 36, 37]. HHχPT is a combination of χPT and HQET. Here the heavy hadrons are considered as nonrelativistic particles, so the expansion corresponding to heavy quark spin symmetry is in the powers of the derivatives acting on the rotated heavy hadron fields, because each derivative brings a heavy quark residual momentum down from the exponent.

4) X-EFT [38]. This is a particular type of HHχPT concerning the physics of the $X(3872)$ particle [39, 40, 41, 42, 43]. It describes D-mesons and pions near the mass of the $X(3872)$. The power counting in X-EFT is the same as for HHχPT; the operators are arranged in powers of the derivatives acting on them. X-EFT can be used to calculate different decay rates and production mechanisms of the $X(3872)$ [44, 45].

5) Soft-Collinear effective theory (SCET) [46]. SCET is constructed to describe processes that involve energetic quark-gluon jets and not-so-energetic (soft) gluons. The power counting parameter is the ratio of the two lightcone-momentum components of the collinear quarks $\lambda = \frac{p_\perp}{p^-}$. The less λ is the more collinear is the quark [47].

6) Non-relativistic pionless EFT (EFT$_{\not\pi}$) [48]. EFT$_{\not\pi}$ is about nonrelativistic nucleons and their interactions. In the processes analyzed by EFT$_{\not\pi}$ the typical momentum exchange in the scattering must be much smaller than the mass of the pion. The power counting parameter

for EFT$_{\not\pi}$ is the ratio $\frac{Q}{\Lambda_{\not\pi}}$, where Q is the typical momentum exchange in the scattering and $\Lambda_{\not\pi}$ is the EFT$_{\not\pi}$ breakdown scale, $\Lambda_{\not\pi} \lesssim m_\pi$.

1.3 The tale of A_y

In the past several decades there has been much effort put into understanding the nuclear forces at the level of few nucleons [49, 9, 5]. There have been many potentials constructed to describe the interaction between nucleons [4, 5, 6, 7, 8]. To put these potentials to test observables needed to be calculated and measured. So the easiest starting point from the point of view of both theory and experiment, was to look at the processes involving only two nucleons. The quantum mechanical two-body problem is fairly easy to solve; in all the cases of interest it can always be reduced to just a one-body problem in a potential. Several potentials can be constructed and adjusted to reproduce the two-nucleon data. So the next filter to use to rule out the "wrong" potentials or unimportant terms in the potentials is the three-nucleon processes. The three-body problem in quantum mechanics is much harder than the two-body one. The first theoretical calculations involving three nucleons became possible after Faddeev introduced in 1961 an integral equation that the scattering amplitude must satisfy in a non-relativistic scattering process [50]. At the three nucleon-sector some of the possible processes are the nucleon deuteron (Nd) elastic scattering. So we can have either proton deuteron (pd) or neutron deuteron (nd) scatterings. From the point of view of the theory the nd scattering is easier to analyze, because there is only one charged particle in this process, the proton inside the deuteron. Thus, the calculation will avoid all the complications coming from the Coulomb interactions. But from the point of view of experiment the pd scattering is both easier to perform and collect more precise data. This is because the proton beam is easier to control, direct and detect due to the electrical charge. One of the observables in Nd scattering is the total unpolarized cross-section. As this observable is averaged over all incoming and outgoing spins of the scattering particles, it is not very sensitive to the interaction terms in the potentials that have spin-structure. To be able to gather more information about these terms, more sensitive observables are needed. One of those sensitive observables is the vector analyzing power, A_y. This observable measures the asymmetry of the scattering of polarized nucleons on unpolarized deuterons, the nucleon polarization being perpendicular to the beam axis. The asymmetry is between nucleon polarization in opposite directions.

Until the end of 1970s the experimentalists were gathering data on *pd* scattering and the theorists were doing calculations on *nd* scattering. Because of the lack of data and calculations physicists were only able to compare the *pd* data to *nd* calculations. The argument was that the *pd* and *nd* elastic scattering processes are related through isospin symmetry, which is an approximate symmetry. Therefore, if we neglect the Coulomb interactions these two processes should qualitatively look the same. Real comparison of theoretical calculations to data became possible after W. Tornow, *et. al.* published series of experimental papers in 1978, 1982 and 1983 reporting A_y data for *nd* elastic scattering for center of mass energies at 12 MeV, 10 MeV and 14.1 MeV [51, 52, 53]. In 1987 C. R. Howell, *et. al.* published a paper with new data for A_y in *nd* scattering, comparing the existing data from 10 to 14 MeV with theoretical Faddeev calculations [54]. These calculations used many different potentials (Paris, Bonn, etc.), and the data showed preference for some models over the others. However, all of these models had the same problem; they failed to predict the correct magnitude of A_y near its maximum. Since then and until now this problem persists throughout all of the potential models: they predict the correct shape of A_y, the correct position of its maximum, but under-predict its magnitude [55, 56] (see Fig. 1.2 [1]).

This problem is known as the "A_y puzzle" [58], and, because it has been measured for *nd* scattering, there have been many attempts to solve it. C. R. Howell, *et. al.* [54] mentioned in their paper that all of the models see that the A_y is very sensitive to the two-nucleon ^3P_J

---

[1] Reprinted from [56], Nuclear Physics A, Volume 607, Issue 4, A. Kievsky, S. Rosati, W. Tornow, M. Viviani, "Critical comparison of experimental data and theoretical predictions for N-d scattering below the breakup threshold," Pages 402-424, Copyright (1996), with permission from Elsevier.

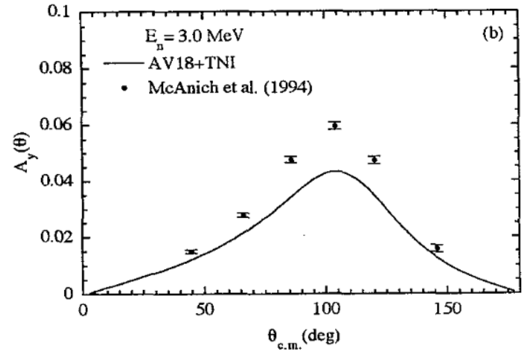

FIGURE 1.2: (Caption and figure reprinted from [56]). Comparison of the neutron analyzing power A_y data of McAninch, *et. al.* [57] with the theoretical predictions obtained in the work of A. Kievsky, *et. al.* [56].

phase shifts. This has motivated several authors to seek for the solution of the A_y puzzle by adjusting the ${}^3P_J$ phase shifts to get the correct magnitude of the A_y. However changing the ${}^3P_J$ phase shifts to get the A_y right led to inconsistencies with other two or three-body observables. In 1998 D. Huber, *et. al.* [59] used the AV18 potential to calculate A_y. In this potential there are eighteen different operator structures, from which D. Huber, *et. al.* determined the five that have non-zero contributions to A_y. They concluded that the A_y puzzle cannot be solved by just adjusting the two-body forces, so likely it will be solved by including some three-body forces that had not been considered before. In 2001 E. Epelbaum et. al. [60] claimed that according to their calculations they are able to find the correct magnitude of A_y by including a new two-body force, which is derived from the chiral EFT, in the potential. But in their calculations for two-nucleon processes they compared their results not to the observables but to the phase-shifts only. Later in 2001 D. R. Entem and R. Machleidt [55] noted that the calculations need to be compared to the two-nucleon data directly, instead of solely to the phase shifts. So they did the comparison and reported that the problem is still not resolved. They also analyzed the possible ways of solving the A_y puzzle and came to the conclusion that, as far as only two-body interactions are used, it is impossible to solve the puzzle without ruining the low energy two-nucleon predictions. There also have been attempts to resolve the puzzle by including some three-body forces into the potentials [61, 62]. However, for all the three-body forces tested, the predictions for the A_y were either not changing or getting worse.

The disadvantage of potential models is that there is no systematic theoretical approach to understand which potential is better than the other and by how much. Hence, to rule out models, physicists have to entirely rely on comparison of the calculations to the experiment. The EFT approach, on the other hand, is constructed with the tool of comparing things in its core. This tool is the power counting parameter, which needs to be determined before an EFT is constructed. The power counting parameter is a small parameter characteristic to the processes that the EFT is constructed for, and all the terms in an EFT Lagrangian, all the calculated amplitudes and observables are expanded in powers of this parameter. As a consequence we get a natural way of determining which term is more significant and to what extent.

The EFT, which is best fit to describe the non-relativistic few-nucleon systems is EFT$_{\not\pi}$ [10]. Up to and including next-to-next-to-leading-order (N^{2}LO) in powers of the power counting parameter, the EFT$_{\not\pi}$ gives very small contributions to the A_y observable. Nevertheless, at the next order (N^{3}LO) the two-nucleon ^3P_J interactions enter into the EFT$_{\not\pi}$ Lagrangian, and these interactions give the first substantial contributions to the A_y. In this dissertation I am going to present the first N^{3}LO calculation of the nd scattering amplitude and show what the EFT$_{\not\pi}$ predictions for A_y look like at this order. The rest of this dissertation is organized as follows: in Chapter 2 EFT$_{\not\pi}$ at two- and three-nucleon sectors up to and including the second order is described, in Chapter 3 EFT$_{\not\pi}$ at two- and three-nucleon sectors at the third order and higher is described. In this chapter the third order calculation of the A_y observable is given. In Chapter 4 the results for the A_y are given along with conclusions and future directions.

2

Non-Relativistic Pionless EFT: Up to Order-2

2.1 Two-nucleon sector at LO

The Lagrangian density for the two-nucleon sector is constructed such that the NN scattering amplitude matches onto the effective range expansion (ERE). The ERE exploits the unitarity of the S-matrix to derive an expression for the scattering amplitude. As the S-matrix must be unitary, the diagonal elements (diagonal in partial wave expansion) must be complex numbers with absolute value 1. So we have:

$$S = e^{2i\delta}, \tag{2.1}$$

where δ is a real number and it is called the phase shift.

From the connection of the S-matrix to the scattering amplitude A: $S = 1 + i\frac{kM}{2\pi}A$, we can derive an expression for A in terms of the phase shift δ. Here k is the absolute value of the nucleon three-momentum in the center of mass (CM) frame and M is the nucleon mass.

$$A = \frac{4\pi}{M}\frac{e^{2i\delta}-1}{2ik} = \frac{4\pi}{M}\frac{1}{ke^{-i\delta}}\frac{e^{i\delta}-e^{-i\delta}}{2i} = \frac{4\pi}{M}\frac{\sin\delta}{k(\cos\delta - i\sin\delta)} = \frac{4\pi}{M}\frac{1}{k\cot\delta - ik} \tag{2.2}$$

Eq. (2.2) is true for any given partial wave and it is shown in [63, 64] that $k\cot\delta$ in the

S-wave is an analytical function of k and that around $k = 0$ the expansion is the following:

$$k \cot(\delta) = -\frac{1}{a} + \frac{1}{2} r_0 k^2 + s k^4 + ... \tag{2.3}$$

Here a is the scattering length, r_0 is the effective range, and s is the shape parameter. The derivation of the last formula in [63] relies on non-relativistic quantum mechanics and investigation of the Schrödinger equation, which is applicable for non-relativistic NN scattering. In the $^3S_1$ channel the deuteron pole exists in the scattering amplitude, so $k \cot \delta$ can be expanded around the deuteron pole.

For the two-nucleon sector at leading order the Lagrange density is:

$$\mathcal{L} = N^\dagger \left(i\partial_0 + \frac{\vec{\nabla}^2}{2M_N} \right) N - C_0 (N^T P N)^\dagger (N^T P N) \tag{2.4}$$

where N is the nucleon field, which technically has two indices, one for spin and one for isospin, each of which has two components. Those indices are suppressed because of the common notation. The operator N only destroys a nucleon, it does not create an antinucleon, because this is a non-relativistic field theory. And P is a spin-isospin projector, not containing any derivatives, because this is at leading order and any derivatives would make the operator higher order. To reproduce the deuteron bound state in NN scattering amplitude all the graphs in Fig 2.1 need to be added up.

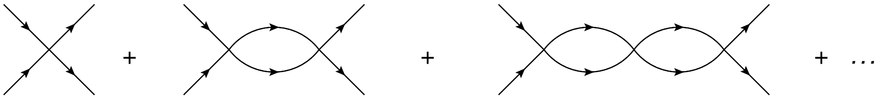

FIGURE 2.1: NN scattering: bubble sum.

Luckily this sum is just a geometric series and can be calculated in closed form. In the center of mass frame we have:

$$A = -C_0 - C_0 I_0 C_0 - C_0 I_0 C_0 I_0 C_0 - ... = \frac{-1}{\frac{1}{C_0} - I_0} \tag{2.5}$$

where I_0 is the one-loop integral:

$$I_0 = -i \int \frac{d^4q}{(2\pi)^4} \frac{i}{E + q_0 - \frac{q^2}{2M} + i\epsilon} \frac{i}{-q_0 - \frac{q^2}{2M} + i\epsilon}. \tag{2.6}$$

Here E is the total incoming momentum in the center of mass frame: $E = \frac{k^2}{M}$. The q_0 integration can be done by closing the contour either in the upper complex plane or the lower, picking up the residue over the pole we find:

$$I_0 = \int \frac{d^3q}{(2\pi)^3} \frac{1}{E - \frac{q^2}{M} + i\epsilon} = -\frac{M}{4\pi}(\frac{2}{\pi}\Lambda + ik) \tag{2.7}$$

where Λ is a sharp cutoff on $|\vec{q}|$. The same result is obtained using the so-called Power Divergence Subtraction (PDS) [65] subtraction scheme. From here we can find the scattering amplitude:

$$A = -\frac{4\pi}{M} \frac{1}{\frac{4\pi}{MC_0} + \frac{2}{\pi}\Lambda + ik}. \tag{2.8}$$

This matches the ERE expression for the scattering amplitude at LO. The pole in this amplitude corresponds to the deuteron bound state:

$$\frac{4\pi}{MC_0} + \frac{2}{\pi}\Lambda = \gamma_t \tag{2.9}$$

where γ_t is the binding momentum and is defined by: $\gamma_t = \sqrt{MB} = 45.70$ MeV, where $B = 2.2$ MeV is the deuteron binding energy. Note that the interaction coefficient C_0 depends on the regulator, the cutoff in our case, so that the observable γ_t matches to its experimental, cutoff-independent value.

2.2 Two-nucleon sector at higher orders

Here I describe the EFT$_{\not\pi}$ in the two-nucleon sector at higher orders, but I only give some of the two-nucleon interactions. Some of the two-nucleon forces such as SD mixing and the P-wave interactions will be discussed in the three-nucleon sector.

To be able to consider three-body scattering problems we first need to construct the two-body Lagrangian to higher orders. It turns out to be very useful to introduce auxiliary dibaryon fields t_i for the deuteron, which is a spin-triplet and isospin-singlet and s_a, which is a spin-singlet and isospin-triplet. The Lagrangian density in the S-wave channel for the two-body sector to all orders is given by:

$$\begin{aligned} \mathcal{L} &= N^\dagger\left(i\partial_0+\frac{\vec{\nabla}^2}{2M_N}\right)N \\ &+ t_i^\dagger\left(\Delta_t-\sum_{n=0}^{\infty}c_{nt}\left(i\partial_0+\frac{\vec{\nabla}^2}{4M_N}+\frac{\gamma_t^2}{M_N}\right)^{n+1}\right)t_i \\ &+ s_a^\dagger\left(\Delta_s+\Delta_s^{N^2LO}\delta^a_{-1}-\sum_{n=0}^{\infty}c_{ns}\left(i\partial_0+\frac{\vec{\nabla}^2}{4M_N}+\frac{\gamma_s^2}{M_N}\right)^{n+1}\right)s_a \\ &+ y_t(t_i^\dagger(N^TP_iN)+\text{h.c.})+y_s(s_a^\dagger(N^TP_aN)+\text{h.c.}), \end{aligned} \tag{2.10}$$

where the projectors are defined by: $P_i=\frac{1}{\sqrt{8}}\sigma_2\sigma_i\tau_2$ and $P_a=\frac{1}{\sqrt{8}}\tau_2\tau_a\sigma_2$. By Gaussian path integration it can be shown that this Lagrangian density is equivalent to a completely general Lagrangian density involving only nucleon fields [11]. The NN elastic scattering amplitude is given by the ERE and the same amplitude can be calculated using this Lagrangian, hence the two answers should match and the c_{nt} (c_{ns}) coefficients should be related to the ERE parameters. We will see this matching in the $^3S_1$ channel where the deuteron lives. The deuteron propagator at LO is given by the infinite bubble sum, as shown in Fig. 2.2.

FIGURE 2.2: Double line is the LO full deuteron propagator, thin solid line is the nucleon propagator, thick solid line is the bare deuteron propagator $\frac{i}{\Delta_t}$.

Without loss of generality the coupling y_t can be chosen to be: $y_t^2 = \frac{4\pi}{M_N}$. This sum is just a geometric series so it can be calculated in a closed form giving the LO deuteron propagator:

$$iD_t^{LO}(p_0, \vec{p}) = \frac{i}{\Delta_t + \Lambda - \sqrt{\frac{\vec{p}^2}{4} - M_N p_0 - i\epsilon}}, \tag{2.11}$$

where Λ is the momentum cutoff (it is actually off by the factor $\frac{2}{\pi}$, which is absorbed by just redefining the cutoff). Using this we can find the exact deuteron propagator to all orders, which will be given by another geometric series shown in the figure:

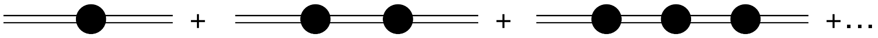

FIGURE 2.3: Deuteron propagator to all orders.

In this figure the solid circle denotes the single insertion of all the c_{nt} interactions summed over all n. This means that the sum given in this figure is not order-by-order, meaning that each of the summands itself has terms at all orders. This sum also can be calculated in a closed form giving:

$$iD_t^{\text{all-orders}}(p_0,\vec{p}) = \frac{i}{\Delta_t + \Lambda - \sqrt{\frac{\vec{p}^2}{4} - M_N p_0 - i\epsilon}} \sum_{m=0}^{\infty} \left(\frac{\sum\limits_{n=0}^{\infty} c_{nt}(p_0 - \frac{\vec{p}^2}{4M_N} + \frac{\gamma_t^2}{M_N})^{n+1}}{\Delta_t + \Lambda - \sqrt{\frac{\vec{p}^2}{4} - M_N p_0 - i\epsilon}} \right)^{m+1} \tag{2.12}$$

Where p_0 and $\vec{p}$ is the energy and the three-momentum of the deuteron. Doing the summation over m gives:

$$iD_t^{\text{all-orders}}(p_0,\vec{p}) = \frac{i}{\Delta_t + \Lambda - \sqrt{\frac{\vec{p}^2}{4} - M_N p_0 - i\epsilon} - \sum\limits_{n=0}^{\infty} c_{nt}\left(p_0 - \frac{\vec{p}^2}{4M_N} + \frac{\gamma_t^2}{M_N}\right)^{n+1}} \tag{2.13}$$

To find the NN scattering amplitude in the center of mass frame we need to attach the nucleon-legs to the deuteron propagator to all-orders and plug in $p_0 = \frac{\vec{k}^2}{M_N}, \vec{p} = 0$, where $\vec{k}$ is the incoming nucleon momentum. This will give for the amplitude:

$$A = -\frac{4\pi}{M_N} \frac{1}{\Delta_t + \Lambda + ik - \sum\limits_{n=0}^{\infty} c_{nt}(\frac{\vec{k}^2}{M_N} + \frac{\gamma_t^2}{M_N})^{n+1}}. \tag{2.14}$$

As was expected this amplitude is exactly the same as the one given by the ERE (2.2). Equating both equations at each order in the $k-$expansion we can match the c_{nt} coefficients to ERE parameters. The ERE parameters are matched to experiment so those are cutoff independent. This forces the parameter Δ_t in the Lagrangian to depend on the cutoff, but all the other parameters c_{nt} are cutoff independent [12].

From the matching the EFT$_{\not\pi}$ and ERE we know that we can do the substitution $\Delta_t + \Lambda = \gamma_t$ in Eq. (2.13). Separating the first term in the sum in the denominator Eq. (2.13) can be rewritten:

$$
\begin{aligned}
& D_t^{\text{all-orders}}(p_0,\vec{p}) \\
= \;& \frac{i}{\gamma_t - \sqrt{\frac{\vec{p}^2}{4} - M_N p_0 - i\epsilon} - \frac{c_{0t}}{M_N}\left(M_N p_0 - \frac{\vec{p}^2}{4} + \gamma_t^2\right) - \sum\limits_{n=1}^{\infty} c_{nt}\left(p_0 - \frac{\vec{p}^2}{4M_N} + \frac{\gamma_t^2}{M_N}\right)^{n+1}} \\
= \;& \frac{1}{\gamma_t - \sqrt{\frac{\vec{p}^2}{4} - M_N p_0 - i\epsilon}} \\
\times \;& \frac{1}{1 - \frac{c_{0t}}{M_N}\left(\gamma_t + \sqrt{\frac{\vec{p}^2}{4} - M_N p_0}\right) - \sum\limits_{n=1}^{\infty} c_{nt}\left(p_0 - \frac{\vec{p}^2}{4M_N} + \frac{\gamma_t^2}{M_N}\right)^{n}\left(\gamma_t + \sqrt{\frac{\vec{p}^2}{4} - M_N p_0}\right)}.
\end{aligned}
\tag{2.15}
$$

From here we can see that around the deuteron pole where $\gamma_t = \sqrt{\frac{\vec{p}^2}{4} - M_N p_0}$ all the terms in the sum in the second denominator do not contribute to the residue and we get for the residue the following expression:

$$
Z_t = \frac{1}{1 - \frac{c_{0t}}{M_N} 2\gamma_t}. \tag{2.16}
$$

The coefficient c_{0t} is matched onto ERE and this matching gives the numerical value for the residue $Z_t = 1.690$. Expressing the coefficient c_{0t} in terms of Z_t we can substitute it into Eq. (2.15) we can re-expand the deuteron propagator in powers of $\frac{Z_t - 1}{2} \approx 0.3$ finding:

$$
\begin{aligned}
& D_t^{\text{all-orders}}(p_0,\vec{p}) \\
= \;& \frac{1}{\gamma_t - \sqrt{\frac{\vec{p}^2}{4} - M_N p_0 - i\epsilon}} \\
& \left[1 + \frac{Z_t - 1}{2\gamma_t}\left(\gamma_t + \sqrt{\frac{\vec{p}^2}{4} - M_N p_0}\right) + \left(\frac{Z_t - 1}{2\gamma_t}\right)^2 \left(\frac{p^2}{4} - M_N p_0 - \gamma_t^2\right) + \ldots\right].
\end{aligned}
\tag{2.17}
$$

Putting the deuteron propagator into this form is called the Z-parametrization [12][13]. The same sort of re-expansion can be done for the spin-singlet dibaryon propagator, and this is what we use in our calculations. This way of expanding the dibaryon propagators has its advantages, one of them being that the dibaryon wave-function renormalization is recovered fully at the NLO of the perturbation, instead of getting contributions at every order. The other advantages and disadvantages are discussed in the references given above in this paragraph.

2.3 Three-nucleon sector at LO, quartet channel

Having the Lagrangian at the two-body sector we are able to consider three-body scattering problems such as neutron-deuteron (nd) or proton-deuteron (pd) elastic scattering [14]. We will consider nd scattering, because there is no Coulomb interaction and we only need the strong interactions which are encoded in the constructed effective Lagrangian. For calculations in $\mathrm{EFT}_{\not\pi}$ about the pd scattering process see for example [66, 67]. As the neutron is a spin $\frac{1}{2}$ particle and the deuteron is a spin 1 particle the scattering can happen in two different channels: total spin-$\frac{1}{2}$, the doublet channel, and total spin-$\frac{3}{2}$, the quartet channel. We will first take a look at the quartet channel scattering. At leading order we have an infinite set of diagrams (see Fig. 2.4) that contributes to nd scattering in the quartet channel much like the two-body case.

The difference between this sum and the sum that we find in the two-body case is that this sum is not a simple geometric series, so we don't find a closed form expression for the amplitude as in the two-body case. Instead we can see that the scattering amplitude satisfies an integral equation represented diagrammatically in the Fig. 2.5 [14]

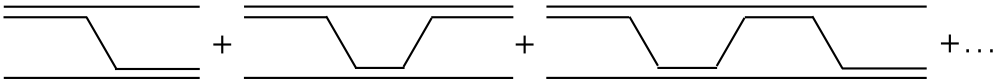

FIGURE 2.4: Pinball diagrams for LO nd scattering.

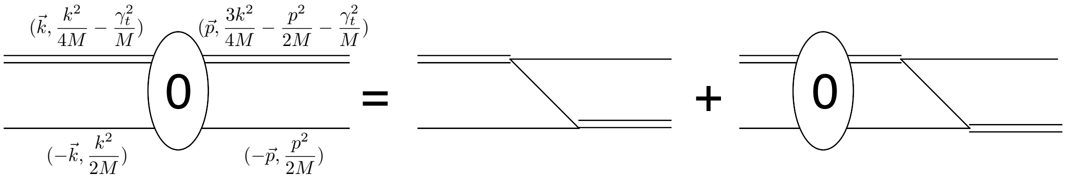

FIGURE 2.5: Quartet channel LO nd equation.

The oval with a "0" in the Fig. 2.5 is the leading order nd scattering amplitude, which is the sum of all the terms in the Fig. 2.4. The explicit form of the integral equation is given by:

$$\begin{aligned}
(it^{ji})^{\beta b}_{\alpha a}(\vec{k}, \vec{p}, \frac{p^2}{2M_N}) &= \frac{y_t^2}{2}(\sigma^i\sigma^j)^{\beta}_{\alpha}\delta^b_a \frac{i}{\frac{k^2}{4M_N} - \frac{p^2}{2M_N} - \frac{\gamma_t^2}{M_N} - \frac{(\vec{k}+\vec{p})^2}{2M_N} + i\epsilon} \\
&+ \frac{y_t^2}{2}(\sigma^i\sigma^k)^{\beta}_{\gamma}\delta^b_c \int \frac{d^4q}{(2\pi)^4}(it^{jk})^{\gamma c}_{\alpha a}(\vec{k}, \vec{q}, q_0) \\
&\times iD_t^{(0)}(E - q_0, \vec{q}) \frac{i}{q_0 - \frac{q^2}{2M_N} + i\epsilon} \frac{i}{E - \frac{p^2}{2M_N} - q_0 - \frac{(\vec{p}+\vec{q})^2}{2M_N} + i\epsilon}
\end{aligned} \tag{2.18}$$

where i and j are the initial and final deuteron polarizations, α and β are the initial and final nucleon spin, and a and b are the initial and final nucleon isospin. The incoming momentum in the CM frame is $\vec{k}$ and the outgoing momentum in the CM frame is $\vec{p}$, the total energy of the system is $E = \frac{3k^2}{4M_N} - \frac{\gamma_t^2}{M_N}$. The leading order dressed deuteron propagator is $D_t^{(0)}(p_0, \vec{p})$, where the superscript 0 stands for LO.

Here we have put the incoming nucleon, deuteron and the outgoing nucleon on-shell, while the outgoing deuteron is off-shell. The energy and momentum of the outgoing deuteron is determined by the conservation of energy-momentum. The amplitude t in this equation depends on three entries which are respectively the incoming momentum $\vec{k}$, the outgoing momentum $\vec{p}$ and the energy of the outgoing nucleon, which is $\frac{\vec{p}^2}{2M_N}$ on the left hand side and q_0 on the right hand side. On the right hand side inside the loop the nucleon that is attached to the scattering amplitude has energy-momentum $(q_0, \vec{q})$ and this is the loop energy-momentum that we are integrating over.

The first step towards solving this integral equation is to simplify it by doing the q_0 integration on the right hand side. Each of the three propagators in the loop has a pole in the complex q_0 plane and it is easy to see that the two poles coming from the deuteron propagator and the exchanged nucleon propagator are on one side of the real axis and the second nucleon propagator is on the other side of the real axis. So we can close the contour of integration so that we pick up only one pole coming from the second nucleon propagator hence putting it on shell: $q_0 = \frac{q^2}{2M_N}$. After doing this we can drop the third variable from the amplitude t and interpret the function $t(\vec{k}, \vec{p})$ as the amplitude that has incoming momentum $\vec{k}$, outgoing momentum $\vec{p}$, the incoming particles on-shell and the outgoing nucleon on-shell.

$$\begin{aligned}
(it^{ji})^{\beta b}_{\alpha a}(\vec{k},\vec{p}) &= \frac{y_t^2}{2}(\sigma^i\sigma^j)^{\beta}_{\alpha}\delta^b_a \frac{i}{E - \frac{k^2}{2M_N} - \frac{p^2}{2M_N} - \frac{(\vec{k}+\vec{p})^2}{2M_N}} \\
+ & \frac{y_t^2}{2}(\sigma^i\sigma^k)^{\beta}_{\gamma}\delta^b_c \int \frac{d^3q}{(2\pi)^3}(it^{jk})^{\gamma c}_{\alpha a}(\vec{k},\vec{q}) \\
\times & \; iD_t^{(0)}(E - \frac{q^2}{2M_N}, \vec{q}) \frac{i}{E - \frac{p^2}{2M_N} - \frac{q^2}{2M_N} - \frac{(\vec{p}+\vec{q})^2}{2M_N}}
\end{aligned} \tag{2.19}$$

Now we can project this equation onto the spin quartet channel and do the partial wave decomposition projecting on the l-th partial wave. To do this we put the z axis along $\vec{p}$, we multiply both sides of the equation by $Y_l^m(\hat{k})$ and integrate by the angles of $\hat{k}$: $d\Omega_{\hat{k}}$. From the previous equation we see that the amplitude depends only on the angle θ between the vectors $\vec{k}$ and $\vec{p}$ and does not depend on the angle ϕ, which is the azimuthal coordinate of the vector $\vec{k}$. Doing the integration on the left hand side we will find the projected amplitude for $m = 0$ which is denoted by $t(k,p)$, and we will find 0 for all the other values of m. The same way for the first first term on the right hand side we will find something proportional to $\int d\Omega_{\hat{k}} Y_l^m(\hat{k}) \frac{1}{E - \frac{k^2}{2M_N} - \frac{p^2}{2M_N} - \frac{(\vec{k}+\vec{p})^2}{2M_N}}$, which is zero for non-zero values of m and for $m = 0$ equals to $\int dx\ P_l(x) \frac{1}{E - \frac{k^2}{M_N} - \frac{p^2}{M_N} - \frac{kpx}{M_N}}$, where $x = \cos(\theta)$. This will give Legendre polynomials of the second kind. The tricky part of this calculation is the second term of the right hand side. Here again we find $m = 0$, so from $Y_l^m(\hat{k})$ we have $P_l(\hat{k} \cdot \hat{p})$, which can be expanded using the addition theorem:

$$P_l(\hat{k} \cdot \hat{p}) = \frac{4\pi}{2l+1} \sum_{m=-l}^{l} Y_l^m(\hat{k}) Y_l^{*m}(\hat{p}) \tag{2.20}$$

In the last equation the z axis is arbitrary so we can chose it to be along $\vec{q}$. No matter whether the z axis is along $\vec{p}$ or $\vec{q}$ the weight $d\Omega_{\hat{k}}$ does not change. So we can integrate the amplitude $(it^{jk})^{\gamma c}_{\alpha a}(\vec{k}, \vec{q})$ with $Y_l^m(\hat{k})$ over the angles of $\vec{k}$: $d\Omega_{\hat{k}}$ to find that the only contribution comes from $m = 0$ and is proportional to the projected amplitude $t(k,q)$. Then using the second spherical harmonic with the nucleon propagator, we can do the integration over the angles of $\vec{q}$ to again find something in terms of Legendre polynomials of the second kind. The final expression after doing all of these manipulations is:

$$\begin{aligned} t_0^l(k,p) &= -\frac{y_t^2 M_N}{pk} Q_l\left(\frac{p^2+k^2-M_N E}{pk}\right) \\ -&\quad \frac{2}{\pi}\int dq q^2 t_0^l(k,q) \frac{1}{\sqrt{\frac{3q^2}{4}-M_N E-i\epsilon}-\gamma_t}\frac{1}{pq}Q_l\left(\frac{p^2+q^2-M_N E-i\epsilon}{pq}\right) \end{aligned} \tag{2.21}$$

Here the Legendre polynomials of the second kind are (this differs from the conventional definition by a phase factor $(-1)^l$):

$$Q_l(a) = \frac{1}{2}\int_{-1}^{1} dx\ \frac{P_l(x)}{x+a} \tag{2.22}$$

This is the equation that the leading order quartet channel l-th partial wave amplitude satisfies. It was first derived by Skornyakov and Ter-Martirosian [68] and it can be solved numerically using the Hetherington-Schick method [69]. It is easy to see that discretizing the integral turns the equation into a system of algebraic equations, which is then solved numerically. I will give more details on the numerical methods used and on the general theory of integral equations in Appendix B.

Originally we had a three-dimensional integral equation, but after projecting it on different partial waves we get an infinite set of one-dimensional integral equations, one for each partial wave. At low energies however, the contributions from higher partial waves gets smaller, so we keep only up to and including G-waves.

We can write the projected integral equation in the following form:

$$t_0^l(k,p) = B_0^l(k,p) + K_0^l(q,p,E)\otimes t_0^l(k,q), \tag{2.23}$$

here the $\otimes$ operation is defined by the following equation:

$$A(q)\otimes B(q) = \frac{2}{\pi}\int dq\ q^2 A(q)B(q), \tag{2.24}$$

also $B_0^l(k,p)$ and $K_0^l(q,p,E)$ are given by:

$$B_0^l(k,p) = -\frac{y_t^2 M_N}{pk} Q_l\left(\frac{p^2+k^2-M_N E}{pk}\right), \tag{2.25}$$

and

$$K_0^l(q,p,E) = -\frac{1}{\sqrt{\frac{3q^2}{4} - M_N E - i\epsilon} - \gamma_t} \frac{1}{pq} Q_l\left(\frac{p^2+q^2-M_N E}{pq}\right). \tag{2.26}$$

2.4 Three-nucleon sector at NLO, quartet channel

At NLO the scattering amplitude gets a correction which itself satisfies an integral equation given in the following Fig. 2.6 [18]:

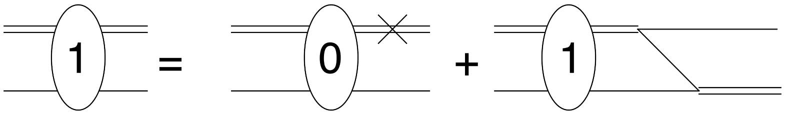

Figure 2.6: Quartet channel NLO *nd* equation.

The oval with “1” inside is the NLO correction to the *nd* scattering amplitude and the cross on the deuteron represents the effective range correction to the deuteron propagator. Explicitly, this integral equation can be written as:

$$t_1^l(k,p) = t_0^l(k,p) R_1(p,E) + K_0^l(q,p,E) \otimes t_1^l(k,q), \tag{2.27}$$

where $R_1(p,E)$ is the effective range insertion which is the first order correction to the deuteron propagator, and is given by:

$$R_1(p,E) = \frac{Z_t - 1}{2\gamma_t}\left(\gamma_t + \sqrt{\frac{3}{4}p^2 - M_N E}\right). \tag{2.28}$$

2.5 Three-nucleon sector at N^{2}LO, quartet channel

The integral equation satisfied by the N^{2}LO correction to the scattering amplitude is given in the Fig. 2.7:

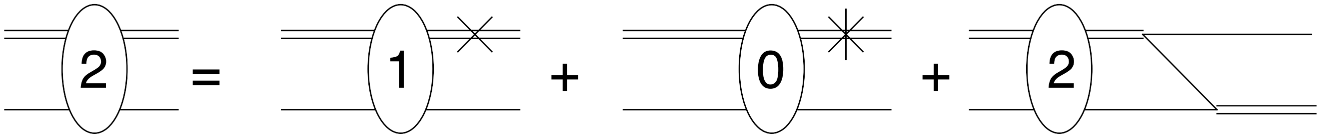

FIGURE 2.7: Quartet channel N^{2}LO *nd* equation.

Here the oval with the "2" in it is the second order correction to the amplitude, also the star on the deuteron is a higher order effective range correction to the deuteron propagator. Explicitly:

$$t_2^l(k,p) = [t_1^l(k,p) - (Z_t - 1)t_0^l(k,p)]R_1(p,E) + K_0^l(q,p,E) \otimes t_2^l(k,q). \tag{2.29}$$

Note that the kernels of the LO, NLO and N^{2}LO integral equations are all the same, which makes the numerical solution of those equations easier. This point is also discussed in the beginning of chapter 3.

The reason why we look at the quartet channel first is two-fold. Firstly in the quartet channel the diagrams involving the spin-singlet auxiliary field s_a do not contribute, because this field has spin zero. In the doublet channel on the other hand, diagrams that involve s_a fields do contribute. As a result in the quartet channel we have one integral equation for each partial wave, but in the doublet channel we have a system of two coupled integral equations for each partial wave (more on this in chapter 3). Secondly the asymptotic analysis of the solutions for the quartet channel integral equations shows that these solutions become independent of the cutoff as the cutoff goes to infinity. The same result is found by numerically looking at the cutoff dependence of the solution. This is not always the case for the doublet channel. The doublet S-wave amplitude shows a very strong dependence on the cutoff which does not go away for big cutoffs, which makes it necessary to include a three-body counterterm into the Lagrangian. This modifies the doublet S-wave equation so that the solution of the new equation becomes cutoff independent for large cutoffs. The same type of problem arises when one considers the three-body scattering problem in an EFT that is the equivalent of the EFT$_{\not\pi}$ when instead of spin-$\frac{1}{2}$ nucleons one considers spinless bosons. So now I will describe the three-boson problem and show how the asymptotic analysis is done in this simpler setting. Then we can go on to the discussion of the doublet channel nd scattering.

2.6 Three-boson system in EFT$_{\not\pi}$ and asymptotic analysis

Following [70], the Lagrangian describing non-relativistic bosons with contact interactions is given by:

$$\mathcal{L} = \psi^\dagger \left(i\partial_0 + \frac{\vec{\nabla}^2}{2M} \right) \psi + \Delta T^\dagger T - \frac{g}{\sqrt{2}}(T^\dagger \psi\psi + h.c.) + hT^\dagger T \psi^\dagger \psi. \tag{2.30}$$

Here ψ is the non-relativistic boson field and T is the dimeron field which represents the bound state of the two bosons. The field T is the analog to the t_i and s_a fields in EFT$_{\not\pi}$ for nucleons. Here too one can recover the Lagrangian involving only the ψ field by integrating the T field out of the theory. In this Lagrangian the parameter Δ is a constant unphysical parameter, the dimeron field has a bare propagator equal to i/Δ. The parameter g determines the two body interaction and we have inserted the three-body interaction term determined by the parameter h. For now we will consider h to be zero and show that the scattering amplitudes have strong cutoff dependence, this will prove the need to insert the three-body interaction.

The process of calculating the three-body scattering amplitude is the same as for nucleons, but without having to do the spin-isospin projections. We first calculate the dressed dimeron propagator, then write the integral equation that the three-body scattering amplitude must satisfy, then solve it numerically. So let's start with the dressed dimeron propagator.

The propagator of the bosonic field ψ with four momentum p is just the usual non-relativistic propagator:

$$iS(p) = \frac{i}{p_0 - \frac{p^2}{2m} + i\epsilon}. \tag{2.31}$$

From here the dressed dimeron propagator is represented by the same figure as the dressed deuteron propagator (see Fig. 2.2) and it is also given by a geometric series which sums up to:

$$i\Delta(p) = \frac{-i}{-\Delta + \frac{mg^2}{4\pi}\sqrt{-mp_0 + \frac{p^2}{4} - i\epsilon}}. \tag{2.32}$$

Now we can look at the boson-dimeron scattering amplitude. This amplitude satisfies an analogous integral equation as before and we can again perform partial wave decomposition for this equation. The complications arise only in the S-wave channel, so we will only look at the integral equation in this channel.

$$\begin{aligned} t(k,p) &= \frac{mg^2}{pk}\log\left(\frac{p^2+pk+k^2-mE}{p^2-pk+k^2-mE}\right) \\ + \quad & \frac{2}{\pi}\int dq q^2 t(k,q)\frac{1}{\sqrt{\frac{3q^2}{4} - M_N E - i\epsilon} - \frac{1}{a_2}}\frac{1}{pq}\log\left(\frac{p^2+pq+q^2-mE-i\epsilon}{p^2-pq+q^2-mE-i\epsilon}\right) \end{aligned} \tag{2.33}$$

Here a_2 is the two body scattering length and $t(k,p)$ is the boson-dimeron scattering amplitude in the S-wave channel. On the right hand side inside the loop integration we have the dimeron propagator which has a pole, so to make this pole structure simpler and to get rid of the square root structure from the kernel it is customary to do the following substitution:

$$\frac{a(k,p)}{p^2-k^2} = \frac{1}{mg^2}\frac{t(k,p)}{\sqrt{\frac{3p^2}{4}-M_N E}-\frac{1}{a_2}}. \tag{2.34}$$

Substituting this back into the integral equation gives an equation for the new function $a(k,p)$. To derive the equation for this new function we use the facts that the total energy E is given by $E = \frac{3k^2}{4m} - B_2$, where B_2 is the two body binding energy and it is related to the two body scattering length by: $B_2 = \frac{1}{ma_2^2}$. After all the simplifications the equation we get is:

$$a(k,p) = M(k,p,k) + \frac{2}{\pi}\int dq M(q,p,k)\frac{q^2}{q^2-k^2-i\epsilon}a(k,q) \tag{2.35}$$

where $M(q,p,k)$ is the new kernel and is defined by:

$$M(q,p,k) = \frac{4}{3}\left(\sqrt{\frac{3p^2}{4}-M_N E}+\frac{1}{a_2}\right)\frac{1}{pq}\log\left(\frac{p^2+pq+q^2-mE-i\epsilon}{p^2-pq+q^2-mE-i\epsilon}\right) \tag{2.36}$$

To understand the behavior of the function $a(k,p)$ for large p we can derive an approximate equation from Eq. (2.35). We can see that the inhomogeneous part of this equation can be neglected as p gets large, also the main contribution in the integral comes from the region where the argument of the log is the biggest, which is the region where $q \sim p$. After doing all of these approximations the integral equation simplifies to:

$$a(k,p) = \frac{4}{\sqrt{3}\pi}\int \frac{dq}{q}\log\left(\frac{q^2+pq+p^2}{q^2-pq+p^2}\right)a(k,q) \tag{2.37}$$

The solution to Eq. (2.35) is unique for any given cutoff Λ, but Eq. (2.37) does not have to have a unique solution. In fact it is obvious that from any given solution to Eq. (2.37) one can construct infinitely many solutions by just multiplying it with any number C. So the most general solution to Eq. (2.37) will be parametrized by some family of parameters. The solution to Eq. (2.35) then has to be matched to the solution of Eq. (2.37) at some intermediate region of the variable p and this matching will give one condition that this family of parameters has to satisfy.

At this point the solution for this integral equation is just guessed to be of the form $a(k,p) = p^s$ and to find s we just substitute it into the equation:

$$p^s = \frac{4}{\sqrt{3}\pi} \int_0^\infty dq \; q^{s-1} \log\left(\frac{q^2 + pq + p^2}{q^2 - pq + p^2}\right) \tag{2.38}$$

The integration limits in this equation are from 0 to ∞, so we can change the integration variable $q \to xp$ without changing the integration limits. After doing this, p^s cancels out and what we are left with is an equation for s:

$$1 = \frac{4}{\sqrt{3}\pi} \int_0^\infty dx \; x^{s-1} \log\left(\frac{x^2 + x + 1}{x^2 - x + 1}\right). \tag{2.39}$$

Denote the integral on the right hand side $I = \int_0^\infty dx \; x^{s-1} \log\left(\frac{x^2+x+1}{x^2-x+1}\right)$. Doing change of integration variable $x \to -x$ we find $\int_{-\infty}^0 dx \; x^{s-1} \log\left(\frac{x^2+x+1}{x^2-x+1}\right) = (-1)^s I$. Note that it may seem like doing the same change of integration variable twice we find $(-1)^{2s} = 1$ which is obviously not the case if s is anything but an integer. In case s is not an integer we have the formula $(-x)^{s-1} = (-1)^{s-1} x^{s-1}$ only if $x > 0$.

From the previous paragraph we find:

$$(1 + (-1)^s) I = \int_{-\infty}^\infty dx \; x^{s-1} \log\left(\frac{x^2 + x + 1}{x^2 - x + 1}\right) \tag{2.40}$$

Substitute Eq. (2.39) into the previous equation to find:

$$(1 + (-1)^s) = \frac{4}{\sqrt{3}\pi} \int_{-\infty}^{\infty} dx \; x^{s-1} \log \left(\frac{x^2 + x + 1}{x^2 - x + 1} \right) \tag{2.41}$$

To calculate the integral on the right hand side we can do integration by parts taking x^{s-1} under the differential:

$$(1 + (-1)^s) = \frac{4}{\sqrt{3}s\pi} \left(x^s \log \left(\frac{x^2 + x + 1}{x^2 - x + 1} \right) \Bigg|_{-\infty}^{\infty} - \int_{-\infty}^{\infty} dx \; x^s \frac{f'(x)}{f(x)} \right) \tag{2.42}$$

where $f(x) = \left(\frac{x^2+x+1}{x^2-x+1} \right)$ is the argument of the log.

For Eq. (2.39) to be valid s has to be so that the first term on the right hand side of the last equation goes to zero in the limits $-\infty$ and ∞. This puts a restriction on possible values for s: $Re(s) < 1$. So we are left with:

$$(1 + (-1)^s) = -\frac{4}{\sqrt{3}s\pi} \int_{-\infty}^{\infty} dx \; x^s \frac{f'(x)}{f(x)} \tag{2.43}$$

To calculate the integral on the right hand side we can close the integration contour in the upper half complex plane and find a complex integral over a contour.

In general if we have an integral of the form $\int dx \; g(x) \frac{f'(x)}{f(x)}$ over a closed contour where $g(x)$ is a regular function inside the contour, $f(x)$ has zeros a_i of order α_i and poles b_j of order β_j then this integral can be calculated with the following formula:

$$\frac{1}{2\pi i} \int dx \; g(x) \frac{f'(x)}{f(x)} = \sum_i \alpha_i g(a_i) - \sum_j \beta_j g(b_j) \tag{2.44}$$

This formula can be easily verified by expanding the functions f and g around the zeros and the poles of f and using the residue theorem.

We use this formula to calculate the integral in Eq. (2.43). In the upper half complex plane the function $f(x)$ has one zero $a = e^{i\frac{2}{3}\pi}$ of order one and one pole $b = e^{i\frac{1}{3}\pi}$ of order one. Using this Eq. (2.43) becomes:

$$(1 + e^{is\pi}) = -\frac{8i}{\sqrt{3}s}(e^{i\frac{2}{3}s\pi} - e^{i\frac{1}{3}s\pi}), \tag{2.45}$$

which simplifies to:

$$s = \frac{8}{\sqrt{3}} \frac{\sin\frac{\pi s}{6}}{\cos\frac{\pi s}{2}}. \tag{2.46}$$

To see another derivation of this equation see [71]. This equation has two complex solutions $s = \pm i s_0$, with s_0 approximately equal to $s_0 \approx 1.00624$. Those two solutions give two different linearly independent solutions to Eq. (2.37) from which one can construct a general solution that is real and has two arbitrary undetermined parameters:

$$a(k, p) = C \cos\left(s_0 \log \frac{p}{p_*}\right) \tag{2.47}$$

with undetermined constants C and p_*.

If we take the solution to Eq. (2.35) with very large cutoff Λ, and look at its form when $\Lambda > p \gg$ then we see that Eq. (2.35) reduces to Eq. (2.37), where there are no k-related scales left, and this solution approaches to Eq. (2.47), with parameters C and p_* that can't depend on k. All that they can depend on is the cutoff Λ used in the original Eq. (2.35). So this solution does not converge to a unique function when $\Lambda \to \infty$.

To regulate the theory and get rid of this cutoff dependence we have to have a cutoff dependent counterterm added to the Lagrangian, which will modify the integral equation that the amplitude must satisfy, and will render it cutoff independent. This counterterm is given in the Lagrangian in Eq. (2.30) by the interaction term proportional to h. It will modify Eq. (2.35) to an equation that looks the same but has a different function $M(q, p, k)$:

$$M(q, p, k) = \frac{4}{3}\left(\sqrt{\frac{3p^2}{4} - M_N E} + \frac{1}{a_2}\right)\left[\frac{1}{pq}\log\left(\frac{p^2 + pq + q^2 - mE}{p^2 - pq + q^2 - mE}\right) + \frac{h}{mg^2}\right] \tag{2.48}$$

with cutoff dependent $h = h(\Lambda)$. To determine h the modified Eq. (2.35) is solved numerically, then from the solution an observable is constructed, such as the three-body scattering length or three-body binding energy and it is held fixed but the cutoff is varied. Doing this the dependence of $h(\Lambda)$ on the cutoff is determined numerically. The approximate form of the function $h(\Lambda)$ can be derived analytically too when the cutoff approaches to infinity by choosing the function $h = h(\Lambda)$ so that the cutoff dependence of the solution of Eq. (2.35) goes away [72, 73]. Here I will only mention that the function $h(\Lambda)$ shows a non-trivial, oscillatory cutoff dependence and that this is a purely non-perturbative effect and it cannot be seen at any order of perturbation theory [70]. In the next section, when I discuss the doublet channel nd scattering, I'll show why a three-body interaction counterterm is needed there for the same reason as it is needed for the three-boson case. I will also show the numerically determined function $h(\Lambda)$.

2.7 Three-nucleon sector at LO, doublet channel: S-wave

The purpose of this section is to show the equivalence of the cutoff dependence problems of the two situations: one with spin-$\frac{1}{2}$ nucleons, the other with spin-0 bosons [15]. Diagrammatically the equations for nd scattering in the S-wave doublet channel without any three-body forces can be expressed as in the following Fig. 2.8:

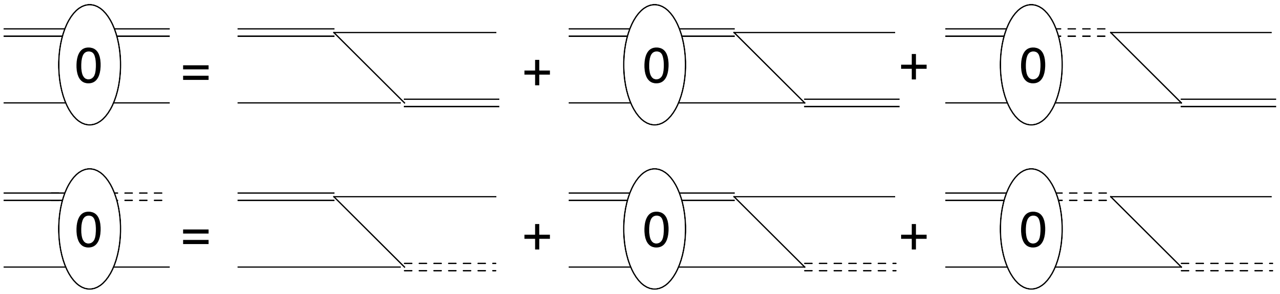

FIGURE 2.8: Doublet channel S-wave LO nd equation without three-body forces.

Here the oval with a "0" is the leading order amplitude, the double lines stand for the deuteron and the double dashed lines stand for the spin-singlet isospin-triplet dibaryon s_a. We can see that here we have two coupled integral equations as opposed to the quartet channel nd scattering. After writing the equations explicitly and projecting on the appropriate channel the following explicit form is obtained:

$$\frac{3}{2}\left(\frac{1}{a_2^t}+\sqrt{\frac{3p^2}{4}-M_N E}\right)^{-1} a(p,k) = K(p,k)+\frac{2}{\pi}\int_0^\Lambda \frac{q^2 dq}{q^2-k^2-i\epsilon}K(p,q)(a(q,k)+3b(q,k)) \tag{2.49}$$

$$2\frac{\left(-\frac{1}{a_2^s}+\sqrt{\frac{3p^2}{4}-M_N E}\right)}{p^2-k^2} b(p,k) = 3K(p,k)+\frac{2}{\pi}\int_0^\Lambda \frac{q^2 dq}{q^2-k^2-i\epsilon}K(p,q)(3a(q,k)+b(q,k)) \tag{2.50}$$

where

$$K(p,q)=\frac{1}{2pq}\log\left(\frac{p^2+pq+q^2-mE-i\epsilon}{p^2-pq+q^2-mE-i\epsilon}\right), \tag{2.51}$$

also $a(p,k)$ and $b(p,k)$ are the two scattering amplitudes corresponding to the left hand sides of the equations in the Fig. 2.8. a_2^t and a_2^s are the two-body scattering lengths in the ${}^3S_1$ and ${}^1S_0$ channels respectively.

As we are only interested in the cutoff dependence of the amplitudes $a(p,k)$ and $b(p,k)$, we want to apply the same kind of asymptotic analysis as in the 3-boson case. In the limit where the cutoff Λ is large and p is large with $p<\Lambda$ the difference between a_2^t and a_2^s does not play an important role hence to figure out the cutoff dependence of the solutions we can take $a_2^t = a_2^s = a_2$. In this case we can define new amplitudes formed from $a(p,k)$ and $b(p,k)$ so that the equations for the new amplitudes decouple. The new amplitudes are $a_+ = a(p,k)+b(p,k)$ and $a_- = a(p,k)-b(p,k)$ and the decoupled equations that they need to satisfy are:

$$\frac{3}{4}\left(\frac{1}{a_2}+\sqrt{\frac{3p^2}{4}-M_NE}\right)^{-1}a_+(p,k)=2K(p,k)+\frac{2}{\pi}\int_0^\Lambda\frac{q^2dq}{q^2-k^2-i\epsilon}2K(p,q)a_+(q,k) \quad (2.52)$$

$$\frac{3}{4}\left(\frac{1}{a_2}+\sqrt{\frac{3p^2}{4}-M_NE}\right)^{-1}a_-(p,k)=-K(p,k)-\frac{2}{\pi}\int_0^\Lambda\frac{q^2dq}{q^2-k^2-i\epsilon}2K(p,q)a_-(q,k) \quad (2.53)$$

Comparing these two equations to Eq. (2.35) and Eq. (2.21) we see that a_- satisfies that same equation as the quartet channel nd scattering amplitude, hence it has no cutoff dependence as $\Lambda \to \infty$, and a_+ satisfies the same equation as the three boson scattering amplitude, so it has cutoff dependence as $\Lambda \to \infty$. This indicates that a three-body force is necessary to regulate this cutoff dependence and ultimately render the nd scattering amplitude and other observables cutoff independent. The interaction Lagrangian that describes this three-body force is given by:

$$\mathcal{L}=\frac{M_NH_0(\Lambda)}{3\Lambda^2}\left(y_tN^\dagger(\vec{t}\cdot\vec{\sigma})^\dagger-y_sN^\dagger(\vec{s}\cdot\vec{\tau})^\dagger\right)\left(y_tN(\vec{t}\cdot\vec{\sigma})-y_sN(\vec{s}\cdot\vec{\tau})\right). \quad (2.54)$$

This will modify the integral equations satisfied by the doublet channel nd scattering amplitude and the modified equations will be given diagrammatically by the following Fig. 2.9.

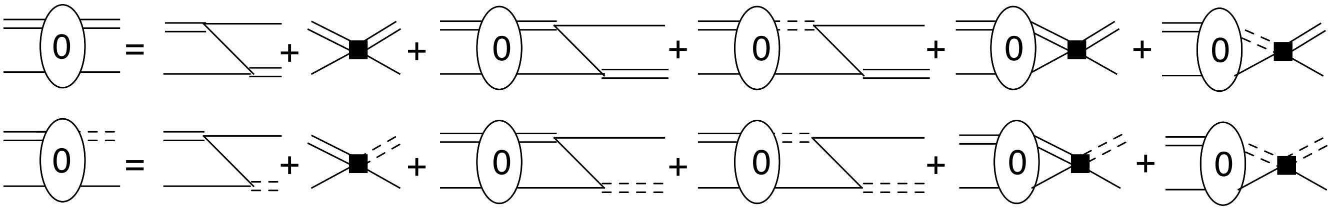

FIGURE 2.9: Doublet channel S-wave LO nd equation with three-body forces.

and have the form:

$$
\begin{aligned}
t^{0}_{0,Nt\to Nt}(k,p) &= 2\pi\left(\frac{1}{pk}\log\left(\frac{p^2+pk+k^2-mE}{p^2-pk+k^2-mE}\right)+\frac{2H_0(\Lambda)}{\Lambda^2}\right)\\
+&\int\left[\frac{1}{2pq}\log\left(\frac{p^2+pq+q^2-mE-i\epsilon}{p^2-pq+q^2-mE-i\epsilon}\right)+\frac{H_0(\Lambda)}{\Lambda^2}\right]\\
\times&\left(-D^{(0)}_t(E,q)t^{0}_{0,Nt\to Nt}(k,q)+3D^{(0)}_s(E,q)t^{0}_{0,Nt\to Ns}(k,q)\right)\\
\\
t^{0}_{0,Nt\to Ns}(k,p) &= -6\pi\left(\frac{1}{pk}\log\left(\frac{p^2+pk+k^2-mE}{p^2-pk+k^2-mE}\right)+\frac{2H_0(\Lambda)}{\Lambda^2}\right)\\
+&\int\left[\frac{1}{2pq}\log\left(\frac{p^2+pq+q^2-mE-i\epsilon}{p^2-pq+q^2-mE-i\epsilon}\right)+\frac{H_0(\Lambda)}{\Lambda^2}\right]\\
\times&\left(3D^{(0)}_t(E,q)t^{0}_{0,Nt\to Nt}(k,q)-D^{(0)}_s(E,q)t^{0}_{0,Nt\to Ns}(k,q)\right).
\end{aligned}
\tag{2.55}
$$

These equations are solved numerically and the three-body force $H_0(\Lambda)$ is fixed by an observable such as the three-body scattering length or the three-body binding energy. The dependence of the three-body force on the cutoff is oscillatory, this RG behavior is called a limit-cycle [15, 16, 17, 70] (see Fig. 2.10[1] [72]). This three body force gets corrections at all higher orders of perturbation theory, at each order being fixed to the same observable.

---

[1] Reprinted from [72], Phys. Rev. Lett., Volume 82, Bedaque, Paulo F. and Hammer, H. W. and van Kolck, U., "Renormalization of the three-body system with short range interactions," Pages 463-467, Copyright (1999), by the American Physical Society.

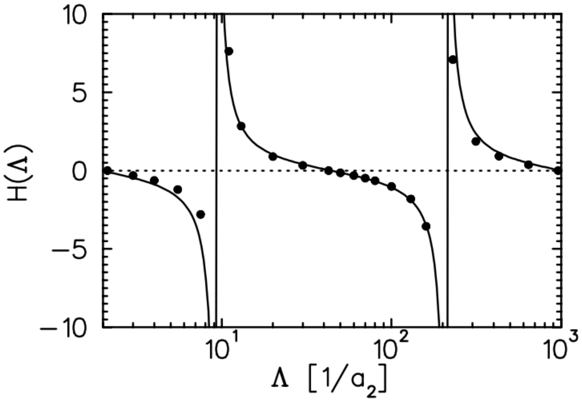

FIGURE 2.10: (Caption and figure reprinted from [72]). Three-body force as a function of the cutoff Λ: numerical solution (dots) and the analytical approximate solution (solid line).

2.8 Three-nucleon sector at LO, doublet channel: Higher partial waves

For higher partial waves the LO equations are expressed by the same diagrams as the S-wave equation without the three-body force, as shown if Fig. 2.11. Explicitly these equation are Eq. (2.56) [14].

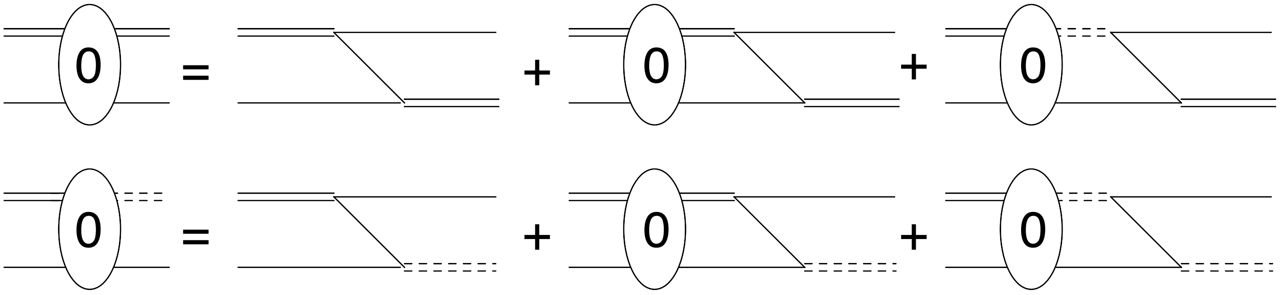

FIGURE 2.11: Doublet channel LO nd equation higher partial waves.

$$t^l_{0,d}(k,p) = B^l_0(k,p,E) + K^l_0(q,p,E) \otimes t^l_{0,d}(k,q). \tag{2.56}$$

where $t^l_{0,d}(k,p)$ is the doublet channel scattering amplitude in so-called cluster configuration space, with the first component being the $Nt \to Nt$ scattering amplitude and the second component being the $Nt \to Ns$ scattering amplitude:

$$t^l_{n,d}(k,p) = \begin{pmatrix} t^l_{n,Nt\to Nt}(k,p) \\ t^l_{n,Nt\to Ns}(k,p) \end{pmatrix}, \tag{2.57}$$

where the superscript l stands for the l-th partial wave. The subscript n stands for n-th order, and d for doublet channel.

$B^l_0(k,p,E)$ is defined by:

$$B^l_0(k,p,E) = \begin{pmatrix} \frac{2\pi}{pk} Q_l(\frac{p^2+k^2-ME}{pk}) \\ -\frac{6\pi}{pk} Q_l(\frac{p^2+k^2-ME}{pk}) \end{pmatrix} \tag{2.58}$$

and the kernel matrix is given by:

$$K^l_0(q,p,E) =$$

$$\frac{1}{2qp} Q_l\left(\frac{p^2+q^2-M_NE-i\epsilon}{pq}\right) \begin{pmatrix} \frac{1}{\sqrt{\frac{3q^2}{4}-M_NE-i\epsilon}-\gamma_t} & \frac{-3}{\sqrt{\frac{3q^2}{4}-M_NE-i\epsilon}-\gamma_s} \\ \frac{-3}{\sqrt{\frac{3q^2}{4}-M_NE-i\epsilon}-\gamma_t} & \frac{1}{\sqrt{\frac{3q^2}{4}-M_NE-i\epsilon}-\gamma_s} \end{pmatrix}. \tag{2.59}$$

The symbol $\otimes$ is defined in Eq. (2.24), but it is also accompanied by a matrix multiplication:

$$\begin{pmatrix} A(q) & B(q) \\ C(q) & D(q) \end{pmatrix} \otimes \begin{pmatrix} U(q) \\ V(q) \end{pmatrix} = \begin{pmatrix} A(q)\otimes U(q) + B(q)\otimes V(q) \\ C(q)\otimes U(q) + D(q)\otimes V(q) \end{pmatrix}. \tag{2.60}$$

2.9 Three-nucleon sector at NLO, doublet channel

The NLO correction to the amplitude is determined from an integral equation diagrammatically expressed in the following Fig. 2.12:

and explicitly by the equation Eq. (2.61):

$$t^l_{1,d}(k,p) = t^l_{0,d}(k,p) \circ R_1(p,E) + K^l_0(q,p,E) \otimes t^l_{1,d}(k,q), \tag{2.61}$$

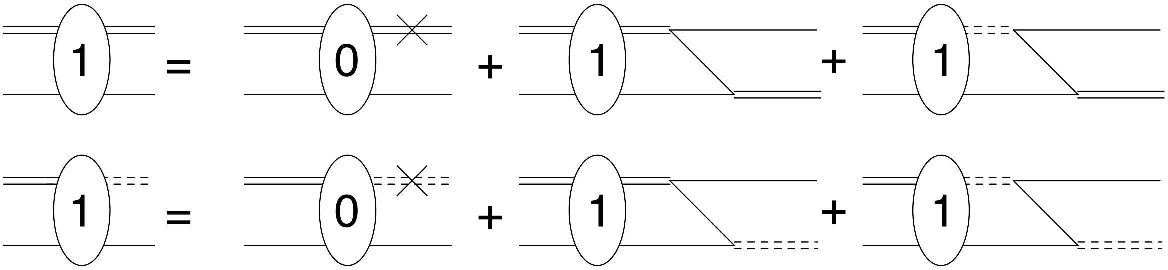

FIGURE 2.12: Doublet channel NLO nd equation.

where:

$$R_1(p,E)=\begin{pmatrix}\frac{z_t-1}{2\gamma_t}(\gamma_t+\sqrt{\frac{3p^2}{4}-M_NE})\\ \frac{z_s-1}{2\gamma_s}(\gamma_s+\sqrt{\frac{3p^2}{4}-M_NE})\end{pmatrix}, \tag{2.62}$$

and the $\circ$ is the Schur product:

$$\begin{pmatrix}A\\B\end{pmatrix}\circ\begin{pmatrix}C\\D\end{pmatrix}=\begin{pmatrix}AC\\BD\end{pmatrix}. \tag{2.63}$$

2.10 Three-nucleon sector at N^{2}LO, doublet channel

The N^{2}LO correction also satisfies similar diagrammatic equation Fig. 2.13:

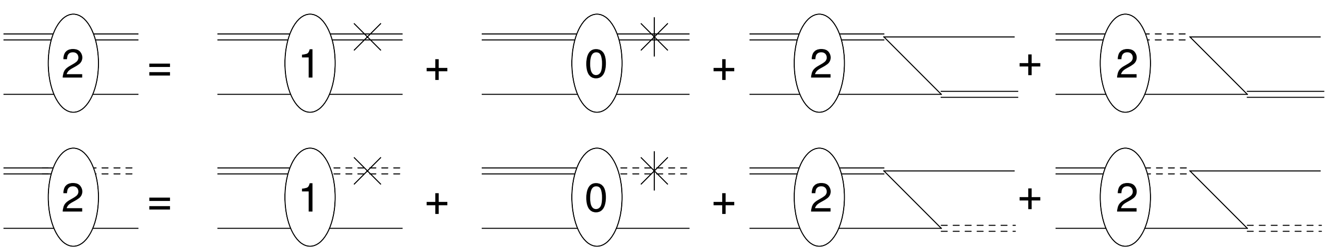

FIGURE 2.13: Doublet channel N^{2}LO nd equation.

which explicitly becomes Eq. (2.64):

$$t^l_{2,d}(k,p)=(t^l_{1,d}(k,p)-c_1\circ t^l_{0,d}(k,p))\circ R_1(p,E)+K^l_0(q,p,E)\otimes t^l_{2,d}(k,q), \tag{2.64}$$

where c_1 is given by:

$$c_1 = \begin{pmatrix} Z_t - 1 \\ Z_s - 1 \end{pmatrix} . \tag{2.65}$$

Note that the kernels of the LO, NLO and N^{2}LO equations are all the same, which makes the numerical part of the calculations easier; once the (1−Kernel) matrix is inverted to solve the LO equation, that inverse can be used to calculate higher order amplitudes. This statement generalizes to higher orders as we will see later. The LO amplitude contributes only to the inhomogeneous parts of the NLO and the N^{2}LO equations, the same way the NLO amplitude only contributes to the inhomogeneous part of the N^{2}LO equation.

At N^{2}LO there is a new interaction that enters in the two-body sector called the SD mixing. It gives a vertex that is an incoming deuteron with two outgoing nucleons attached to it or vise versa. In the deuteron the nucleons are in relative S-wave and the other two nucleons that are attached to this vertex are always in a relative D-wave, otherwise this interaction vertex is just zero, and hence the name. There are two derivatives acting on the nucleon fields, which makes this term enter at N^{2}LO, also making the two nucleons outside of the deuteron to be in relative a D-wave. This interaction is given by the Lagrangian:

$$\mathcal{L}_2^{SD} = y_{SD} \hat{t}_i^\dagger \left[\hat{N}^T \left((\overrightarrow{\partial} - \overleftarrow{\partial})^i (\overrightarrow{\partial} - \overleftarrow{\partial})^j - \frac{1}{3}\delta^{ij} (\overrightarrow{\partial} - \overleftarrow{\partial})^2 \right) P_j \hat{N} \right] + \text{H.c.}, \tag{2.66}$$

where, just like before, the projector is defined by $P_j = \frac{1}{\sqrt{8}}\sigma_2\sigma_j\tau_2$. The coupling constant y_{SD} is fixed by the two-body scattering data. A detailed discussion of how to fix y_{SD} and the calculation of the contributions of this term to the three-body scattering amplitude can be found in [18, 74]. Here I will just note that this is the first interaction term that gives a non-zero contribution to the observable A_y. At N^{3}LO new interaction terms enter (see section 2.11) into the Lagrangian giving more substantial contributions to this observable.

2.11 Two-body P-wave interactions at two-nucleon sector

Two-body P-wave contact interactions first occur at N^{3}LO. The ^3P_J terms are given by the ^3P_J Lagrangian [75],

$$\mathcal{L}_2^{^3P_J} = \left(C_2^{(^3P_0)} \delta_{xy}\delta_{wz} + C_2^{(^3P_1)} [\delta_{xw}\delta_{yz} - \delta_{xz}\delta_{yw}] + C_2^{(^3P_2)} \left[2\delta_{xw}\delta_{yz} + 2\delta_{xz}\delta_{yw} - \frac{4}{3}\delta_{xy}\delta_{wz} \right] \right) \tag{2.67}$$

$$\times \frac{1}{4} (\hat{N}^T \mathcal{O}^{(1,P)}_{xyA} \hat{N})^\dagger (\hat{N}^T \mathcal{O}^{(1,P)}_{wzA} \hat{N})$$

where

$$\mathcal{O}^{(1,P)}_{ijA} = \overleftarrow{\nabla}_i \, P^P_{jA} - P^P_{jA} \, \overrightarrow{\nabla}_i \tag{2.68}$$

and the projector is defined as $P^P_{iA} = \frac{1}{\sqrt{8}} \sigma_2 \sigma_i \tau_2 \tau_A$. This interaction Lagrangian is also considered in the paper Ref. [75], in which the authors consider the process $np \to d\gamma$. To calculate this particular scattering amplitude they need the projector P^P_{iA} to be something particular so that it projects to the isospin quantum numbers of the initial state np. In our case we are interested in nd scattering, hence we can have nn and np scattering through this interaction. For this reason we need the projector P^P_{iA} to be a more general one than given in Ref. [75].

At this order also the two-body $^1P_1$ contact interaction appears:

$$\mathcal{L}_2^{^1P_1} = C_2^{(^1P_1)} \frac{1}{4} (\hat{N}^T \mathcal{O}^{(0,P)}_x \hat{N})^\dagger (\hat{N}^T \mathcal{O}^{(0,P)}_x \hat{N}), \tag{2.69}$$

The operator $\mathcal{O}^{(0,P)}_i$ is defined by

$$\mathcal{O}^{(0,P)}_i = \overleftarrow{\nabla}_i \, P^P - P^P \, \overrightarrow{\nabla}_i, \tag{2.70}$$

where the projector is $P^P = \frac{1}{\sqrt{8}} \sigma_2 \tau_2$.

To understand the index structure of the projectors $P^P_{iA} = \frac{1}{\sqrt{8}} \sigma_2 \sigma_i \tau_2 \tau_A$ and $P^P = \frac{1}{\sqrt{8}} \sigma_2 \tau_2$ consider the following. The nucleons interacting through the ^3P_J interaction terms have to be in relative a $P-$wave, which is antisymmetric, with total spin $S = 1$, which is symmetric, so to have in total an antisymmetric configuration the total isospin should be also symmetric hence $I = 1$. This is why the projector $P^P_{iA} = \frac{1}{\sqrt{8}}\sigma_2\sigma_i\tau_2\tau_A$ has a spin index i and an isospin index A. The same way in ${}^1P_1$ channel we have antisymmetric $P-$wave, antisymmetric $S = 0$ state, so we must have antisymmetric $I = 0$ state hence there are no spin and isospin indices on the $P^P = \frac{1}{\sqrt{8}}\sigma_2\tau_2$ projector.

The interaction coefficients are $C_2^{{}^3P_J}$ with $J = 1, 2, 3$ and $C_2^{{}^1P_1}$. The subscript 2 refers to two-body, in the superscripts ${}^3P_J$ and ${}^1P_1$ the standard spectroscopic notation is used: ${}^{(2S+1)}L_J$. If $S = 1$ and $L = 1$ then $J = S + L$ can be only $1, 2$, and 3, so we have three terms here. The same with ${}^1P_1$: $S = 0$, $L = 1$ hence $J = 1$ and we have one interaction term here. These interaction are constructed so that each of these interaction terms only contributes to the NN scattering amplitude in the corresponding channel.

To determine the interaction coefficients we use these interactions to calculate the np scattering amplitude in the CM frame. This calculation is fairly straightforward, because we already know the channels in which we are going to get non-zero contributions. As an example let's do the calculation of the contribution that comes from C^{3P_0} term. Denoting the incoming momentum by $\vec{k}$ and the outgoing momentum by $\vec{p}$ we get for this amplitude:

$$T^J_{LS,L'S'} = 4\frac{1}{4}\frac{1}{8}C_2^{3P_0} \sum_{i,j,m_1,m_2,m_1',m_2'} C^{m_L,m_S,M}_{L,S,J} C^{m_L',m_S',M'}_{L',S',J'} C^{m_1,m_2,m_S}_{\frac{1}{2},\frac{1}{2},S} C^{m_1',m_2',m_S'}_{\frac{1}{2},\frac{1}{2},S}$$
$$\left\langle L', m_L' \right| 2k_i 2p_j \left| L, m_L \right\rangle \left\langle \frac{1}{2}m_2 \right| \sigma_2\sigma_i \left| \frac{1}{2}m_1 \right\rangle \left\langle \frac{1}{2}m_2' \right| \sigma_j\sigma_2 \left| \frac{1}{2}m_1' \right\rangle \tag{2.71}$$

in this equation the first factor 4 is a symmetry factor, the ratio $\frac{1}{4}$ comes from the operator, the ratio $\frac{1}{8}$ comes from the projectors. The first Clebsch-Gordan coefficient combines the spin and the orbital angular momentum S and L into the total angular momentum J in the initial state, the second does the same for the final state. The third and fourth Clebsch-

Gordan coefficients combine the spins of the nucleons into the total spins S and S'. m_1 and m_2 stand for initial nucleons' spin magnetic quantum numbers, and correspondingly m_1' and m_2' for final.

The sum in Eq. (2.71) is easily calculated using the methods described in Appendix A. The answer turns out to be non-zero only if $J = J' = 0$, $L = L' = 1$, $S = S' = 1$ as was expected, because the operators by construction should give contributions only in the corresponding channels. After we have the amplitude $T^J_{LS,L'S'}$, the phase shift is calculated by the Eq. (2.72).

$$\delta = \frac{Mk}{4\pi} T^J_{LS,L'S'}, \tag{2.72}$$

where we have assumed δ to be small and we have expanded $e^{2i\delta}$, keeping only the linear term in δ. Having a numerical value for δ at a given scattering energy we find the coefficient $C_2^{3P_0}$. And the same way we can determine all the other interaction coefficients in the Lagrangians in Eqs.(2.67) and (2.69). The numerical values for the phase shifts are taken from the Nijmegen phase shifts [5]. The coefficients we get are:

$$C^{^3P_0} = 6.27 \text{ fm}^4, \quad C^{^3P_1} = -5.75 \text{ fm}^4, \quad C^{^3P_2} = .522 \text{ fm}^4, \text{ and } C^{^1P_1} = -19.8 \text{ fm}^4. \tag{2.73}$$

3

Non-Relativistic Pionless EFT: Order-3 and Higher

3.1 Three-nucleon sector at N^{n}LO, both channels

The process of going to higher orders is the same as before. We solve the LO equation, getting the LO amplitude numerically. Then this amplitude contributes to the inhomogeneous part of the NLO equation. Then the LO and NLO amplitudes contribute to the inhomogeneous part of the N^{2}LO equation, etc. At each subsequent order all of the lower order amplitudes, which are known numerically, contribute to the inhomogeneous parts of the equations at that order and not to the kernel. The kernel of the equations is always determined by just one nucleon exchange, which contributes in all channels, and the LO three-body force, which only contributes in the doublet S-wave channel. Using the technology developed earlier to represent the LO, NLO and N^{2}LO equations diagrammatically we can generalize it to represent the N^{n}LO equations diagrammatically as in Fig. 3.1 (caption and figures are from [76]).

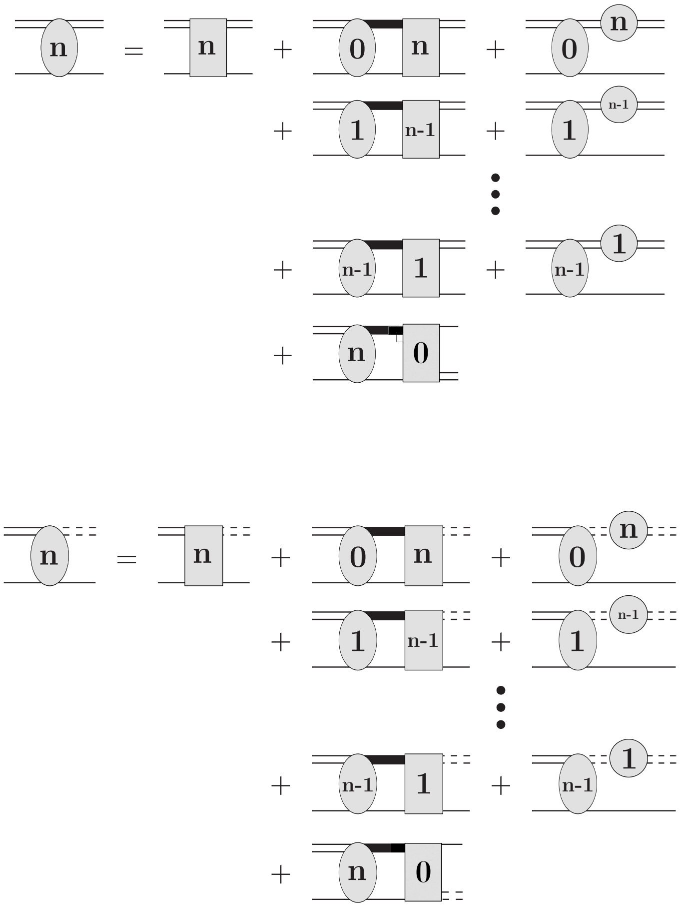

FIGURE 3.1: (Caption and figures are from [76]). Single lines represent nucleons, double lines spin-triplet dibaryons, and double dashed lines spin-singlet dibaryons. Thick solid lines denote a sum over both spin-triplet and spin-singlet dibaryons. The LO *nd* scattering amplitude is the oval with a "0" inside and the oval with the *n* inside is the N^{n}LO correction to the *nd* scattering amplitude. The circle with the *n* inside is the N^{n}LO correction to the dibaryon propagators (see Fig. 3.3), and the rectangle with the *n* inside is the *n*th order "three-body" correction (see Fig. 3.2).

In the Fig. 3.1 we use the same notation as before, except a few things need to be generalized:

1) Note that this system of equations is for the *n*-th order amplitude, which is the oval with an "*n*."

2) The n-th order, not-resummed , and using only the leading order dibaryon propagators, contributions to the n-th order amplitude are collected in the rectangle with an "n" inside, see Fig. 3.1 and Fig. 3.2 (caption and figures are from [76]); this only makes contributions to the inhomogeneous parts of the equations except for the leading order.

At LO this box is the one-nucleon exchange contributing in all channels plus the LO three-body force contributing only in the doublet S-wave channel. This is the only order when the box has a contribution to the kernel: it is the kernel.

At NLO it is only the first order correction to the LO three-body force and nothing else.

At N^{2}LO it has contributions from SD mixing, the N^{2}LO correction to the LO three-body force and the new energy-dependent three-body force $H_2^{(\mathrm{N^2LO})}$).

At N^{3}LO it gets the expected contributions, which are the third order correction to the LO three-body force and the first order correction to the energy-dependent three-body force. Most importantly it gets a contribution from the two-body P-wave interactions (see Fig. 3.2, in the box on the third line, first contribution to the rectangle with a "3" in it), which determine the leading magnitude and behavior of the A_y observable.

3) We also generalized the ERE corrections to the dibaryon propagators [12]. We collect all the $n-$th order corrections to the dibaryon propagator into a circle with an "n" on the dibaryon double line Fig. 3.3 (caption and figures are from [76]).

4) The last piece of new notation used here is the thick line, which denotes a sum over spin-triplet and spin-singlet leading order dibaryon propagators. This notation is used to make the picture more concise.

This coupled system of integral equations is not yet projected onto spin-angular momentum channels. The nd scattering can happen in either spin-quartet or spin-doublet channel. After projecting this system of equations onto the spin-quartet channel we get only one integral equation instead of two coupled ones. The reason for this is that the spin-singlet dibaryon can combine with a spin-doublet nucleon only to form a total spin-doublet state, so the amplitudes involving the double dashed lines do not exist in the quartet channel and we

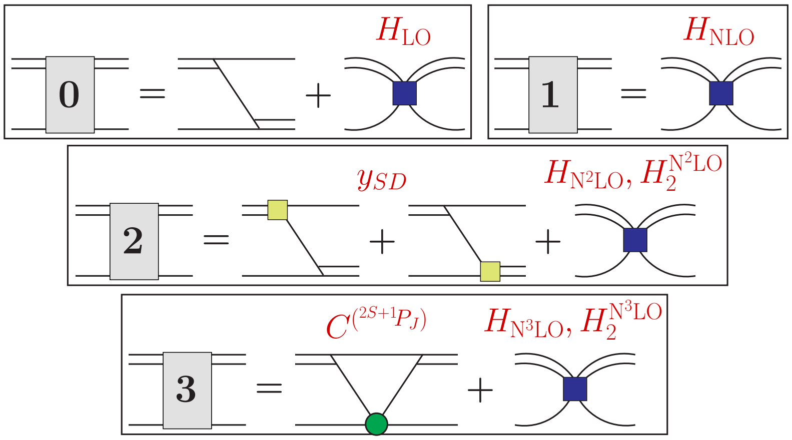

FIGURE 3.2: (Caption and figures are from [76]). "three-body" contributions to integral equations (used in the diagrams of Fig. 3.1). The LO terms are nucleon exchange plus in the doublet S-wave channel the LO three-body force (dark square) . The NLO term is a NLO correction to the LO three-body force. At N^{2}LO there are contributions from the two-body SD-mixing term (coupling indicated by pale square), the N^{2}LO correction to the LO three-body force, $H_{\mathrm{N^2LO}}$, and a new energy dependent three-body force, $H_2^{\mathrm{N^2LO}}$. The N^{3}LO contributions are from the two-body P-wave contact interactions (green circle), the N^{3}LO correction to the LO three-body force, and the N^{3}LO correction to the N^{2}LO energy dependent three-body force.

are left with only one integral equation. After doing the spin-angular momentum projections these equations can be put in the following general form:

$$\mathbf{t}^J_{n;L'S',LS}(k,p,E) = \mathbf{K}^J_{n;L'S',LS}(k,p,E)\mathbf{v}_p + \sum_{i=1}^{n} \mathbf{t}^J_{n-i;L'S',LS}(k,p,E) \circ \mathbf{R}_i(p,E) \tag{3.1}$$

$$+ \sum_{L'',S''} \sum_{i=0}^{n-1} \mathbf{K}^J_{n-i;L'S',L''S''}(q,p,E)\ \mathbf{D}\left(E - \frac{q^2}{2M_N}, \vec{\boldsymbol{q}}\right) \otimes \mathbf{t}^J_{i;L''S'',LS}(k,q,E)$$

$$+ \sum_{L'',S''} \mathbf{K}^J_{0;L'S',L''S''}(q,p,E)\ \mathbf{D}\left(E - \frac{q^2}{2M_N}, \vec{\boldsymbol{q}}\right) \otimes \mathbf{t}^J_{n;L''S'',LS}(k,q,E),$$

where the $\otimes$ symbol is defined by:

$$A(q) \otimes B(q) = \frac{1}{2\pi^2} \int dq\ q^2 A(q) B(q). \tag{3.2}$$

Note that this definition is different from Eq. (2.24). This equation is written in cluster configuration space as were our equations for the doublet channel amplitudes given before in

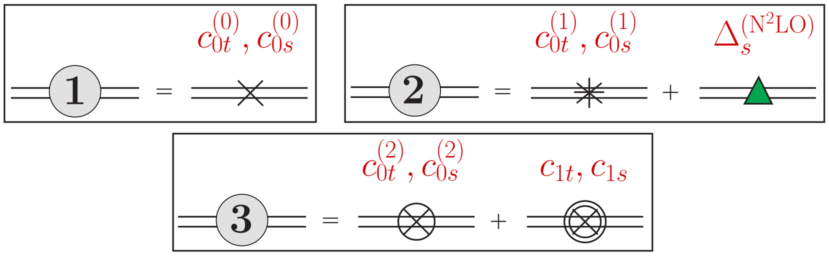

FIGURE 3.3: (Caption and figures are from [76]). Higher order corrections to dibaryon propagators (used in the diagrams of Fig. 3.1). The NLO (n=1) corrections are range corrections from $c_{0t}^{(0)}$ and $c_{0s}^{(0)}$. At N^{2}LO (n=2) the dibaryons receive further range corrections $c_{0t}^{(1)}$ and $c_{0s}^{(1)}$ in the Z-parametrization, as well as the $\Delta^{(\mathrm{N^2LO})}$ correction from splitting between the nn and np spin-singlet scattering lengths. The N^{3}LO (n=3) corrections are from higher order range corrections $c_{0t}^{(2)}$ and $c_{0s}^{(2)}$ in the Z-parametrization, and shape parameter corrections c_{1t} and c_{1s}.

Eq. (2.56), Eq. (2.61), Eq. (2.64). Everything is collected into two dimensional vectors and matrices in cluster configuration space.

$\mathbf{D}(E,\vec{\boldsymbol{q}})$ is given by:

$$\mathbf{D}(E,\vec{\boldsymbol{q}}) = \begin{pmatrix} D_t(E,\vec{\boldsymbol{q}}) & 0 \\ 0 & D_s(E,\vec{\boldsymbol{q}}) \end{pmatrix}, \tag{3.3}$$

where D_t and D_s are the LO dibaryon propagators.

$\mathbf{t}^J_{n,L'S',LS}(k,p,E)$ is the n-th order correction to the scattering amplitude in cluster configuration space, with the first component being the $Nt \to Nt$ scattering amplitude and the second component being the $Nt \to Ns$ scattering amplitude:

$$\mathbf{t}^J_{n,L'S',LS}(k,p,E) = \begin{pmatrix} t^{J;Nt\to Nt}_{n;L'S',LS}(k,p,E) \\ t^{J;Nt\to Ns}_{n;L'S',LS}(k,p,E) \end{pmatrix}. \tag{3.4}$$

The K-matrices are defined by the boxes introduced in Fig. 3.1 as in Fig 3.4.

$$\mathbf{K}^{J}_{n;L'S',LS}(k,p,E) =$$

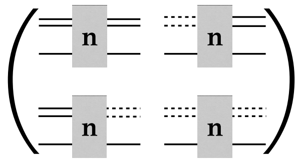

FIGURE 3.4: Diagrammatic definition of K-matrices.

Note that the actual kernel of these equations is only the matrix $\mathbf{K}^{J}_{0;L'S',LS}(q,p,E)$, which is the matrix of the rectangles with a "0" in them. The functions $\mathbf{R}_n(p,E)$ (in what follows I call those R-functions) are defined as two dimensional vectors in cluster configuration space with entries equal to the n-th order corrections to the dibaryon propagators ($n = 1, 2, 3...$) Fig 3.5.

$$\mathbf{R}_n(p,E) =$$

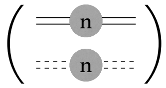

FIGURE 3.5: Diagrammatic definition of R-functions.

I have already described the explicit forms of these equations up to and including N^{2}LO. Here I will summarize all of that, talk about two-body P-wave interactions that enter at N^{3}LO and give the explicit forms of the equations satisfied by scattering amplitudes up to and including N^{3}LO.

At LO we only have the LO K-matrix, which is the kernel for the integral equations at all orders:

$$\mathbf{K}^{J}_{0;L'S',LS}(q,p,E) = \tag{3.5}$$

$$\delta_{LL'}\delta_{SS'}\begin{cases} -\frac{2\pi}{qp}Q_L\left(\frac{q^2+p^2-M_NE-i\epsilon}{qp}\right)\begin{pmatrix} 1 & -3 \\ -3 & 1 \end{pmatrix} - \pi H_{\mathrm{LO}}\delta_{L0}\begin{pmatrix} 1 & -1 \\ -1 & 1 \end{pmatrix} & , \quad S = 1/2 \\ \\ -\frac{4\pi}{qp}Q_L\left(\frac{q^2+p^2-M_NE-i\epsilon}{qp}\right)\begin{pmatrix} 1 & 0 \\ 0 & 0 \end{pmatrix} & . \quad S = 3/2 \end{cases}$$

At this order we don't have any R-functions.

At NLO the K-matrix is:

$$\mathbf{K}^{J}_{1;L'S',LS}(q,p,E) = -\pi H_{\mathrm{NLO}}\delta_{L0}\delta_{LL'}\delta_{SS'}\delta_{S1/2}\begin{pmatrix} 1 & -1 \\ -1 & 1 \end{pmatrix}. \tag{3.6}$$

H_{NLO} is the first order correction to the LO three-body force, and the R-function at this order is:

$$\mathbf{R}_1(p,E) = \begin{pmatrix} \frac{(Z_t-1)}{2\gamma_t}\left(\gamma_t + \sqrt{\frac{3}{4}p^2 - M_NE - i\epsilon}\right) \\ \frac{(Z_s-1)}{2\gamma_s}\left(\gamma_s + \sqrt{\frac{3}{4}p^2 - M_NE - i\epsilon}\right) \end{pmatrix}. \tag{3.7}$$

At N^{2}LO the K-matrix is:

$$\begin{aligned} \left[\mathbf{K}^{J}_{2;L'S',LS}(q,p,E)\right]_{zx} = \frac{y\,y_{SD}\,M_N}{2}\Bigg(& Z^{(1)}_{SD}(J,L',S',L,S,x,z)\frac{1}{kp}\left[4p^2Q_L(a) + k^2Q_{L'}(a)\right] \\ & + Z^{(1)}_{SD}(J,L,S,L',S',z,x)\frac{1}{kp}\left[p^2Q_L(a) + 4k^2Q_{L'}(a)\right] \\ & + \sum_{L''}\left[Z^{(2)}_{SD}(J,L',S',L,S,x,z,L'') + Z^{(2)}_{SD}(J,L,S,L',S',z,x,L'')\right]Q_{L''}(a)\Bigg) \\ & - \pi(H_{\mathrm{N^2LO}} + \frac{4}{3}(M_NE+\gamma_t^2)H_2^{(\mathrm{N^2LO})})\delta_{L0}\delta_{LL'}\delta_{SS'}\delta_{S1/2}(-1)^{x+z}, \end{aligned} \tag{3.8}$$

where the subscripts x and z determine the matrix element of the K-matrix in cluster configuration space. They run over the values zero and one, zero standing for spin-singlet dibaryon and one standing for the deuteron.

Functions $Z^{(1)}_{SD}(\cdots)$ and $Z^{(2)}_{SD}(\cdots)$ are calculated using the Pauli-matrix structure of the SD mixing diagrams. These functions calculate the spin-angular momentum projections of the diagrams onto particular scattering channels. I will show an example calculation of similar projection functions for the P-wave contribution diagrams in Appendix A. The functions $Z^{(1)}_{SD}(\cdots)$ and $Z^{(2)}_{SD}(\cdots)$ are defined by the equations:

$$Z^{(1)}_{SD}(J,L',S',L,S,x,z) = 2\sqrt{\hat{x}\hat{z}\widehat{(1-z)}\widehat{S}\widehat{S'}\widehat{L}}\sqrt{\frac{10}{3}}\,(-1)^{1/2+x+z+L+S+S'-J}\begin{Bmatrix} z & \frac{1}{2} & \frac{1}{2} \\ 1 & S' & \frac{1}{2}\end{Bmatrix} \tag{3.9}$$

$$\times\begin{Bmatrix} 2 & 1 & x \\ \frac{1}{2} & S & S'\end{Bmatrix}\begin{Bmatrix} S' & 2 & S \\ L & J & L'\end{Bmatrix}C^{0,0,0}_{L,2,L'},$$

and

$$Z^{(2)}_{SD}(J,L',S',L,S,x,z,L'') = \sum_{L''}8\sqrt{\hat{x}\hat{z}\widehat{(1-z)}\widehat{S}\widehat{S'}\widehat{L}\widehat{L''}}\,(-1)^{z+L''+L}\begin{Bmatrix} 1 & \frac{1}{2} & \frac{1}{2} \\ z & S' & \frac{1}{2}\end{Bmatrix} \tag{3.10}$$

$$\times\left(\begin{Bmatrix} \frac{1}{2} & x & S \\ 1 & L'' & L \\ S' & L' & J\end{Bmatrix} + \begin{Bmatrix} \frac{1}{2} & 1 & S' \\ L' & J & L''\end{Bmatrix}\begin{Bmatrix} L & x & L'' \\ \frac{1}{2} & J & S\end{Bmatrix} + \frac{1}{3}(-1)^{1+L''+L}\frac{1}{\widehat{S}\widehat{L}}\delta_{LL'}\delta_{SS'}\right)C^{0,0,0}_{L,1,L''}C^{0,0,0}_{L'',1,L'},$$

where the hat is defined by $\hat{x} = 2x+1$. The R-function at this order is:

$$\mathbf{R}_2(p,E) = -\begin{pmatrix} \frac{(Z_t-1)^2}{2\gamma_t}\left(\gamma_t + \sqrt{\frac{3}{4}p^2 - M_NE - i\epsilon}\right) \\ \frac{(Z_s-1)^2}{2\gamma_s}\left(\gamma_s + \sqrt{\frac{3}{4}p^2 - M_NE - i\epsilon}\right) \quad -\frac{2}{3}\Delta_s^{(\mathrm{N^2LO})}D_s\left(E - \frac{p^2}{2M_N}, p\right)\end{pmatrix}. \tag{3.11}$$

At N^{3}LO the K-matrix gets three different contributions: the N^{3}LO correction to the LO three-body force, the NLO correction to the energy dependent three-body force and the P-wave diagram.

$$\mathbf{K}^J_{3;L'S',LS}(q,p,E) = \mathbf{K}_{3-bforces} + \mathbf{K}_{P-wave} \tag{3.12}$$

The first term is given by:

$$\mathbf{K}_{3-bforces} = -\pi \left(H_{\mathrm{N^3LO}} + \frac{4}{3}(M_N E + \gamma_t^2) H_2^{\mathrm{N^3LO}} \right) \delta_{L0}\delta_{LL'}\delta_{SS'}\delta_{S1/2} \begin{pmatrix} 1 & -1 \\ -1 & 1 \end{pmatrix}, \tag{3.13}$$

and the $\mathrm{N^3LO}$ R-function is given by:

$$\mathbf{R}_3(p,E) = \left(\begin{array}{c} \left(\gamma_t + \sqrt{\frac{3}{4}p^2 - M_N E - i\epsilon}\right) \left[\frac{(Z_t-1)^3}{2\gamma_t} + \rho_{t1}\left(\frac{3}{4}p^2 - M_N E - \gamma_t^2\right) \right] \\ \left(\gamma_s + \sqrt{\frac{3}{4}p^2 - M_N E - i\epsilon}\right) \left[\frac{(Z_s-1)^3}{2\gamma_s} + \rho_{s1}\left(\frac{3}{4}p^2 - M_N E - \gamma_s^2\right) \right] \end{array} \right). \tag{3.14}$$

The only thing that I have not talked about yet is the $\mathbf{K}_{P-wave}$ contribution to the K-matrix. I want to mention again that this is the most important piece that contributes to the A_y observable up to $\mathrm{N^3LO}$. The calculation of $\mathbf{K}_{P-wave}$ can be done in two different ways. First we can calculate directly the one-loop Feynman diagram given in Fig. 3.2, in the box on the third line, first contribution to the rectangle with a “3” in it. The second way, suggested by Jared Vanasse, is to introduce a new set of auxiliary fields, which have quantum numbers corresponding to a dibaryon in which the two nucleons are in a relative P-wave state. This second way is completely equivalent to the direct calculation, but more preferable because it makes the coding easier. I will elaborate on this at the end of section 3.3. Practically all it does is to change the order of some of the steps in the calculation.

In what follows I describe both of the ways of calculating $\mathbf{K}_{P-wave}$. I note that we have done the third order calculation in both ways and gotten the same results for the amplitude.

3.2 First way of computing P-wave contribution: direct calculation

The first way of calculating the P-wave contributions to the nd scattering amplitude is to calculate directly the one-loop Feynman diagram given in Fig. 3.2, in the box on the third line, first contribution to the rectangle with a “3” in it. Then we can do the spin-angular momentum projections and use that in the third order equations. Here I will only show the calculation of this diagram. The results of the spin projections are given in the appendices.

Denoting this diagram by t we have:

$$64t = \int \frac{d^3q}{(2\pi)^3} \frac{1}{\frac{k^2}{4M} - \frac{\gamma^2}{M} - \frac{q^2}{2M} - \frac{(\vec{k}-\vec{q})^2}{2M}} \frac{1}{\frac{k^2}{4M} - \frac{\gamma^2}{M} + \epsilon - \frac{q^2}{2M} - \frac{(\vec{p}-\vec{q})^2}{2M}} \frac{1}{4}(2\vec{k} - \vec{q})_w (2\vec{p} - \vec{q})_x$$

$$\times \quad \Bigg[\sigma_y\sigma_i\sigma_j\sigma_z\Bigg(C_2^{^3P_0}\delta^{xy}\delta^{wz} + C_2^{^3P_1}[\delta^{xw}\delta^{yz} - \delta^{xz}\delta^{yw}] + C_2^{^3P_2}[2\delta^{xw}\delta^{yz} + 2\delta^{xz}\delta^{yw} - \frac{4}{3}\delta^{xy}\delta^{wz}]\Bigg)$$

$$+ \quad \delta^{xw}C_2^{^1P_1}\sigma_i\sigma_j\Bigg], \tag{3.15}$$

where $\epsilon = \frac{k^2-p^2}{2M_N}$.

After some notations and simplifications the integration part of this expression is reduced to three different types of integrals given by the Eqs. (C.1), (C.2) and (C.3) respectively. Introducing more notations given in Eqs. (3.17), (3.18) we get for t Eq. (3.16).

$$64t = Z_{wx}\Bigg[\sigma_y\sigma_i\sigma_j\sigma_z\Bigg(C_2^{^3P_0}\delta^{xy}\delta^{wz} + C_2^{^3P_1}[\delta^{xw}\delta yz - \delta^{xz}\delta^{yw}]$$

$$+ C_2^{^3P_2}[2\delta^{xw}\delta^{yz} + 2\delta^{xz}\delta^{yw} - \frac{4}{3}\delta^{xy}\delta^{wz}]\Bigg) + \delta^{xw}C_2^{^1P_1}\sigma_i\sigma_j\Bigg], \tag{3.16}$$

where,

$$a^2 = \gamma^2, \tag{3.17}$$

$$b^2 = \gamma^2 + \frac{\vec{p}^2}{4} - \frac{\vec{k}^2}{4} - \epsilon M, \tag{3.18}$$

which after simplifications becomes:

$$64t = (C_2^{^3P_1} + 2C_2^{^3P_2})Z^2\sigma_k\sigma_i\sigma_j\sigma_k + (2C_2^{^3P_2} - C_2^{^3P_1})Z_{kl}\sigma_k\sigma_i\sigma_j\sigma_l$$

$$+ (C_2^{^3P_0} - \frac{4}{3}C_2^{^3P_2})Z_{lk}\sigma_k\sigma_i\sigma_j\sigma_l + Z^2C_2^{^1P_1}\sigma_i\sigma_j, \tag{3.19}$$

where $Z^2 = Z_{kk}$ and:

$$Z_{kl} = M^2\Big(\frac{I_{kl}(\vec{k},\vec{p},a^2,b^2)}{4} - k_k\frac{I_l(\vec{k},\vec{p},a,b))}{2} - p_l\frac{I_k(\vec{k},\vec{p},a,b)}{2} + k_kp_lI(\vec{k},\vec{p},a,b)\Big) \tag{3.20}$$

Eqs. (C.1), (C.2) and (C.3) are substituted into the previous equation giving the result:

$$\begin{aligned}
Z_{kl}/M^2 &= \frac{\pi}{3(2\pi)^3}\Lambda\delta_{kl} \\
&- \frac{\pi^2}{16(2\pi)^3}\delta_{kl}\Bigg\{a+b-\frac{4(a^2-b^2)^2}{(a+b)(\vec{k}-\vec{p})^2}+8\frac{\tan^{-1}(\alpha)}{|\vec{k}-\vec{p}|}\frac{(a^2-b^2)^2+(a^2+b^2)\frac{(\vec{k}-\vec{p})^2}{2}+\frac{(\vec{k}-\vec{p})^4}{16}}{(\vec{k}-\vec{p})^2}\Bigg\} \\
&- \frac{\pi^2}{16(2\pi)^3}k_kk_l\Bigg\{\frac{12(a^2-b^2)^2}{(a+b)(\vec{k}-\vec{p})^4}+\frac{13b-11a}{(\vec{k}-\vec{p})^2} \\
&- 8\frac{\tan^{-1}(\alpha)}{|\vec{k}-\vec{p}|}\frac{3(a^2-b^2)^2+(-5a^2+7b^2)\frac{(\vec{k}-\vec{p})^2}{2}+\frac{13(\vec{k}-\vec{p})^4}{16}}{(\vec{k}-\vec{p})^4}\Bigg\} \\
&- \frac{\pi^2}{16(2\pi)^3}p_kp_l\Bigg\{\frac{12(b^2-a^2)^2}{(a+b)(\vec{k}-\vec{p})^4}+\frac{13a-11b}{(\vec{k}-\vec{p})^2} \\
&- 8\frac{\tan^{-1}(\alpha)}{|\vec{k}-\vec{p}|}\frac{3(a^2-b^2)^2+(-5b^2+7a^2)\frac{(\vec{k}-\vec{p})^2}{2}+\frac{13(\vec{k}-\vec{p})^4}{16}}{(\vec{k}-\vec{p})^4}\Bigg\} \\
&+ \frac{\pi^2}{16(2\pi)^3}k_lp_k\Bigg\{\frac{12(a^2-b^2)^2}{(a+b)(\vec{k}-\vec{p})^4}+\frac{a+b}{(\vec{k}-\vec{p})^2}-8\frac{\tan^{-1}(\alpha)}{|\vec{k}-\vec{p}|}\frac{3(a^2-b^2)^2+(a^2+b^2)\frac{(\vec{k}-\vec{p})^2}{2}-\frac{(\vec{k}-\vec{p})^4}{16}}{(\vec{k}-\vec{p})^4}\Bigg\} \\
&+ \frac{\pi^2}{16(2\pi)^3}k_kp_l\Bigg\{\frac{12(a^2-b^2)^2}{(a+b)(\vec{k}-\vec{p})^4}+\frac{a+b}{(\vec{k}-\vec{p})^2}-8\frac{\tan^{-1}(\alpha)}{|\vec{k}-\vec{p}|}\frac{3(a^2-b^2)^2+(a^2+b^2)\frac{(\vec{k}-\vec{p})^2}{2}-\frac{97(\vec{k}-\vec{p})^4}{16}}{(\vec{k}-\vec{p})^4}\Bigg\}.
\end{aligned} \tag{3.21}$$

Defining:

$$Z_{kl} = A\delta_{kl} + Bk_kk_l + Cp_kp_l + Dk_lp_k + Ek_kp_l, \tag{3.22}$$

and this gives:

$$Z^2 = 3A + Bk^2 + Cp^2 + (D+E)\vec{k}\cdot\vec{p}. \tag{3.23}$$

Substituting into the expression for t we get:

$$\begin{aligned}
&64t = (C_2^{^3P_1} + 2C_2^{^3P_2})Z^2\sigma_k\sigma_i\sigma_j\sigma_k + (2C_2^{^3P_2} - C_2^{^3P_1})Z_{kl}\sigma_k\sigma_i\sigma_j\sigma_l \\
+\ & (C_2^{^3P_0} - \frac{4}{3}C_2^{^3P_2})Z_{lk}\sigma_k\sigma_i\sigma_j\sigma_l + Z^2C_2^{^1P_1}\sigma_i\sigma_j \\
=\ & \left\{Z^2(C_2^{^3P_1} + 2C_2^{^3P_2}) + A(C_2^{^3P_0} - C_2^{^3P_1} + \frac{2}{3}C_2^{^3P_2})\right\}\sigma_k\sigma_i\sigma_j\sigma_k \\
+\ & B(C_2^{^3P_0} - C_2^{^3P_1} + \frac{2}{3}C_2^{^3P_2})k_kk_l\sigma_k\sigma_i\sigma_j\sigma_l \\
+\ & C(C_2^{^3P_0} - C_2^{^3P_1} + \frac{2}{3}C_2^{^3P_2})p_kp_l\sigma_k\sigma_i\sigma_j\sigma_l \\
+\ & \left\{D(2C_2^{^3P_2} - C_2^{^3P_1}) + E(C_2^{^3P_0} - \frac{4}{3}C_2^{^3P_2})\right\}k_lp_k\sigma_k\sigma_i\sigma_j\sigma_l \\
+\ & \left\{E(2C_2^{^3P_2} - C_2^{^3P_1}) + D(C_2^{^3P_0} - \frac{4}{3}C_2^{^3P_2})\right\}k_kp_l\sigma_k\sigma_i\sigma_j\sigma_l \\
+\ & Z^2C_2^{^1P_1}\sigma_i\sigma_j.
\end{aligned} \tag{3.24}$$

In this expression the index i is contracted with final deuteron polarization and the index j is contracted with initial deuteron polarization. Appendix A gives the results of spin-angular momentum and isospin projections of all the pieces of this expression.

3.3 Second way of computing P-wave contribution: introducing P-wave auxiliary fields

Before we turn to the introduction of P-wave auxiliary fields let's separate the P-wave contribution to the full third order scattering amplitude from the equation that this amplitude satisfies. To do that consider the integral equation:

$$t(p) = f(p) + g(p) + \int K(p,q)t(q)dq, \tag{3.25}$$

where $K(p,q)$ is the kernel of this equation and $f(p)$ and $g(p)$ are known functions. The sum $f(p)+g(p)$ is the inhomogeneous part of this integral equation.

If we have a solution $t_f(p)$ to an integral equation with the same kernel, but with inhomogeneous part equal to $f(p)$ only, and we have a solution $t_g(p)$ to an integral equation with the same kernel, but with inhomogeneous part equal to $g(p)$ only, then the sum $t_f(p)+t_g(p)$ is a solution for the original equation: indeed summing the two equations:

$$t_f(p) = f(p) + \int K(p,q)t_f(q)dq, \tag{3.26}$$

$$t_g(p) = g(p) + \int K(p,q)t_g(q)dq, \tag{3.27}$$

we see that the function $t(p) = t_f(p)+t_g(p)$ satisfies the original equation. Now returning to our third order equation (Eq. (3.1) with $n=3$), we see that the three-body diagram with the two-body P-wave interactions contributes to only the inhomogeneous part of the equation and not the kernel. So we can take two integral equations with the same kernel but one with inhomogeneous part equal to everything else except the two-body P-wave contributions and another with only the two-body P-wave contributions. Here we only consider the second equation, the solution to which we call the "3_P amplitude": $\mathbf{t}^J_{3_{\rm P};L'S',LS}(k,p,E)$.

Let's take a look at the 2-body P-wave interaction Lagrangian again:

$$\mathcal{L}_2^{^3P_J} = \left(C_2^{(^3P_0)}\delta_{xy}\delta_{wz} + C_2^{(^3P_1)}[\delta_{xw}\delta_{yz}-\delta_{xz}\delta_{yw}] + C_2^{(^3P_2)}\left[2\delta_{xw}\delta_{yz}+2\delta_{xz}\delta_{yw}-\frac{4}{3}\delta_{xy}\delta_{wz}\right]\right) \tag{3.28}$$

$$\times\,\frac{1}{4}(\hat{N}^T\mathcal{O}^{(1,P)}_{xyA}\hat{N})^\dagger(\hat{N}^T\mathcal{O}^{(1,P)}_{wzA}\hat{N})$$

where

$$\mathcal{O}^{(1,P)}_{ijA} = \overleftarrow{\nabla}_i\, P^P_{jA} - P^P_{jA}\,\overrightarrow{\nabla}_i \tag{3.29}$$

and the projector is defined as $P^P_{iA} = \frac{1}{\sqrt{8}}\sigma_2\sigma_i\tau_2\tau_A$.

$$\mathcal{L}_2^{^1P_1} = C_2^{(^1P_1)}\frac{1}{4}(\hat{N}^T\mathcal{O}^{(0,P)}_{x}\hat{N})^\dagger(\hat{N}^T\mathcal{O}^{(0,P)}_{x}\hat{N}), \tag{3.30}$$

The operator $\mathcal{O}_i^{(0,P)}$ is defined by

$$\mathcal{O}_i^{(0,P)} = \overleftarrow{\nabla}_i \; P^P - P^P \; \overrightarrow{\nabla}_i, \tag{3.31}$$

where the projector is $P^P = \frac{1}{\sqrt{8}}\sigma_2\tau_2$.

We can introduce a new set of auxiliary fields $\left(\hat{\mathcal{P}}_{kA}^{^3\mathrm{P}_J}\right)$ through a new interaction Lagrangian given by:

$$\begin{aligned}\mathcal{L}_2^P = & -\hat{\mathcal{P}}_{0A}^{^3\mathrm{P}_0\dagger}\Delta^{(^3\mathrm{P}_0)}\hat{\mathcal{P}}_{0A}^{^3\mathrm{P}_0} - \hat{\mathcal{P}}_{iA}^{^3\mathrm{P}_1\dagger}\Delta^{(^3\mathrm{P}_1)}\hat{\mathcal{P}}_{iA}^{^3\mathrm{P}_1} - \hat{\mathcal{P}}_{iA}^{^3\mathrm{P}_2\dagger}\Delta^{(^3\mathrm{P}_2)}\hat{\mathcal{P}}_{iA}^{^3\mathrm{P}_2} - \hat{\mathcal{P}}_{i}^{^1\mathrm{P}_1\dagger}\Delta^{(^1\mathrm{P}_1)}\hat{\mathcal{P}}_{i}^{^1\mathrm{P}_1} \\ & + \frac{1}{2}\sum_{J=0}^{2} y^{^3\mathrm{P}_J}\left[C_{1,1,J}^{i,j,k}\left(\hat{\mathcal{P}}_{kA}^{^3\mathrm{P}_J}\right)^\dagger \hat{N}^T i\mathcal{O}_{jiA}^{(1,P)}\hat{N} + \mathrm{H.c.}\right] \\ & + \frac{1}{2}y^{^1\mathrm{P}_1}\left[\left(\hat{\mathcal{P}}_{i}^{^1\mathrm{P}_1}\right)^\dagger \hat{N}^T i\mathcal{O}_{i}^{(0,P)}\hat{N} + \mathrm{H.c.}\right],\end{aligned} \tag{3.32}$$

so that if we integrate out the $\left(\hat{\mathcal{P}}_{kA}^{^3\mathrm{P}_J}\right)$ fields we will recover the original form of the P-wave interaction Lagrangian Eq. (3.28) and Eq. (3.30). In Eq. (3.32) all of the $\Delta^{(^3\mathrm{P}_J)}$ coefficients are unphysical constants that are just chosen so that this Lagrangian matches onto the original P-wave interaction Lagrangian Eq. (3.28) and Eq. (3.30). The indices i, j, k are spherical indices, they take values $-1, 0, 1$.

To see the matching between the two Lagrangians at the two-body sector we can calculate the two-body elastic scattering with the new Lagrangian. The tree diagram that contributes to this scattering is given by the Fig. 3.6.

Given two vectors $\vec{v}$ and $\vec{w}$ the dot product in terms of space indices is given by $\sum_i v_i w_i$, but when these vectors are given in terms of spherical indices the same dot product is given by $\sum_i (-1)^i v_i w_{-i}$. Using this the diagram in Fig. 3.6 can be calculated to give (here I only do the matching for the $^3\mathrm{P}_J$ channel, the $^1\mathrm{P}_1$ is analogous and easier):

$$it = \frac{(y^{^3\mathrm{P}_J})^2}{4\Delta^{^3\mathrm{P}_J}} \sum_{i,j.m.l.k;A} (-1)^k C_{1,1,J}^{i,j,k} C_{1,1,J}^{m,l,-k} (i\mathcal{O}_{jiA}^{(1,P)})(i\mathcal{O}_{lmA}^{(1,P)})^\dagger \tag{3.33}$$

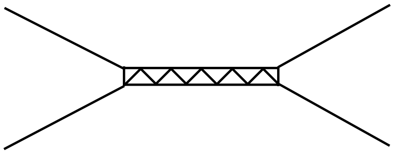

FIGURE 3.6: Two-body P-wave elastic scattering. The $\hat{\mathcal{P}}_{kA}^{^3\mathrm{P}_J}$ field propagator is the double line with a zig-zag in it and is given by the constant $\frac{i}{\Delta^{^3\mathrm{P}_J}}$.

In this expression the operators $\mathcal{O}$ are supposed to be calculated between nucleon spin states, but that part matches automatically, so I just skip it. It can be shown that going between spherical coordinates and cartesian coordinates the following substitutions can be made:

$$C_{1,1,0}^{i,j,0} C_{1,1,0}^{m,l,0} \rightarrow \frac{1}{3}\delta_{ij}\delta_{ml}, \tag{3.34}$$

$$\sum_k C_{1,1,1}^{i,j,k} C_{1,1,1}^{m,l,-k}(-1)^k \rightarrow \frac{1}{2}(\delta_{il}\delta_{jm} - \delta_{im}\delta_{jl}), \tag{3.35}$$

$$\sum_k C_{1,1,2}^{i,j,k} C_{1,1,2}^{m,l,-k}(-1)^k \rightarrow \frac{1}{2}(\delta_{il}\delta_{jm} + \delta_{im}\delta_{jl} - \frac{2}{3}\delta_{ij}\delta_{ml}) \tag{3.36}$$

In here the coordinates on the left hand side are spherical and the ones on the right hand side are cartesian. Using these relations it becomes clear how Eq. (3.33) matches onto the $^3\mathrm{P}_J$ interaction terms in the original Lagrangian Eq. (3.28) giving the following relations between the different parameters in the two Lagrangians:

$$C^{^3P_0} = \frac{1}{3}\frac{(y^{^3P_0})^2}{\Delta^{(^3P_0)}}, \quad C^{^3P_1} = -\frac{1}{2}\frac{(y^{^3P_1})^2}{\Delta^{(^3P_1)}}, \quad C^{^3P_2} = \frac{1}{4}\frac{(y^{^3P_2})^2}{\Delta^{(^3P_2)}}, \quad C^{^1P_1} = \frac{(y^{^1P_1})^2}{\Delta^{(^1P_1)}}. \tag{3.37}$$

At this point we can describe the second way of calculating the 3_P amplitude. Instead of calculating the one loop diagram as in the previous section we can just calculate the tree diagram given in the Fig 3.7 and do the spin-angular momentum projections for this diagram

(In the figure I only give the diagram with the initial dibaryon being the deuteron, but the second diagram with initial dibaryon being the spin-singlet also has to be calculated).

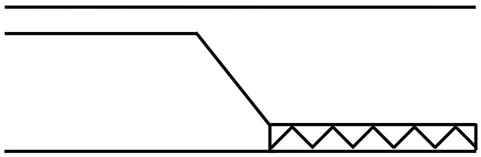

FIGURE 3.7: Tree-level contribution to $nd \rightarrow nP$-wave dibaryon.

After this we can construct the P-wave amplitude as in the boxed area in Fig 3.8, which attached to the same diagram will give the inhomogeneous part of the equation that the 3_P amplitude satisfies (the first terms of the right hand side of the first two lines of Fig 3.8).

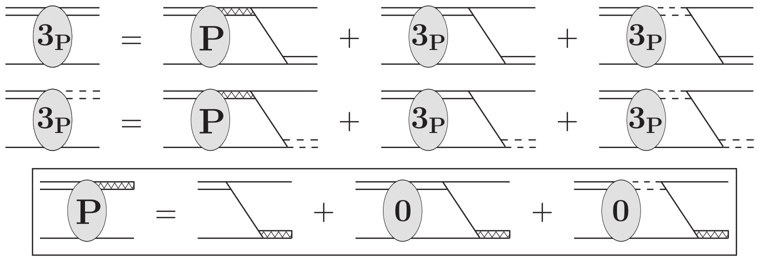

FIGURE 3.8: (Caption and figures are from [76]). Unboxed diagrams are the integral equations for the N^{3}LO contribution to the nd scattering amplitude from the two-body P-wave contact interactions. The double lines with a zig-zag in the middle are the P-wave dibaryon propagator, given by $i/\Delta^{^{2R+1}\mathrm{P}_J}$. The boxed diagrams represent the equation for the “P” amplitude used in the unboxed integral equations above. The notation “3$_\mathrm{P}$” in the oval indicates that this is a N^{3}LO correction but one that only involves the two-body P-wave contributions.

Explicitly the P-wave amplitude, which is the boxed area in Fig 3.8 is given by:

$$t^{J(^{2R+1}P_z)}_{L'S',LS}(k,p,E) = \left[\mathbf{K}^{J(^{2R+1}P_z)}_{L'S',LS}(k,p,E)\right]_1 + \mathbf{K}^{J(^{2R+1}P_z)}_{L'S',LS}(q,p,E)\otimes \mathbf{t}^{J}_{0;LS,LS}(k,q,E), \tag{3.38}$$

where the K-matrices are determined by the diagram in Fig 3.7 and are given by:

$$\left[\mathbf{K}^{J(^{3}P_z)}_{L'S',LS}(k,p,E)\right]_x = -\frac{M_N\, y\, y^{^3\mathrm{P}_z}}{4kp}\mathcal{Z}^{^3\mathrm{P}_z}\left(J,L',S',L,S,x,z\right)\left(2k\, Q_{L'}(a) + p\, Q_L(a)\right) \tag{3.39}$$

$$\left[\mathbf{K}^{J(^1P_1)}_{L'S',LS}(k,p,E)\right]_x = -\frac{M_N\, y\, y^{^1\mathrm{P}_1}}{4kp}\mathscr{Z}^{^1\mathrm{P}_1}\left(J,L',S',L,S,x\right)\left(2k\,Q_{L'}(a)+p\,Q_L(a)\right) \tag{3.40}$$

and the Z-functions are the spin-angular momentum projections of the diagram in Fig 3.7, given by:

$$\begin{aligned}\mathscr{Z}^{^3\mathrm{P}_z}\left(J,L',S',L,S,x,z\right) &= 12(-1)^{3/2+S+S'+L-J}\sqrt{\widehat{x}\widehat{(1-x)}\widehat{z}\widehat{S}\widehat{S}'\widehat{L}}\begin{Bmatrix} x & 1/2 & 1/2 \\ 1 & S & 1/2 \end{Bmatrix} \\ &\times\begin{Bmatrix} 1/2 & 1 & S \\ 1 & S' & z \end{Bmatrix}\begin{Bmatrix} S & 1 & S' \\ L' & J & L \end{Bmatrix}\begin{Bmatrix} 1-x & 1/2 & 1/2 \\ 1 & 1/2 & 1/2 \end{Bmatrix} C^{0,0,0}_{L,1,L'},\end{aligned} \tag{3.41}$$

and

$$\mathscr{Z}^{^1\mathrm{P}_1}\left(J,L',S',L,S,x\right) = (-1)^{3/2+L-J}\sqrt{\widehat{x}\widehat{(1-x)}\widehat{S}'\widehat{L}}\begin{Bmatrix} S & 1 & S' \\ L' & J & L \end{Bmatrix}\delta_{S,1/2}C^{0,0,0}_{L,1,L'}. \tag{3.42}$$

In terms of all of these newly defined objects the equation that the 3_P amplitude satisfies is:

$$\begin{aligned}\mathbf{t}^J_{3\mathrm{P};L'S',LS}(k,p,E) &= \\ &\sum_{R=0}^{1}\sum_{z=|R-1|}^{R+1}\sum_{L'',S''}\frac{(-1)^z}{\Delta^{(^{2R+1}P_z)}}\left[\mathbf{K}^{J(^{2R+1}P_z)}_{L''S'',L'S'}(p,q,E)\right]^T\otimes t^{J(^{2R+1}P_z)}_{L''S'',LS}(k,q,E) \\ &+\mathbf{K}^J_{0;L'S',L'S'}(q,p,E)\otimes\mathbf{t}^J_{3\mathrm{P};L'S',LS}(k,q,E).\end{aligned} \tag{3.43}$$

From how the new Lagrangian with auxiliary P fields matches onto the original Lagrangian the equivalence of the two methods, described in the previous sections, for calculating the P-wave contributions to the three-body scattering amplitude becomes obvious. The only essential difference is that in the method of direct calculation we do the loop-integration analytically first, then we do the spin-angular momentum projections, but in the second method the order is changed. In the second method we do the spin-angular momentum projections first, then the loop-integration, but the loop-integration is done numerically. The second method proves to be preferable because in calculating the angular momentum projections we only see functions like the Legendre polynomials of the second kind, the analytical properties of which are well understood and which are already coded, because the same functions arise in the angular momentum projections of the lower order equations. As opposed to this, in the method of direct calculation, the loop-integration is done analytically, but in the angular momentum projections we get much more complicated functions then the Legendre polynomials of the second kind. With these new functions new numerical issues arise associated with the analytical behavior of these functions near the collinear limit where the vectors $\vec{k}$ and $\vec{p}$ become parallel.

3.4 Power Counting

The power of an EFT is that when we calculate an observable using it, we are also able to make a prediction on the accuracy of the calculation. To construct an EFT in the first place we need to identify the relevant scales of the theory. Having done that we can form a small parameter in powers of which we can organize the infinite number of interaction terms in the Lagrangian. Also all the observables are calculated order by order, as a power series expansion in powers of this small parameter. The EFT$_{\not\pi}$ is constructed to describe non-relativistic nucleons which interact through contact interactions, so pions are integrated out. From here we see that the small energy scale in this theory is the typical momentum exchange in Feynman diagrams denoted by Q, and the large energy scales are the EFT$_{\not\pi}$ breaking scale $\Lambda_{\not\pi}$, which is of the order of the pion mass $\Lambda_{\not\pi} \sim m_\pi$ and the nucleon mass M_N. The binding momentum of the deuteron $\gamma_t = 45.7025$ MeV is much smaller than the pion mass $m_\pi \approx 140$ MeV, so it is also considered to be a small energy scale $\sim Q$. All of the interactions in the Lagrangian and the observables are ordered in the powers of Q. For instance the more derivatives in an interaction term the higher order that term is in the Lagrangian. The scaling of an interaction in EFT$_{\not\pi}$ is not always easy to figure out, and it can depend on the regularization scheme used to render the loop-integrals finite [11, 12]. Here I will talk about the scaling of some of the interactions and diagrams. Let's start with the only-nucleon-fields formulation of EFT$_{\not\pi}$ at the LO two-body sector:

$$\mathcal{L} = N^\dagger \left(i\partial_0 + \frac{\vec{\nabla}^2}{2M_N} \right) N - C_0 (N^T P N)^\dagger (N^T P N). \tag{3.44}$$

From this Lagrangian we see that in loops with nucleon propagators, if we denote the loop four momentum by $(l^0, \vec{l})$, the l^0 integration picks up a pole at a nucleon energy, so we have that l^0 integration scales like $\frac{Q^2}{M_N}$ and each component of the $\vec{l}$ integration scales like Q. Also the non-relativistic nucleon propagator scales like $\frac{M_N}{Q^2}$. Using naive dimensional analysis (NDA) the scaling of the interaction coefficient C_0 in Eq. (3.44) can be estimated to be $C_0 \sim \frac{1}{M_N \Lambda_{\not\pi}}$. As it was shown in Section 2.1 with this Lagrangian we can calculate the sum of all the diagrams contributing to the NN scattering amplitude given in Fig. 3.9.

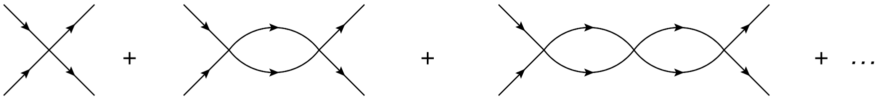

FIGURE 3.9: NN scattering: bubble sum.

Using the scalings described above and the NDA estimate for C_0, we can see that each subsequent term in the series given in Fig. 3.9 is suppressed by a factor of $\frac{Q}{\Lambda_{\not\pi}}$. This makes each subsequent term in this series to be of higher order in EFT$_{\not\pi}$ power counting. If this was the correct scaling of the terms then, to do a calculation to a given order we would have to truncate the series. This would have been a valid conclusion if the NN scattering length was of the natural or "naive" size $a \sim \frac{1}{\Lambda}$. But as we know this is not the case, in fact the scattering length is unnaturally large $a = \frac{1}{\gamma_t} \sim \frac{1}{Q}$. Hence we need to find the deuteron pole at the leading order in EFT$_{\not\pi}$. In order to generate the deuteron bound state at LO, the appropriate power counting needs to find that all the terms in the series in Fig. 3.9 contribute at the same leading order. This is impossible to achieve using NDA to estimate the size of C_0. To make the power counting correct PDS was invented [65]. In PDS regularization scheme for the calculation of the loop integrals in Fig. 3.9 the momentum cutoff Λ is replaced by an unphysical arbitrary parameter μ and since it is arbitrary we can choose it to be of the order Q. With this choice for μ, matching the calculated NN scattering amplitude to the ERE result gives a different scaling for the interaction coefficient $C_0 \sim \frac{1}{M_N Q}$. Motivated by the need of getting the shallow deuteron pole at the LO the auxiliary field t was introduced into the Lagrangian:

$$\begin{aligned} \mathcal{L} &= N^\dagger(i\partial_0 + \frac{\vec{\partial}^2}{2M_N})N \\ &+ \ t_i^\dagger\,(\Delta_t)\,t_i \\ &+ \ y_t(t_i^\dagger(N^T P_i N) + h.c.). \end{aligned} \tag{3.45}$$

It was shown in [11] by integrating out the auxiliary field t that this Lagrangian is physically equivalent to the one given in Eq. (3.44). The field t is constructed such that it has the quantum numbers of a deuteron. From this Lagrangian we can find the following list for the scaling of different things.

$\gamma_t \sim Q$
dressed deuteron propagator $\sim \frac{1}{Q}$ (this is proven below)
the non-relativistic nucleon propagator $\sim \frac{M_N}{Q^2}$
as a convention we use $y_t^2 \sim \frac{1}{M_N}$
non-relativistic loop integration $\sim \frac{Q^5}{M_N}$

From the Lagrangian in Eq. (3.45) the dressed deuteron propagator can be calculated as a geometric series given in Fig. 3.10.

Here again to regulate the loop integrals in Fig. 3.10 PDS is used and the scaling of the parameter Δ_t is $\Delta_t \sim Q$. Using the list given above we can power count all the terms in

FIGURE 3.10: Double line is the LO full deuteron propagator, thin solid line is the nucleon propagator, thick solid line is the bare deuteron propagator $\frac{i}{\Delta_t}$.

the series in Fig. 3.10. The first term scales as $\sim \frac{1}{Q}$. The second term-y_t^2∗(bare deuteron propagator)^2∗(nucleon propagator)^2∗ loop integration $=\sim \frac{1}{M_N}\frac{1}{Q^2}\frac{M_N^2}{Q^4}\frac{Q^5}{M_N} = \frac{1}{Q}$. From here it becomes clear that all the terms in this series contribute at the LO and scale as $\sim \frac{1}{Q}$ (which was the purpose of PDS) justifying the need to sum all the terms. Looking at the dressed deuteron propagator,

$$iD_t^{LO}(p_0, \vec{p}) = \frac{i}{\gamma_t - \sqrt{\frac{\vec{p}^2}{4} - M_N p_0 - i\epsilon}}, \tag{3.46}$$

we see that it also scales as $\sim \frac{1}{Q}$. This is the advantage of using PDS instead of cutoff with NDA. With PDS all the terms contributing to the dressed deuteron are of the same order (LO) as the final result.

Using dimensional analysis, from the requirement that the action is dimensionless and from the nucleon kinetic term in Eq. (3.45) we see that the mass dimension of a nucleon field is $[N] = M^{\frac{3}{2}}$ (here I use the notation that the square brackets denote the mass dimension). From the convention we use for the dNN coupling constant: $y_t^2 = \frac{4\pi}{M_N}$ and from the third term in Eq. (3.45) we see that the mass dimension of a dibaryon field is the same as for the nucleon field $[t] = M^{\frac{3}{2}}$. From this and the second term in Eq. (3.45) we find the mass dimension of Δ_t to be $[\Delta_t] = M$.

From the SD-mixing Lagrangian:

$$\mathcal{L}_2^{SD} = y_{SD}\hat{t}_i^\dagger \left[\hat{N}^T\left((\overrightarrow{\partial}-\overleftarrow{\partial})^i(\overrightarrow{\partial}-\overleftarrow{\partial})^j - \frac{1}{3}\delta^{ij}(\overrightarrow{\partial}-\overleftarrow{\partial})^2\right)P_j\hat{N}\right] + \text{H.c.}, \tag{3.47}$$

and the dimensions of the nucleon and deuteron fields we find the dimension and the scaling of the SD-mixing interaction coefficient $y_{SD} \sim \frac{1}{M_N^{\frac{5}{2}}}$. The same way from the two-body P-wave interaction Lagrangian:

$$\begin{aligned}\mathcal{L}_2^{{}^3P_J} = &\left(C_2^{({}^3P_0)}\delta_{xy}\delta_{wz} + C_2^{({}^3P_1)}[\delta_{xw}\delta_{yz} - \delta_{xz}\delta_{yw}] + C_2^{({}^3P_2)}\left[2\delta_{xw}\delta_{yz} + 2\delta_{xz}\delta_{yw} - \frac{4}{3}\delta_{xy}\delta_{wz}\right]\right) \\ &\times\frac{1}{4}(\hat{N}^T\mathcal{O}^{(1,P)}_{xyA}\hat{N})^\dagger(\hat{N}^T\mathcal{O}^{(1,P)}_{wzA}\hat{N})\end{aligned} \tag{3.48}$$

we can find the dimensions of the interaction coefficients $C_2^{({}^3P_J)}$. Each of the operators $\mathcal{O}$ in Eq. (3.48) has one derivative, which has mass dimension one. With this and the dimension of the nucleon fields we find for the dimension of the interaction coefficients $C_2^{({}^3P_J)} \sim \frac{1}{M_N^4}$.

As we just showed NDA fails to give the correct scaling of the interaction coefficient C_0. In general NDA can not be trusted to give to correct scaling of operators in the Lagrangian or to give the correct scaling of the interaction coefficients. In order to find the correct scaling one needs to understand the renormalization conditions and use RG analysis.

We can also use the Z-parametrization to compute the dressed deuteron propagator as described in section 2.2. The deuteron propagator in the Z-parametrization [12] up to N^{2}LO is given by:

$$\begin{aligned}iD_t(p_0,\vec{p}) = &\frac{i}{\gamma_t - \sqrt{\frac{\vec{p}^2}{4} - M_Np_0 - i\epsilon}} \\ \times &\left[1 + \frac{Z_t-1}{2\gamma_t}\left(\gamma_t + \sqrt{\frac{\vec{p}^2}{4} - M_Np_0 - i\epsilon}\right) + \left(\frac{Z_t-1}{2\gamma_t}\right)^2\left(-\gamma_t^2 + \frac{\vec{p}^2}{4} - M_Np_0\right)\right]\end{aligned} \tag{3.49}$$

In the Z-parametrization, since $\frac{Z_t-1}{2}$ is about 0.3, $Z_t - 1$ is also considered to be of order Q. Using that we see that each subsequent term is one order higher in powers of Q. So we conclude that the circle with an "n" in it on the dibaryon line (the R-functions) scales like Q^n.

To see how things scale at the three-body sector let's look at the diagrams contributing to the nd scattering amplitude at the leading order Fig 3.11.

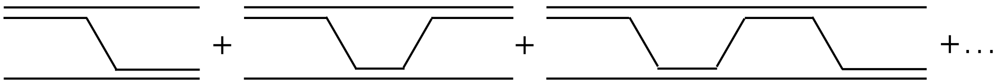

FIGURE 3.11: Pinball diagrams for LO nd scattering.

The first diagram is just a tree and using our rules we get that it scales like $\sim \frac{1}{Q^2}$. In the second diagram we have one loop and three more propagators, it scales like $\sim (y_t)^4 \frac{M_N^3}{Q^6} \frac{1}{Q} \frac{Q^5}{M_N} = \frac{1}{Q^2}$. Again we see that all the diagrams in the expansion are going to contribute to the same order, again justifying the need to sum all of them at the LO. From here naively we would assume that the LO nd scattering amplitude scales like $\sim \frac{1}{Q^2}$.

Let's also look at the three-body contributions which previously were defined as the rectangles with an "n" in them, except without all of the three-body forces as in the Fig 3.12.

Here we have already figured out that the rectangle with the number "0" scales like $\sim \frac{1}{Q^2}$.

The rectangle with "1" is zero, so we can think of it as scaling like $\sim \frac{1}{Q}$.

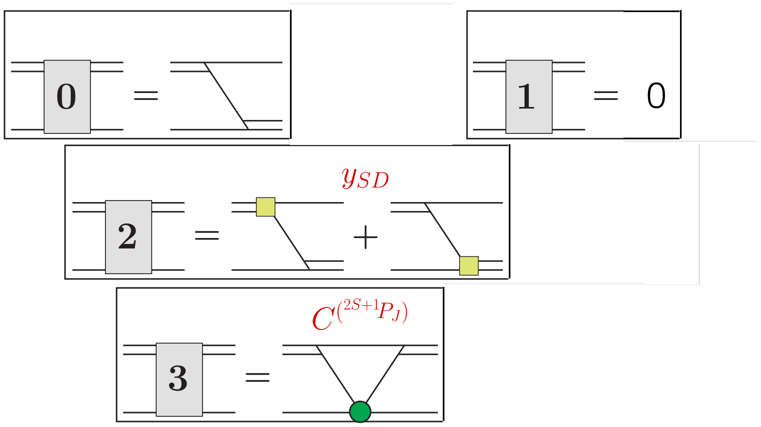

FIGURE 3.12: Three-body diagrams without three-body forces.

The rectangle with "2" has the SD mixing interaction, which has two derivatives, so it scales like $\sim y_{SD}Q^2 y_t \frac{M_N}{Q^2}$, and as $(y_{SD}y_t)$ scales as $\sim \frac{1}{M_N^3}$, we get that this rectangle scales as $\sim \frac{1}{M_N^2} \sim \frac{1}{Q^2}\frac{Q^2}{M_N^2}$.

The rectangle with "3" has the P-wave interactions, which have two derivatives, so it scales like $\sim (y_t)^2 C^{^3P_J} Q^2 \frac{M_N^3}{Q^6}\frac{Q^5}{M_N}$, and the coefficient $C^{^3P_J}$ scales like $\frac{1}{M_N^4}$, giving for the rectangle scaling $\sim \frac{Q}{M_N^3} \sim \frac{1}{Q^2}\frac{Q^3}{M_N^3}$.

Generalizing the previous results we conclude that the rectangle with an "n" in it by construction scales like $\sim Q^{n-2}$ in powers of Q.

At this point we are ready to power count all the terms appearing on the right hand side of the n-th order equations given in the Fig 3.1. As I already mentioned above with the naive approach to how things scale we conclude that the LO nd scattering amplitude scales like each of the terms contributing to it, which is $\frac{1}{Q^2}$. Here I prove that with the same naive approach we will come to the conclusion that the N^{n}LO nd scattering amplitude (the oval with an "n" in it, Fig 3.1) scales like each of the terms contributing to it: $\sim Q^{n-2}$. To prove this we can induce on n; assuming that everything works at up to and including N^{n-1}LO we can look at the two general types of diagrams contributing to the n-th order amplitude

Fig 3.13.

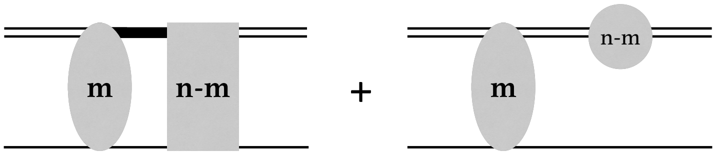

FIGURE 3.13: General terms in n-th order equation.

Using our rules for power counting we see that the first term scales like: $\sim$ m-th order amplitude $*$ $(n-m)$-th order rectangle $*$ dibaryon propagator $*$ nucleon propagator $*$ loop integration $= Q^{m-2}Q^{n-m-2}\frac{1}{Q}\frac{M_N}{Q^2}\frac{Q^5}{M_N} = Q^{n-2}$. And the second term: $\sim Q^{m-2}Q^{n-m} = Q^{n-2}$. Now assuming that this amplitude also scales as all the terms contributing to it we find that it scales like $\sim Q^{n-2}$, which is the naive conclusion.

In reality though things are not so simple. At each order we have infinite number of diagrams contributing to the amplitude. Although each one of these contributions scales the same, there is no guarantee that the total amplitude will scale the same. One of the most important examples when this analysis fails is the LO doublet channel S-wave amplitude. According to the analysis this amplitude should be well-behaved and scale like $\frac{1}{Q^2}$, but as it is shown it has strong cutoff dependence. To regulate this cutoff dependence we are forced to include a three-body contact interaction at LO, which is naturally expected to be included at N^{2}LO [15, 16, 17, 70]. To see this let's look at the interaction Lagrangian for the three-body force again:

$$\mathcal{L} = \frac{M_N H_0(\Lambda)}{3\Lambda^2}\left(y_t N^\dagger(\vec{t}\cdot\vec{\sigma})^\dagger - y_s N^\dagger(\vec{s}\cdot\vec{\tau})^\dagger\right)\left(y_t N(\vec{t}\cdot\vec{\sigma}) - y_s N(\vec{s}\cdot\vec{\tau})\right). \tag{3.50}$$

We can easily find the scaling of the contribution of this term to the three-body scattering amplitude. This contribution is just a tree diagram and it scales as $\sim \frac{1}{\Lambda^2} = \frac{1}{Q^2}\frac{Q^2}{\Lambda^2}$ (here Λ is the momentum cutoff in three-body loop diagrams). From the analysis of the terms in Fig 3.11 we know that the LO contribution to the three-body scattering amplitude scales as $\frac{1}{Q^2}$. From here we find that using NDA we would conclude that the three-body force contribution comes at N^{2}LO, which is the wrong conclusion as we found in Section 2.7.

4

Results and conclusions

4.1 Observables

In nd scattering there are several observables related to initial beam and target polarizations. Let's take for example initial polarized neutron beam and unpolarized deuteron target. We need to define a coordinate system to describe the observables. We define two coordinate systems (see Fig. 4.1) in the laboratory reference frame; one attached to the initial neutron (x, y, z) and the other attached to final (scattered) neutron (x', y', z'). In the laboratory frame denote the initial neutron momentum as $\vec{k}_i$ and the final neutron momentum as $\vec{k}_f$. The z axis is defined along $\vec{k}_i$, the y axis is defined along the cross product $\vec{k}_i \times \vec{k}_f$ and the x axis is defined so that (x, y, z) is right handed. The same way z' axis is defined along $\vec{k}_f$, the y' axis is defined along the cross product $\vec{k}_i \times \vec{k}_f$ and the x' axis is defined so that (x', y', z') is right handed.

We can denote the spinor that describes the initial nucleon by χ_i and the final nucleon by χ_f. The transition matrices M are related to the amplitudes that we calculate solving the integral equations numerically. These matrices depend on the incoming energy, the scattering angle θ, also they have indices corresponding to the initial and the final deuteron

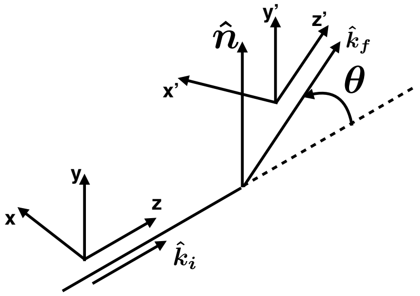

FIGURE 4.1: Coordinate systems.

spin components and the initial and final neutron spin components. As, for now we are only considering unpolarized deuteron target the indices that correspond to the deuterons are going to be summed over, so for now we suppress those indices to make the notations more concise. The transition matrix for this process is $M_{m_i m_f}$, where m_i and m_f are the initial and final neutron spin components. This matrix connects the initial and final neutron spinors so we have:

$$\chi_f = M\chi_i. \tag{4.1}$$

If we have a beam of N neutrons in the initial state then the density matrix that describes it can be written as:

$$\rho_i = \sum_{n=1}^{N} \chi_i^{(n)} \left[\chi_i^{(n)}\right]^{\dagger}, \tag{4.2}$$

and the same way for the final state we have:

$$\rho_f = \sum_{n=1}^{N} \chi_f^{(n)} \left[\chi_f^{(n)}\right]^{\dagger}, \tag{4.3}$$

where the superscript (n) denotes the particle number. Putting the Eqs. (4.1), (4.2), (4.3) together it is easy to see:

$$\rho_f = M\rho_i M^{\dagger}. \tag{4.4}$$

Denoting the components of a spinor:

$$\chi^{(n)} = \begin{pmatrix} a_1^{(n)} \\ a_2^{(n)} \end{pmatrix} \tag{4.5}$$

and using the definition for the density matrix we find:

$$\rho = \begin{pmatrix} \sum\limits_{n=1}^{N} |a_1^{(n)}|^2 & \sum\limits_{n=1}^{N} a_1^{(n)} a_2^{(n)*} \\ \sum\limits_{n=1}^{N} a_2^{(n)} a_1^{(n)*} & \sum\limits_{n=1}^{N} |a_2^{(n)}|^2 \end{pmatrix}. \tag{4.6}$$

The total averaged spin polarization components of the beam can be calculated using the Pauli matrices and the density matrix Eq. (4.6) finding the expressions in Eq. (4.7).

$$\begin{aligned} p_x &= \mathrm{Tr}(\rho\sigma_x) = \sum_{n=1}^{N} 2\,\mathrm{Re}(a_1^{(n)} a_2^{(n)*}), \\ p_y &= \mathrm{Tr}(\rho\sigma_y) = \sum_{n=1}^{N} 2\,\mathrm{Im}(a_1^{(n)} a_2^{(n)*}), \\ p_z &= \mathrm{Tr}(\rho\sigma_z) = \sum_{n=1}^{N} (|a_1^{(n)}|^2 - |a_2^{(n)}|^2). \end{aligned} \tag{4.7}$$

These spin polarization components components correspond to the initial beam as a whole. To find the average spin polarization per particle we need to divide the three lines of the Eq. (4.7) by N. From Eq. (4.7) we see that if the initial beam is not polarized then from the requirements $p_x = p_y = p_z = 0$ we find that the density matrix describing that beam will be proportional to the 2×2 identity matrix I, Eq. (4.8).

$$\rho_i = \frac{N}{2} I = \frac{N}{2} \begin{pmatrix} 1 & 0 \\ 0 & 1 \end{pmatrix}. \tag{4.8}$$

Here we assumed that the spinors $\chi_i^{(n)}$ are normalized to one: $|a_1^{(n)}|^2 + |a_2^{(n)}|^2 = 1$.

As the density matrix is a hermitian operator and as the identity matrix together with the Pauli matrices span the space of the 2×2 hermitian matrices, we can express the density matrix in terms of the identity matrix and the Pauli matrices. Denoting the 2×2 identity matrix as σ_0 we have Eq. (4.9).

$$\rho = \sum_{j=0}^{3} a_j \sigma_j \tag{4.9}$$

To find the coefficients a_j in Eq. (4.9) note that the matrices σ_j with $j = 0, 1, 2, 3$, satisfy an orthogonality relation with a scalar product defined as the trace of the product (see Eq. (4.10)).

$$\mathrm{Tr}(\sigma_i \sigma_j) = 2\delta_{ij}. \tag{4.10}$$

From Eq. (4.9) and Eq. (4.10) we find:

$$a_j = \frac{1}{2}\,\mathrm{Tr}(\rho\sigma_j) = \frac{1}{2}p_j,\ \ j = 1, 2, 3 \tag{4.11}$$

where p_j is defined for $j = 1, 2, 3$ in Eq. (4.7) and for $j = 0$ we have:

$$a_0 = \frac{1}{2}\,\mathrm{Tr}(\rho\sigma_0) = \frac{1}{2}\,\mathrm{Tr}(\rho) = \frac{N}{2}. \tag{4.12}$$

For the density matrix we find:

$$\rho = \frac{1}{2}(N\sigma_0 + \sum_{j=1}^{3} p_j \sigma_j). \tag{4.13}$$

Again we see that if the beam is not polarized we recover Eq. (4.8) for the density matrix.

In terms of the density matrices the total cross section of the scattering of a polarized beam on an unpolarized target is given by (noting that $\mathrm{Tr}(\rho_i) = N$):

$$\frac{d\sigma}{d\Omega}(\theta, \phi) = \frac{\mathrm{Tr}(\rho_f)}{\mathrm{Tr}(\rho_i)} = \frac{\mathrm{Tr}\big(M\rho_i M^\dagger\big)}{N}, \tag{4.14}$$

and for the completely unpolarized scattering, for which the initial beam is non-polarized and hence ρ_i is given by Eq. (4.8), the cross section Eq. (4.14) reduces to:

$$\frac{d\bar{\sigma}}{d\Omega}(\theta) = \frac{\mathrm{Tr}(\rho_f)}{\mathrm{Tr}(\rho_i)} = \frac{1}{2}\,\mathrm{Tr}\big(MM^\dagger\big), \tag{4.15}$$

where the bar over the σ indicates that this is the unpolarized cross section. Using the expansion Eq. (4.13) for the initial density matrix the polarized cross section Eq. (4.14) can be put into the following form:

$$\frac{d\sigma}{d\Omega}(\theta,\phi) = \frac{d\bar{\sigma}}{d\Omega}(\theta)(1 + \sum_{j=1}^{3} \frac{p_j}{N} A_j(\theta)), \tag{4.16}$$

where the $A_j(\theta)$ are the analyzing powers and are given by:

$$A_j(\theta) = \frac{\mathrm{Tr}\big(M\sigma_j M^\dagger\big)}{\mathrm{Tr}(MM^\dagger)}. \tag{4.17}$$

If we have an initial beam that is polarized along the y axis, then in Eq. (4.16) we only have the term proportional to p_y:

$$\frac{d\sigma}{d\Omega}(\theta,\phi) = \frac{d\bar{\sigma}}{d\Omega}(\theta)(1 + \frac{p_y}{N} A_y(\theta)), \tag{4.18}$$

where the fraction $\frac{p_y}{N}$ is the average polarization per particle. The function $A_y(\theta)$ is the A_y observable that is called the transverse asymmetry. To give it the interpretation of an "asymmetry" note that from rotational symmetry the unpolarized cross section has to be an even function of θ: $\frac{d\bar{\sigma}}{d\Omega}(-\theta) = \frac{d\bar{\sigma}}{d\Omega}(\theta)$ and $A_y(\theta)$ has to be an odd function of θ: $A_y(-\theta) = -A_y(\theta)$. Taking all the particles in the initial beam polarized along the y axis we can substitute $\frac{p_y}{N} = 1$ in Eq. (4.18). Writing this equation for $\pm\theta$, then adding and subtracting from each other we get:

$$\frac{d\sigma}{d\Omega}(\theta,\phi) + \frac{d\sigma}{d\Omega}(-\theta,\phi) = 2\frac{d\bar{\sigma}}{d\Omega}(\theta) \tag{4.19}$$

and

$$A_y(\theta) = \frac{\frac{d\sigma}{d\Omega}(\theta,\phi) - \frac{d\sigma}{d\Omega}(-\theta,\phi)}{\frac{d\sigma}{d\Omega}(\theta,\phi) + \frac{d\sigma}{d\Omega}(-\theta,\phi)}. \tag{4.20}$$

Using Eq. (4.20) we interpret A_y as the asymmetry between the number of the left- and right-scattered particles. We also see that the denominator in Eq. (4.20) is the total unpolarized cross section. For practical calculations of A_y though we use Eq. (4.17) with $j = 2$. The Pauli matrix σ_2 is given by:

$$\begin{pmatrix} 0 & -i \\ i & 0 \end{pmatrix}. \tag{4.21}$$

Substituting this into Eq. (4.17) we get for A_y:

$$A_y(\theta) = \frac{\mathrm{Tr}\big(M\sigma_2 M^\dagger\big)}{\mathrm{Tr}(MM^\dagger)} = \frac{\sum\limits_{m_f,m_1,m_2} (M_{m_f m_1}(\sigma_2)_{m_1 m_2} M^\dagger_{m_2 m_f})}{\mathrm{Tr}(MM^\dagger)}. \tag{4.22}$$

Using the definition of $M^\dagger$:

$$A_y(\theta) = \frac{\sum\limits_{m_f,m_1,m_2} (M_{m_f m_1}(\sigma_2)_{m_1 m_2} M^*_{m_f m_2})}{\mathrm{Tr}(MM^\dagger)}, \tag{4.23}$$

and using the explicit from of σ_2 Eq. (4.21):

$$A_y(\theta) = \frac{\sum\limits_{m_f} i(-M_{m_f\frac{1}{2}} M^*_{m_f-\frac{1}{2}} + M_{m_f-\frac{1}{2}} M^*_{m_f\frac{1}{2}})}{\mathrm{Tr}(MM^\dagger)} = \frac{\sum\limits_{m_f} 2\,\mathrm{Im}(M_{m_f\frac{1}{2}} M^*_{m_f-\frac{1}{2}})}{\mathrm{Tr}(MM^\dagger)}. \tag{4.24}$$

Now redefining magnetic quantum numbers as m_1 and m_1' for the initial and final deuteron, and m_2 and m_2' for initial and final neutron we get the final form of the formula to calculate A_y:

$$A_y(\theta,\phi) = \frac{\sum\limits_{m_1}\sum\limits_{m_1',m_2'} 2\,\mathrm{Im}\left[M_{m_1',m_2';m_1,1/2}\, M^*_{m_1',m_2';m_1,-1/2}\right]}{\sum\limits_{m_1,m_2}\sum\limits_{m_1',m_2'} \left|M_{m_1',m_2';m_1,m_2}\right|^2}. \tag{4.25}$$

The connection between the transition matrix M and the on-shell scattering amplitude calculated solving the integral equations is given by Eq. (4.26).

$$M^J_{L'S',LS}(k) = Z_{\mathrm{LO}}\, t^{J;Nt\to Nt}_{L'S',LS}(k,k,E), \tag{4.26}$$

where Z_{LO} is the leading order deuteron wavefunction renormalization given by: $Z_{LO} = \frac{2\gamma_t}{M_N}$. If the deuterons in the target are polarized we get more polarization observable, for which formulas analogous to Eq. (4.25) can be derived using the density-matrix formulation described earlier [77, 78, 79, 80]. Here are the formulas we use to compute these observables:

$$iT_{11}(\theta,\phi) = -\sqrt{\frac{3}{2}}\,\frac{\sum\limits_{m_2}\sum\limits_{m_1',m_2'} \mathrm{Im}\left[M_{m_1',m_2';-1,m_2}M^*_{m_1',m_2';0,m_2} + M_{m_1',m_2';0,m_2}M^*_{m_1',m_2';1,m_2}\right]}{\sum\limits_{m_1,m_2}\sum\limits_{m_1',m_2'}\left|M_{m_1',m_2';m_1,m_2}\right|^2}, \quad (4.27)$$

$$T_{20}(\theta) = \frac{1}{\sqrt{2}}\,\frac{\sum\limits_{m_2}\sum\limits_{m_1',m_2'} \left\{\left|M_{m_1',m_2';1,m_2}\right|^2 - 2\left|M_{m_1',m_2';0,m_2}\right|^2 + \left|M_{m_1',m_2';-1,m_2}\right|^2\right\}}{\sum\limits_{m_1,m_2}\sum\limits_{m_1',m_2'}\left|M_{m_1',m_2';m_1,m_2}\right|^2}, \quad (4.28)$$

$$T_{21}(\theta,\phi) = -\sqrt{\frac{3}{2}}\,\frac{\sum\limits_{m_2}\sum\limits_{m_1',m_2'} \mathrm{Re}\left[M_{m_1',m_2';0,m_2}\left(M^*_{m_1',m_2';1,m_2} - M^*_{m_1',m_2';-1,m_2}\right)\right]}{\sum\limits_{m_1,m_2}\sum\limits_{m_1',m_2'}\left|M_{m_1',m_2';m_1,m_2}\right|^2}, \quad (4.29)$$

and

$$T_{22}(\theta,\phi) = \sqrt{3}\,\frac{\sum\limits_{m_2}\sum\limits_{m_1',m_2'} \mathrm{Re}\left[M_{m_1',m_2';1,m_2}M^*_{m_1',m_2';-1,m_2}\right]}{\sum\limits_{m_1,m_2}\sum\limits_{m_1',m_2'}\left|M_{m_1',m_2';m_1,m_2}\right|^2}, \quad (4.30)$$

4.2 Results

Here I present the up to N^{2}LO results of the EFT$_{\not\pi}$ calculation for the total unpolarized cross-section and the N^{3}LO results for the observables discussed in the previous section for the elastic *nd* scattering in comparison to the data and some potential model calculations.

The results for the cross section calculations at 3 MeV-nucleon energy are given in Fig. 4.2 (caption and figures are from [76]). In this figure we can clearly see that the EFT$_{\not\pi}$ results get better order by order. There is an excellent agreement of the N^{2}LO result with the experiment. The curve that corresponds to the N^{2}LO calculation is given with a band that represents the estimated theoretical error.

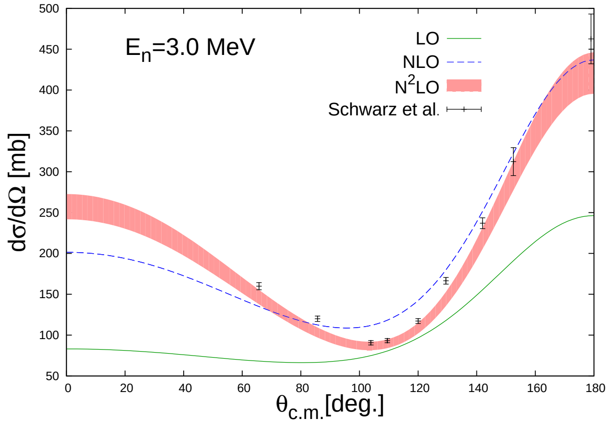

FIGURE 4.2: (Caption and figures are from [76]). *nd* scattering cross section for $E_n = 3.0$ MeV with experimental data from Schwarz, *et. al.* [81]. The LO prediction (without theoretical errors) is the solid green line, the dashed blue line the NLO prediction (without theoretical errors), and the solid red band the N^{2}LO prediction with a 6% error estimate.

A good energy range of processes that we expect EFT$_{\not\pi}$ to work well is given by typical momentum exchange Q such that the power counting parameter is about $\frac{Q}{\Lambda_{\not\pi}} \sim 0.3$, which is used to estimate the theoretical error. As the terms in the Lagrangian and the amplitudes are calculated as a power series in powers of 0.3 we can estimate that each subsequent term is going to be of the order of $0.3\times$ previous term. So we estimate that the N^{3}LO correction to an amplitude is of the order of $0.3 \times 0.3 \times 0.3\times$ the LO result$\approx 0.03\times$the LO result, which is the 3% of the LO result. Cross sections, being proportional to the square of the amplitudes, get the double of that error estimate. This is why we give a 6% theoretically estimated error band on the N^{2}LO cross section in Fig. 4.2 [76]. Our N^{3}LO results for the observable A_y are given in Fig. 4.3 (caption and figures are from [76]) for three different energies. Just as we calculated an estimate for the theoretical error for the cross section, we can do the same also for A_y. The main contributions to this observable come from the ^3P_J interactions Eq. (2.67) with interaction coefficients $C_2^{^3P_J}$. At the next order of the EFT$_{\not\pi}$ the correction to the observable is estimated to be the same order as the change in the observable if we vary the $C_2^{^3P_J}$ interaction coefficients within a 30% (±15%) band around their central values given in Eq. (2.73). Fig. 4.3 contains various curves corresponding to different values of the $C_2^{^3P_J}$ coefficients [76]. We can make a couple different conclusions from the results in Fig. 4.3. First of all we see that the A_y observable is indeed very sensitive to the ^3P_J interactions as was already discovered by various potential model calculations previously. Secondly we can see from the 3 MeV plot that the maximum of A_y is around $\theta = 105^\circ$, which coincides with the minimum of the unpolarized cross-section (see Fig. 4.2). This is justified by the fact that the total unpolarized cross section is in the denominator in Eq. (4.20). Finally, we see that the experimental data is well within the reach of the EFT$_{\not\pi}$. This means that if the EFT$_{\not\pi}$ at higher than N^{3}LO orders gives corrections according to the given error estimates, as is expected, then the A_y-puzzle could be solved in the next order.

We have previously claimed that the contribution to A_y coming from the two-body SD-mixing term is negligible compared to the contributions that come from the ^3P_J interactions. To see this we plot only the SD-mixing contribution to the A_y in Fig. 4.4. As we can see from the comparison of the two figures Figs. 4.3 and 4.4 the SD-contribution is about three orders of magnitude smaller than the ^3P_J contributions.

To develop a feeling about how well the EFT$_{\not\pi}$ works for few nucleon processes it is also useful to look at the results that it gives for the other nd polarization observables Fig. 4.5 (caption and figures are from [76]). On this figure the EFT$_{\not\pi}$ results for deuteron polarization observables are plotted along with some potential model calculations and experimental data. The experimental data is not for nd elastic scattering though, it is for pd elastic scattering. Given the approximate isospin symmetry and that the Coulomb interactions become less and less important for backward angles and higher scattering energies, we expect qualitative agreement between the theory and experiment, which is observed.

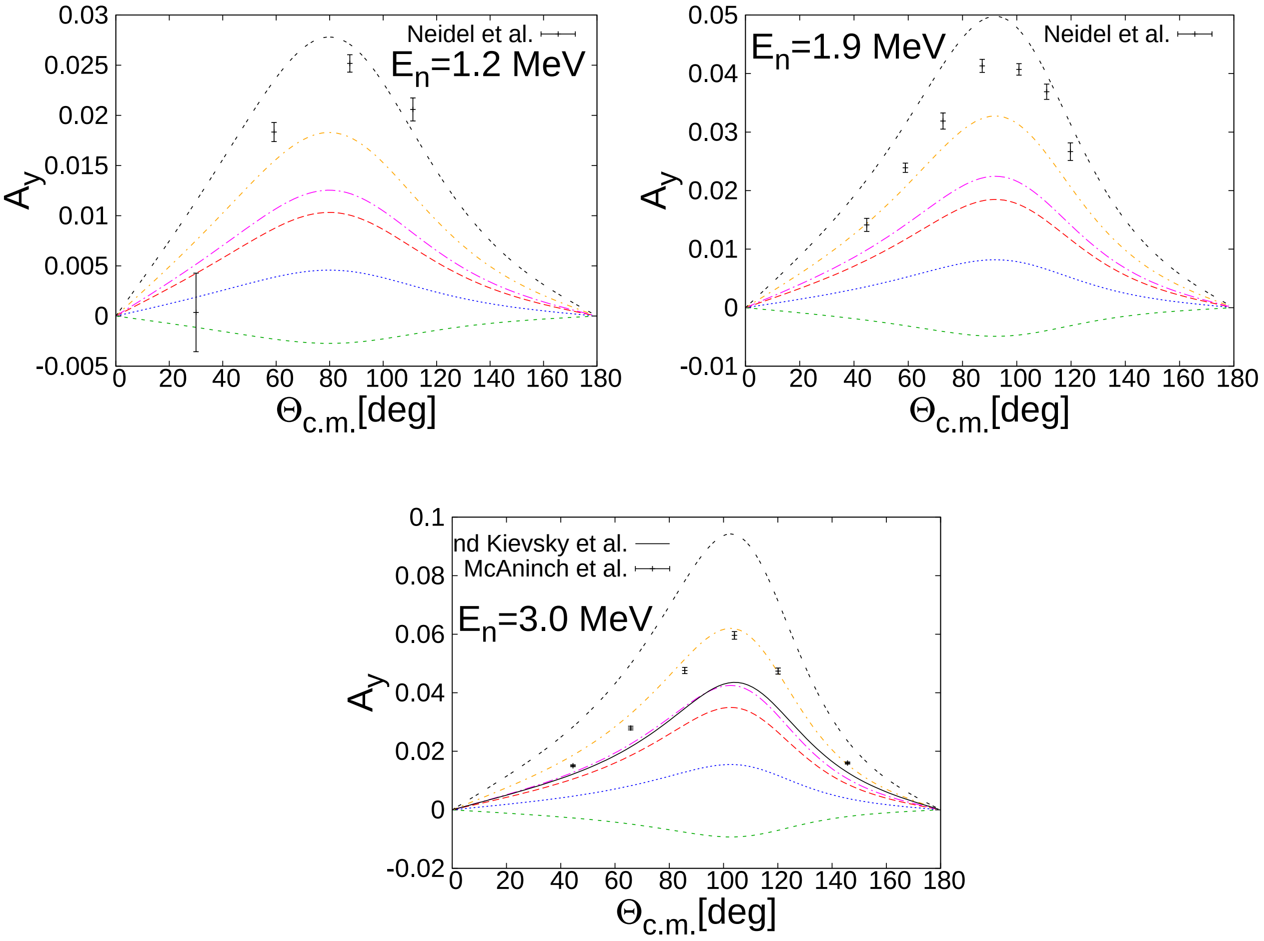

FIGURE 4.3: (Caption and figures are from [76]). The dashed lines are EFT$_{\not\pi}$ results for A_y for several sets of $C^{^3P_J}$ coefficients varied by 15% around their central values. Top Left: $E_n = 1.2$ MeV, experimental data from Neidel et al. [82]. Top Right: $E_n = 1.9$ MeV, experimental data from Neidel, *et. al.* [82]. Bottom: $E_n = 3.0$ MeV, the solid line is a PMC calculation from Kievsky, *et. al.* using AV-18+UR [56], with experimental data from McAninch, *et. al.* [57]. In the following, "+" stands for 15 percent above central values given in Eq. (2.73); "0" is at central value; and "−" is 15 percent below central value. The coefficient values ($C^{^3P_0}$,$C^{^3P_1}$,$C^{^3P_2}$) used to produce the curves shown are (from lowest EFT$_{\not\pi}$ curve to highest EFT$_{\not\pi}$ curve on the plots): big dots (green)$=(+,-,+)$; small dots (blue)$=(+,0,+)$; long dash (red)$=(0,0,0)$; long-dash-dot (purple) $=(0,0,+)$; short-dash-dot (orange) $=(-,0,0)$; double-dot (black) $=(-,+,+)$.

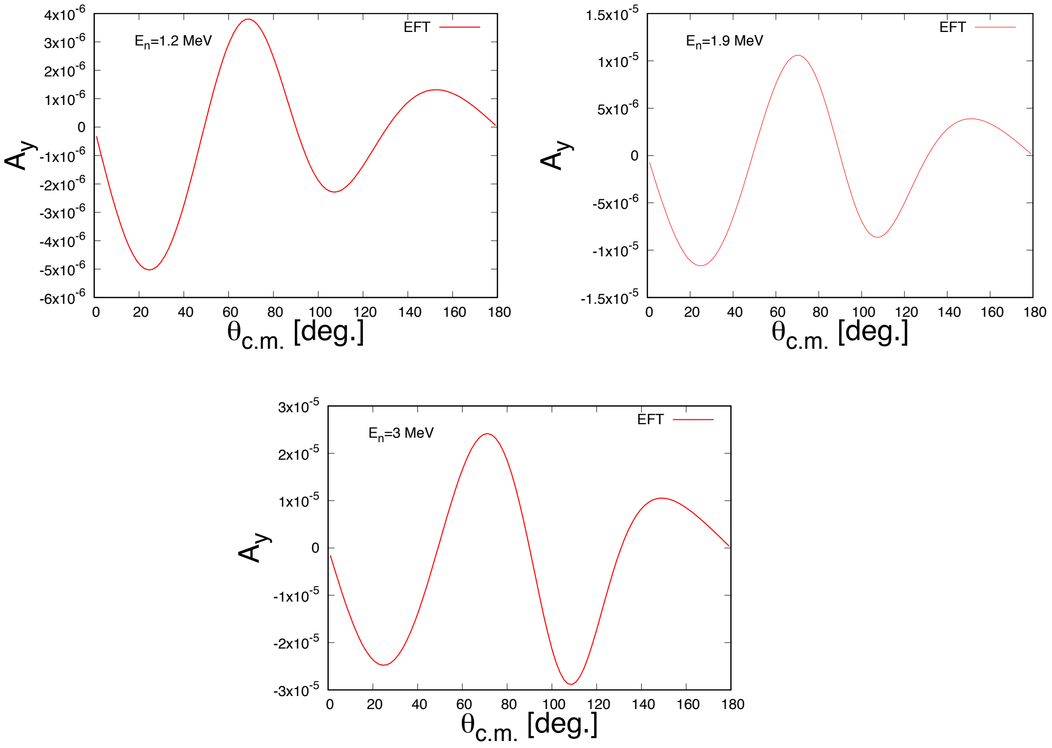

FIGURE 4.4: EFT$_{\not\pi}$ results for A_y only coming from the SD-mixing.

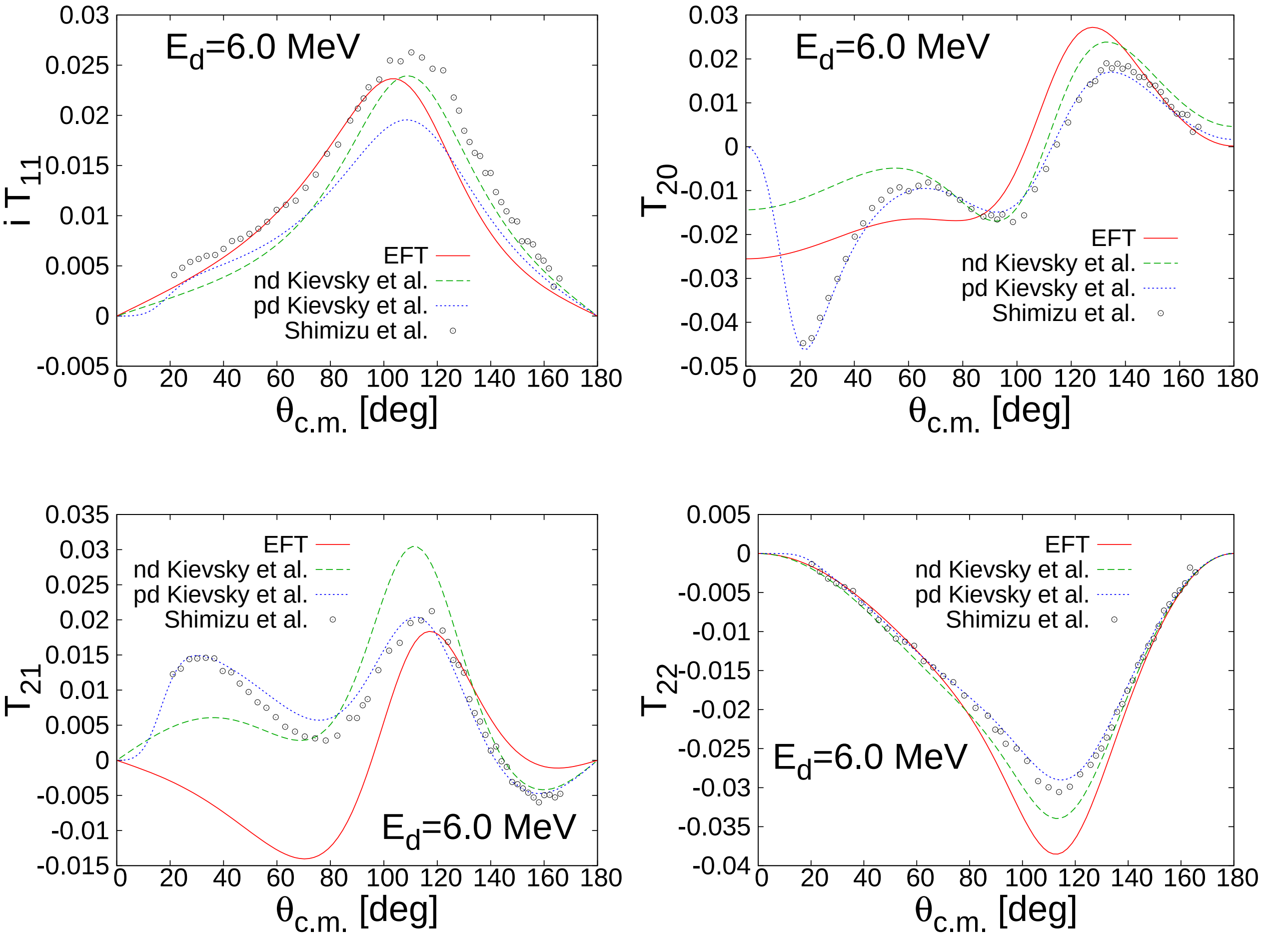

FIGURE 4.5: (Caption and figures are from [76]). The solid red line is the EFT$_{\not\pi}$ prediction (without theoretical error bars) for deuteron polarization observables in nd scattering, the dashed green line PMC calculations using AV18+UR for nd scattering [56] , and the dotted blue line PMC calculations using AV18+UR for pd scattering [56]. All experimental data is for pd scattering from Shimizu, *et. al.* [83] at a laboratory deuteron energy of $E_d = 6.0$ MeV.

4.3 Conclusions

In this dissertation the N^{3}LO calculation of the A_y observable for nd elastic scattering process in EFT$_{\not\pi}$ is described. This observable at N^{3}LO gets contributions from the two-body SD mixing and the two-body P-wave interactions. We find that the contributions from SD mixing are about three orders of magnitude smaller than the contributions from the two-body P-wave interactions. The A_y observable is found to be very sensitive to the two-body P-wave interactions. We see that varying the two-body P-wave interaction coefficients within the estimated theoretical error we find a very wide range of theoretical curves for the A_y observable. Most importantly the experimental data is within this range, which, at this order, eliminates the long-standing disagreement between the theory and the experiment, but dictates that a higher order calculation of this observable is necessary to unambiguously test $\mathrm{EFT}_{\not\pi}$. As we go to higher orders in an EFT we get more interaction terms in the Lagrangian and this increases the number of parameters that can be matched onto the experiment. Some of the possible results of a higher order calculation might be as follows. One of the possibilities is that at the next order the new three-body P-wave interaction coefficient is matched onto the A_y observable at some particular scattering energy and the predictions of the theory for the other energies agree well with the experiment. This would solve the A_y-puzzle and justify $\mathrm{EFT}_{\not\pi}$ as a well-constructed low-energy approximation to QCD, which gives a good description of the low energy nuclear physics at two- and three-body sectors. Another possibility is that the higher order theoretical prediction either grossly disagrees with the experiment or gets better but is still unsatisfactory. This would possibly be an indication of a beyond the standard model physics, but more likely this will be taken as a first sign that the power counting of $\mathrm{EFT}_{\not\pi}$ needs to be modified for this observable. In this case a possible solution might be the extension of $\mathrm{EFT}_{\not\pi}$ in such a way that certain three-body diagrams are resummed in order for the theory to be able to include more of the non-perturbative aspects of QCD.

The A_y observable has the total unpolarized *nd* scattering cross section in its denominator. Strictly perturbatively for N^3LO result this denominator is supposed to be expended and truncated at NLO, because the first nonzero contribution to the numerator of A_y is at N^2LO. Doing so we discovered that the position of the peak of A_y does not match with the experimental result. Keeping the denominator at N^2LO is equivalent to resumming some of the higher order contributions and makes the position of the maximum of A_y to match with the experiment. The total unpolarized *nd* scattering cross section is in the denominators of all of the polarization observables, so the interesting physics about the polarization observables is concentrated in the numerators. This justifies keeping the denominator unexpended when comparing to experiments.

We have not done the calculation of the N^{3}LO total unpolarized cross-section for the *nd* elastic scattering process. The reason is that at this order there is a new three-body force that we have not included in the calculation. This three body force gives zero contribution to the A_y but is important in the calculation of the total cross section, which will be necessary for higher order calculations of A_y (see [76] for a more detailed discussion).

The calculation of the same observable for the *pd* elastic scattering vs *nd* elastic scattering is complicated by Coulomb interactions and by the necessity to include more three-body counter-terms that are not necessary in the *nd* system. Calculations on *pd* system are of interest because there is more experimental data for this system to compare to. The qualitative agreement between the EFT$_{\not\pi}$ calculations for the *nd* system and the experimental data for the *pd* system in Fig. 4.5 is encouraging. This figure shows that as expected the Coulomb interactions are more important for forward angles, so to get the correct behavior for these observables at forward angles it might be necessary to include the Coulomb effects non-perturbatively.

4.4 Future Directions

From the theory point of view nuclear physics is the simplest when the number of nucleons is fewer and the processes happen in the low-energy regime. So this seems to be a good starting point in exploring nuclear forces, and the EFT$_{\not\pi}$ is specifically designed to deal with processes like that. Given this, the next steps to advance our understanding of nuclear physics can be: 1. to increase the accuracy of our predictions in the few-nucleon low-energy regime, 2. to increase the number of particles involved in a process, 3. to consider the higher-energy regimes.

1. We can increase the accuracy of the predictions by just going into higher orders of the $\mathrm{EFT}_{\not\pi}$. In fact our hope and conclusion is that the A_y-puzzle will be solved in the next few orders of the $\mathrm{EFT}_{\not\pi}$, because at N^4LO we will have new 3-body P-wave interactions entering into the Lagrangian, which will probably give the missing contributions to the A_y.

Some of the difficulties with this direction are that in the higher orders the number of diagrams increases excessively and the difficulty of both analytical and numerical calculations increases too. Besides in higher orders we always get new interaction terms allowed by the symmetries, which need to be fixed by implementing more and more experimental data into the theory, losing the predictive power of the theory. For example for the A_y in particular we might have to fix one of the new interactions to this observable at least at some scattering energy and then the prediction of the theory will be perefect at that scattering energy, but it will not really be a prediction, the theory will still be able to provide predictions for other scattering energies.

2. Increasing the number of particles we can explore a wider range of processes involving both short-range and long-range interactions and it should in principle allow us to predict binding energies of the different nuclei. The difficulties in this direction are partly the same as in previous point: it becomes numerically expensive to deal with a larger number of particles and an analytical approach is even harder. We have started to look at the LO four-body problem in $\mathrm{EFT}_{\not\pi}$ and firstly we would like to know whether a four-body contact interaction is needed at LO, as was the case with the three-body sector. To answer this question our strategy is to disregard any -four-body interactions, calculate the four-body binding energy numerically and check to see whether or not this binding energy has cutoff dependence. If it does have a cutoff dependence then it will most definitely prove that a four-body contact interaction will be necessary at LO so that the theory is properly renormalized, but if the predictions are cutoff independent then there is no need for the four-body contact interaction [84, 85, 86, 87, 88].

There is a special family of nuclei though called the halo-nuclei, which have a structure with a dense nuclear core with one or two nucleons on higher orbits. The EFT that is constructed to describe these nuclei is called Halo EFT and has similar features to $\text{EFT}_{\not\pi}$ [89, 90, 91, 92, 93, 94, 95].

3. As we go higher in energy, we will encounter particles that had been integrated out before and we will have to include them into the theory as explicit degrees of freedom. The first particles to come into the theory are the pions. The low-energy effective field theory with pions is the χPT, which was created before the $\text{EFT}_{\not\pi}$. The χPT allows one to do calculations on the same processes that are calculated in the $\text{EFT}_{\not\pi}$ and many more, and the applicability range of the χPT is wider. One of the difficulties of the χPT is its power counting though; as opposed to the $\text{EFT}_{\not\pi}$ its power counting is not un-ambiguous.

And finally one shouldn't lose the hope that QCD will eventually be solved in its non-perturbative regime. That would ultimately give answers to all of our questions about nuclear physics.

Appendix A

Projections

To do the spin-angular momentum projections we use integrals proven in [96] and diagrammatic approach to Clebsch-Gordan coefficients and $3nJ$-symbols described in [97]. Here I will give the integrals used, describe the diagrammatic approach and do a sample calculation of one of the diagrams.

The integrals necessary are given in the following equations.

$$\begin{aligned} & \frac{k^2}{3}\int d\Omega_k \int d\Omega_p f(\cos\theta)(Y_{L'}^{m'_L}(\hat{\mathbf{p}}))^* Y_L^{m_L}(\hat{\mathbf{k}}) Y_1^{m_1}(\hat{\mathbf{k}}) Y_1^{m_2}(\hat{\mathbf{k}}) \\ = \quad & k^2 \sum_{L''}\sum_{m''}\sqrt{\frac{\bar{L}}{\bar{L}'}} C_{1,1,L''}^{m_1,m_2,m''} C_{L,L'',L'}^{m_L,m'',m'_L} C_{1,1,L''}^{0,0,0} C_{L,L'',L'}^{0,0,0} \frac{1}{2}\int_{-1}^{1} P_{L'}(x) f(x) dx \end{aligned} \tag{A.1}$$

$$\begin{aligned}&\frac{p^2}{3}\int d\Omega_k \int d\Omega_p f(\cos\theta)(Y_{L'}^{m'_L}(\hat{\mathbf{p}}))^* Y_L^{m_L}(\hat{\mathbf{k}}) Y_1^{m_1}(\hat{\mathbf{p}}) Y_1^{m_2}(\hat{\mathbf{p}}) \\ = \;& p^2 \sum_{L''}\sum_{m''}\sqrt{\frac{\bar{L}}{\bar{L}'}} C_{1,1,L''}^{m_1,m_2,m''} C_{L,L'',L'}^{m_L,m'',m'_L} C_{1,1,L''}^{0,0,0} C_{L,L'',L'}^{0,0,0} \frac{1}{2}\int_{-1}^{1} P_L(x) f(x)\,dx\end{aligned} \tag{A.2}$$

$$\begin{aligned}&\frac{kp}{3}\int d\Omega_k \int d\Omega_p f(\cos\theta)(Y_{L'}^{m'_L}(\hat{\mathbf{p}}))^* Y_L^{m_L}(\hat{\mathbf{k}}) Y_1^{m_1}(\hat{\mathbf{k}}) Y_1^{m_2}(\hat{\mathbf{p}}) \\ = \;& kp \sum_{L''}\sum_{m''}\sqrt{\frac{\bar{L}}{\bar{L}'}} C_{L,1,L''}^{m_L,m_1,m''} C_{L'',1,L'}^{m'',m_2,m'_L} C_{L,1,L''}^{0,0,0} C_{L'',1,L'}^{0,0,0} \frac{1}{2}\int_{-1}^{1} P_{L''}(x) f(x)\,dx\end{aligned} \tag{A.3}$$

where θ is the angle between $\hat{\mathbf{k}}$ and $\hat{\mathbf{p}}$. These integrals arise when we have to project expressions like $f(\cos\theta)k_ik_j$, $f(\cos\theta)p_ip_j$ and $f(\cos\theta)k_ip_j$ onto an angular-momentum state basis. The vectors $\vec{k}$ and $\vec{p}$ are first represented as spherical vectors arriving at expressions like the left hand sides of the previous equations, then the integrals are evaluated using these equations. Usually for the function $f(x)$ we have $f(x) = \frac{1}{a+x}$, which on the right hand side gives (up to a sign) Legendre polynomials of the second kind.

In evaluating the spin-angular momentum projections we encounter large expressions which are sums of products of many Clebsch-Gordan coefficients. The sums run over magnetic quantum numbers. We simplify these expressions by reducing them into products of $6J$- and $9J$- symbols which are independent of magnetic quantum numbers. In general the $3nJ$-symbols arise when one has to combine more than two angular momenta together to form a total angular momentum of a system. The diagrammatic approach we use is described below. I give identities from [97] which are the most relevant to our calculations.

A Clebsch-Gordan coefficient is drawn as an arrow:

$$C^{m_1,m_2,m_3}_{J_1,J_2,J_3} = \left.\begin{array}{r} m_3 \\ m_1 \\ m_2 \end{array}\right\uparrow \tag{A.4}$$

On the arrow we only put the magnetic quantum numbers, keeping in mind that it is actually a function of six variables: the magnetic quantum numbers and the angular momentum J-values.

With this notation the symmetry properties of Clebsch-Gordan coefficients can be expressed as:

$$\left.\begin{array}{r} m_3 \\ m_2 \\ m_1 \end{array}\right\uparrow = (-1)^{J_1+m_1}(\frac{\bar{J}_3}{\bar{J}_2})^{\frac{1}{2}} \left.\begin{array}{r} m_2 \\ -m_1 \\ m_3 \end{array}\right\uparrow = (-1)^{J_2-m_2}(\frac{\bar{J}_3}{\bar{J}_1})^{\frac{1}{2}} \left.\begin{array}{r} m_1 \\ m_3 \\ -m_2 \end{array}\right\uparrow$$
$$= (-1)^{J_1+J_2-J_3} \left.\begin{array}{r} -m_3 \\ -m_2 \\ -m_1 \end{array}\right\uparrow = (-1)^{J_1+J_2-J_3} \left.\begin{array}{r} m_3 \\ m_1 \\ m_2 \end{array}\right\uparrow \tag{A.5}$$

where $\bar{J} = 2J + 1$.

The orthogonality and completeness relations are written as:

$$\sum_{m_1,m_2} \left.\begin{array}{r} m_3 \\ m_2 \\ m_1 \end{array}\right\uparrow \left.\begin{array}{r} m_3' \\ m_2 \\ m_1 \end{array}\right\uparrow = \delta_{J_3,J_3'}\delta_{m_3,m_3'} \tag{A.6}$$

and

$$\sum_{J_3,m_3} \begin{array}{c|c|} m_3 \uparrow & m_3 \uparrow \\ m_2 & m_2' \\ m_1 & m_1' \end{array} = \delta_{m_1,m_1'}\delta_{m_2,m_2'} \tag{A.7}$$

In the last two equations it is to be understood that the first two J-values in the two arrows are the same.

In our expressions with Clebsch-Gordan coefficients we have each magnetic quantum number appearing either once or twice. If it appears once then it is a free index and the final expression is going to depend on it. If it appears twice, then it is on two different Clebsch-Gordan coefficients, the J- values corresponding to the two places where it appears are always the same (otherwise the expression would not make sense), and it is understood that there is a sum going over that magnetic quantum number. If we have two arrows, which have two coinciding magnetic quantum numbers, meaning there is a sum over it, then we can draw these arrows intersecting or touching at that magnetic quantum number. With this new notation the $6J$-symbols are defined by:

$$(\bar{J}_6\bar{J}_4\bar{J}_5\bar{J}_6)^{\frac{1}{2}}(-1)^{J_1+J_3+J_4+J_5}\begin{Bmatrix} J_1 & J_2 & J_4 \\ J_3 & J_6 & J_5 \end{Bmatrix} = \tag{A.8}$$

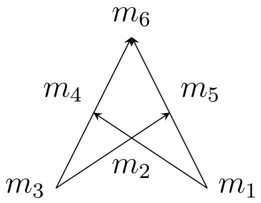

Using the properties of Clebsch-Gordan coefficients and the $6J$-symbols the following equations can be derived:

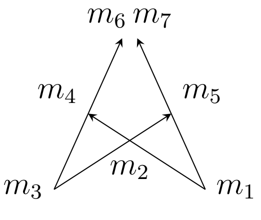

$$= (\bar{J}_4\bar{J}_5)^{\frac{1}{2}}(-1)^{J_1+J_3+J_4+J_5}\begin{Bmatrix} J_1 & J_2 & J_4 \\ J_3 & J_6 & J_5 \end{Bmatrix}\delta_{J_6,J_7}\delta_{m_6,m_7} \tag{A.9}$$

and

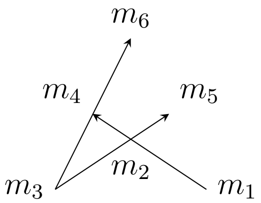

$$= (\bar{J}_4\bar{J}_5)^{\frac{1}{2}}(-1)^{J_1+J_3+J_4+J_5}\begin{Bmatrix} J_1 & J_2 & J_4 \\ J_3 & J_6 & J_5 \end{Bmatrix} \left.\begin{array}{c} m_6 \\ m_5 \\ m_1 \end{array}\right\uparrow \tag{A.10}$$

Using same notation a $9J$-symbol is defined by the following equation:

$$\begin{Bmatrix} J_1 & J_2 & J_3 \\ J_4 & J_5 & J_6 \\ J_7 & J_8 & J_9 \end{Bmatrix} = (\bar{J}_3\bar{J}_6\bar{J}_9\bar{J}_7\bar{J}_8\bar{J}_9)^{-\frac{1}{2}} \tag{A.11}$$

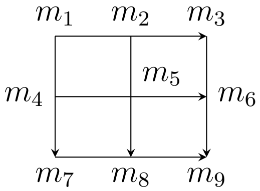

And the following identities can be proven:

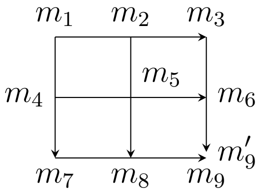

$$= (\bar{J}_8\bar{J}_6\bar{J}_7\bar{J}_3)^{\frac{1}{2}} \begin{Bmatrix} J_1 & J_2 & J_3 \\ J_4 & J_5 & J_6 \\ J_7 & J_8 & J_9 \end{Bmatrix} \delta_{J_9,J_9'}\delta_{m_9,m_9'} \tag{A.12}$$

and

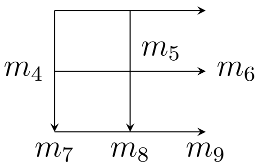

$$= (\bar{J}_8\bar{J}_6\bar{J}_7\bar{J}_3)^{\frac{1}{2}} \begin{Bmatrix} J_1 & J_2 & J_3 \\ J_4 & J_5 & J_6 \\ J_7 & J_8 & J_9 \end{Bmatrix} \left.\begin{array}{c} m_9 \\ m_6 \\ m_3 \end{array}\right\uparrow \tag{A.13}$$

As an example let's calculate the projections of a term in the two-body P-wave loop Feynman diagram derived above:

$$\begin{aligned}
64t = & \left\{ Z^2 (C_2^{^3P_1} + 2C_2^{^3P_2}) + A(C_2^{^3P_0} - C_2^{^3P_1} + \frac{2}{3} C_2^{^3P_2}) \right\} \sigma_k \sigma_i \sigma_j \sigma_k \\
+ & \; B(C_2^{^3P_0} - C_2^{^3P_1} + \frac{2}{3} C_2^{^3P_2}) k_k k_l \sigma_k \sigma_i \sigma_j \sigma_l \\
+ & \; C(C_2^{^3P_0} - C_2^{^3P_1} + \frac{2}{3} C_2^{^3P_2}) p_k p_l \sigma_k \sigma_i \sigma_j \sigma_l \\
+ & \left\{ D(2C_2^{^3P_2} - C_2^{^3P_1}) + E(C_2^{^3P_0} - \frac{4}{3} C_2^{^3P_2}) \right\} k_l p_k \sigma_k \sigma_i \sigma_j \sigma_l \\
+ & \left\{ E(2C_2^{^3P_2} - C_2^{^3P_1}) + D(C_2^{^3P_0} - \frac{4}{3} C_2^{^3P_2}) \right\} k_k p_l \sigma_k \sigma_i \sigma_j \sigma_l \\
+ & \; Z^2 C_2^{^1P_1} \sigma_i \sigma_j
\end{aligned} \tag{A.14}$$

The notation used in what follows is that all the not-primed variables correspond to initial states, all the primed variables correspond to final states,
J stands for total angular momentum and M its projection,
L stands for orbital angular momentum and m_L its projection
S stands for total spin and m_S its projection
m_N stands for nucleon spin projection
m_d stands for deuteron spin projection

Let's take the term proportional to $k_k p_l$. This needs to be projected onto a total angular momentum state basis, so we have:

$$\begin{aligned}
&P_{kl} = \langle J', M'|\, f(\cos\theta) k_k p_l \sigma_k \sigma_i \sigma_j \sigma_l \,|J, M\rangle \\
= \;& C^{m_L,m_S,M}_{L,S,J} C^{m'_L,m'_S,M'}_{L',S',J'} \left\langle L', m'_L\right|\, f(\cos\theta) k_k p_l \,|L, m_L\rangle \langle S', m'_S|\, \sigma_k \sigma_i \sigma_j \sigma_l \,|S, m_S\rangle \\
= \;& C^{m_L,m_S,M}_{L,S,J} C^{m_L,m'_S,M'}_{L',S',J'} C^{m_N,m_d,m_S}_{\frac{1}{2},1,S} C^{m'_N,m'_d,m'_S}_{\frac{1}{2},1,S} \\
& \left\langle L', m'_L\right|\, f(\cos\theta) k_k p_l \,|L, m_L\rangle \left\langle \frac{1}{2}, m'_N \right| \sigma_k \sigma_i \sigma_j \sigma_l \left| \frac{1}{2}, m_N \right\rangle \epsilon_d^{*m'_d} \epsilon_d^{m_d}
\end{aligned} \tag{A.15}$$

In here the first equation is just a notation, the second and third equations come from the definition of Clebsch-Gordan coefficients. $\epsilon_d^{m_d}$ and $\epsilon_d^{*m'_d}$ are the initial and final deuteron polarizations. The indices j and i are contracted with initial and final deuteron polarization projections, so going to spherical indices we can do the substitution $\sigma_j \epsilon_d^{m_d} = \sigma^{m_d}$ and $\sigma_i \epsilon_d^{*m'_d} = (-1)^{m'_d} \sigma^{-m'_d}$, the minus signs come from the complex conjugation on $\epsilon_d^{*m'_d}$.

$$\begin{gathered}
P_{kl} = (-1)^{m'_d} C^{m_L,m_S,M}_{L,S,J} C^{m'_L,m'_S,M'}_{L',S',J'} C^{m_N,m_d,m_S}_{\frac{1}{2},1,S} C^{m'_N,m'_d,m'_S}_{\frac{1}{2},1,S} \\
\left\langle L', m'_L\right|\, f(\cos\theta) k_k p_l \,|L, m_L\rangle \left\langle \frac{1}{2}, m'_N \right| \sigma_k \sigma^{-m'_d} \sigma^{m_d} \sigma_l \left| \frac{1}{2}, m_N \right\rangle
\end{gathered} \tag{A.16}$$

We can also switch to spherical indices for k and l doing the substitutions:

$$k_k \sigma_k = (-1)^{m_k} \frac{1}{\sqrt{3}} k Y_1^{-m_k}(\hat{\mathbf{k}}) \sigma^{m_k} \tag{A.17}$$

and

$$p_l \sigma_l = (-1)^{m_l} \frac{1}{\sqrt{3}} p Y_1^{m_l}(\hat{\mathbf{p}}) \sigma^{-m_l}. \tag{A.18}$$

The placement of the minus sign on the Pauli matrix or the spherical harmonic is unimportant; the equations are true in both ways. With these substitutions we get:

$$P_{kl} = (-1)^{m'_d+m_k+m_l} C_{L,S,J}^{m_L,m_S,M} C_{L',S',J'}^{m'_L,m'_S,M'} C_{\frac{1}{2},1,S}^{m_N,m_d,m_S} C_{\frac{1}{2},1,S}^{m'_N,m'_d,m'_S}$$

$$\frac{1}{3} kp \left\langle L', m'_L \right| f(\cos\theta) Y_1^{-m_k}(\hat{\mathbf{k}}) Y_1^{m_l}(\hat{\mathbf{p}}) \left| L, m_L \right\rangle \left\langle \frac{1}{2}, m'_N \right| \sigma^{m_k} \sigma^{-m'_d} \sigma^{m_d} \sigma^{-m_l} \left| \frac{1}{2}, m_N \right\rangle \tag{A.19}$$

Here we recognize the first matrix element on the second line as the Eq. (A.3). Doing the substitution we find:

$$P_{kl} = (-1)^{m'_d+m_k+m_l} C_{L,S,J}^{m_L,m_S,M} C_{L',S',J'}^{m'_L,m'_S,M'} C_{\frac{1}{2},1,S}^{m_N,m_d,m_S} C_{\frac{1}{2},1,S}^{m'_N,m'_d,m'_S}$$

$$kp \sum_{L''} \sqrt{\frac{\bar{L}}{\bar{L}'}} C_{L,1,L''}^{m_L,-m_k,m''} C_{L'',1,L'}^{m'',m_l,m'_L} C_{L,1,L''}^{0,0,0} C_{L'',1,L'}^{0,0,0} \frac{1}{2} \int_{-1}^{1} P_{L''}(x) f(x) dx$$

$$\left\langle \frac{1}{2}, m'_N \right| \sigma^{m_k} \sigma^{-m'_d} \sigma^{m_d} \sigma^{-m_l} \left| \frac{1}{2}, m_N \right\rangle \tag{A.20}$$

The summation over m'' is understood as are summations over other magnetic quantum numbers. After rearranging the terms in previous equation and denoting $\frac{1}{2}\int_{-1}^{1} P_{L''}(x) f(x) dx = \tilde{Q}_{L''}$ we have:

$$P_{kl} = kp \sum_{L''} \tilde{Q}_{L''} \sqrt{\frac{\bar{L}}{\bar{L}'}} C_{L,1,L''}^{0,0,0} C_{L'',1,L'}^{0,0,0}$$

$$(-1)^{m'_d+m_k+m_l} C_{L,S,J}^{m_L,m_S,M} C_{L',S',J'}^{m'_L,m'_S,M'} C_{\frac{1}{2},1,S}^{m_N,m_d,m_S} C_{\frac{1}{2},1,S}^{m'_N,m'_d,m'_S}$$

$$C_{L,1,L''}^{m_L,-m_k,m''} C_{L'',1,L'}^{m'',m_l,m'_L}$$

$$\left\langle \frac{1}{2}, m'_N \right| \sigma^{m_k} \sigma^{-m'_d} \sigma^{m_d} \sigma^{-m_l} \left| \frac{1}{2}, m_N \right\rangle \tag{A.21}$$

Now we can insert complete set of states $\left|\frac{1}{2}, m^{(1)}\right\rangle\left\langle\frac{1}{2}, m^{(1)}\right|$, $\left|\frac{1}{2}, m^{(2)}\right\rangle\left\langle\frac{1}{2}, m^{(2)}\right|$, $\left|\frac{1}{2}, m^{(3)}\right\rangle\left\langle\frac{1}{2}, m^{(3)}\right|$ between the Pauli matrices and using the fact that $\left\langle\frac{1}{2}, m_1\right| \sigma^m \left|\frac{1}{2}, m_2\right\rangle = \sqrt{3} C^{m_2,m,m_1}_{\frac{1}{2},1,\frac{1}{2}}$, which is proven using the Wigner-Eckart Theorem [98], we find:

$$
\begin{aligned}
P_{kl} &= 9kp \sum_{L''} \tilde{Q}_{L''} \sqrt{\frac{\bar{L}}{\bar{L}'}} C^{0,0,0}_{L,1,L''} C^{0,0,0}_{L'',1,L'} \\
&(-1)^{m'_d+m_k+m_l} C^{m_L,m_S,M}_{L,S,J} C^{m'_L,m'_S,M'}_{L',S',J'} C^{m_N,m_d,m_S}_{\frac{1}{2},1,S} C^{m'_N,m'_d,m'_S}_{\frac{1}{2},1,S} \\
&C^{m_L,-m_k,m''}_{L,1,L''} C^{m'',m_l,m'_L}_{L'',1,L'} \\
&C^{m^{(1)},m_k,m'_N}_{\frac{1}{2},1,\frac{1}{2}} C^{m^{(2)},-m'_d,m^{(1)}}_{\frac{1}{2},1,\frac{1}{2}} C^{m^{(3)},m_d,m^{(2)}}_{\frac{1}{2},1,\frac{1}{2}} C^{m_N,-m_l,m^{(3)}}_{\frac{1}{2},1,\frac{1}{2}}
\end{aligned}
\tag{A.22}
$$

As I described above we found an expression which is a sum of products of Clebsch-Gordan coefficients and the sum runs over all of the magnetic quantum numbers except M and M'. To proceed from here it is convenient to start using the diagrammatic notation for Clebsch-Gordan coefficients.

$$
\begin{aligned}
P_{kl} &= 9kp \sum_{L''} \tilde{Q}_{L''} \sqrt{\frac{\bar{L}}{\bar{L}'}} C^{0,0,0}_{L,1,L''} C^{0,0,0}_{L'',1,L'} \\
&(-1)^{m'_d+m_k+m_l}
\left.\begin{array}{r} M \\ m_L \\ m_S \end{array}\right\uparrow
\left.\begin{array}{r} M' \\ m'_L \\ m'_S \end{array}\right\uparrow
\left.\begin{array}{r} m_S \\ m_N \\ m_d \end{array}\right\uparrow
\left.\begin{array}{r} m'_S \\ m'_N \\ m'_d \end{array}\right\uparrow
\left.\begin{array}{r} m'' \\ m_L \\ -m_k \end{array}\right\uparrow
\left.\begin{array}{r} m'_L \\ m'' \\ m_l \end{array}\right\uparrow
\left.\begin{array}{r} m'_N \\ m^{(1)} \\ m_k \end{array}\right\uparrow
\left.\begin{array}{r} m^{(1)} \\ m^{(2)} \\ -m'_d \end{array}\right\uparrow
\left.\begin{array}{r} m^{(2)} \\ m^{(3)} \\ m_d \end{array}\right\uparrow
\left.\begin{array}{r} m^{(3)} \\ m_N \\ -m_l \end{array}\right\uparrow
\end{aligned}
\tag{A.23}
$$

Now we can use Eq. (A.5) to make the signs of all the magnetic quantum numbers to be the same in our expression:

$$
\begin{aligned}
P_{kl} &= 9kp \sum_{L''} \tilde{Q}_{L''} \sqrt{\frac{\bar{L}}{\bar{L}'}} C^{0,0,0}_{L,1,L''} C^{0,0,0}_{L'',1,L'} \\
&(-1)^{m'_d+m_k+m_l} \left.\begin{matrix} M \\ m_L \\ m_S \end{matrix}\right\uparrow \left.\begin{matrix} M' \\ m'_L \\ m'_S \end{matrix}\right\uparrow \left.\begin{matrix} m_S \\ m_N \\ m_d \end{matrix}\right\uparrow \left.\begin{matrix} m'_S \\ m'_N \\ m'_d \end{matrix}\right\uparrow \left.\begin{matrix} m_L \\ m_k \\ m'' \end{matrix}\right\uparrow \\
&\left(\frac{\bar{L}''}{\bar{L}}\right)^{\frac{1}{2}} (-1)^{1-m_k} \left.\begin{matrix} m'_L \\ m'' \\ m_l \end{matrix}\right\uparrow \left.\begin{matrix} m'_N \\ m^{(1)} \\ m_k \end{matrix}\right\uparrow \left.\begin{matrix} m^{(2)} \\ m'_d \\ m^{(1)} \end{matrix}\right\uparrow \\
&(-1)^{1-m'_d} \left.\begin{matrix} m^{(2)} \\ m^{(3)} \\ m_d \end{matrix}\right\uparrow \left.\begin{matrix} m_N \\ m_l \\ m^{(3)} \end{matrix}\right\uparrow (-1)^{1-m_l} \\
= \quad & -9kp \sum_{L''} \tilde{Q}_{L''} \sqrt{\frac{\bar{L}''}{\bar{L}'}} C^{0,0,0}_{L,1,L''} C^{0,0,0}_{L'',1,L'} \\
&\left.\begin{matrix} M \\ m_L \\ m_S \end{matrix}\right\uparrow \left.\begin{matrix} M' \\ m'_L \\ m'_S \end{matrix}\right\uparrow \left.\begin{matrix} m_S \\ m_N \\ m_d \end{matrix}\right\uparrow \left.\begin{matrix} m'_S \\ m'_N \\ m'_d \end{matrix}\right\uparrow \left.\begin{matrix} m_L \\ m_k \\ m'' \end{matrix}\right\uparrow \left.\begin{matrix} m'_L \\ m'' \\ m_l \end{matrix}\right\uparrow \left.\begin{matrix} m'_N \\ m^{(1)} \\ m_k \end{matrix}\right\uparrow \left.\begin{matrix} m^{(2)} \\ m'_d \\ m^{(1)} \end{matrix}\right\uparrow \left.\begin{matrix} m^{(2)} \\ m^{(3)} \\ m_d \end{matrix}\right\uparrow \left.\begin{matrix} m_N \\ m_l \\ m^{(3)} \end{matrix}\right\uparrow
\end{aligned}
\tag{A.24}
$$

Now again using Eq. (A.5) to change the order of the first two entries in two of the arrows and rearranging the terms we find:

$$P_{kl} = -9kp\sum_{L''}\tilde{Q}_{L''}\sqrt{\frac{\bar{L}''}{\bar{L}'}}C^{0,0,0}_{L,1,L''}C^{0,0,0}_{L'',1,L'}$$

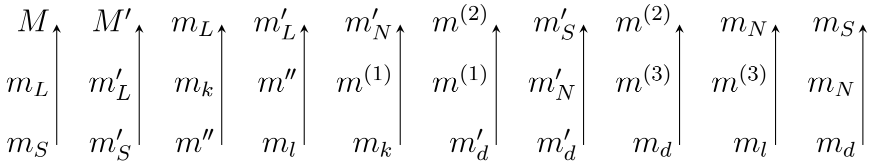

(A.25)

Now we see that the last six arrows fall into patterns as in Eq. (A.10):

$$P_{kl} = -9kp\sum_{L''}\tilde{Q}_{L''}\sqrt{\frac{\bar{L}''}{\bar{L}'}}C^{0,0,0}_{L,1,L''}C^{0,0,0}_{L'',1,L'}$$

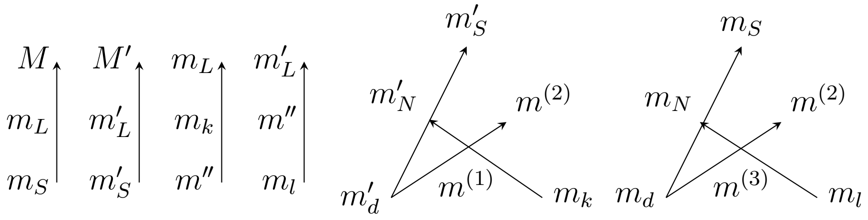

$$= \quad -36kp\sum_{L''}\tilde{Q}_{L''}\sqrt{\frac{\bar{L}''}{\bar{L}'}}C^{0,0,0}_{L,1,L''}C^{0,0,0}_{L'',1,L'}$$

$$\begin{Bmatrix}1 & \frac{1}{2} & \frac{1}{2}\\ 1 & S & \frac{1}{2}\end{Bmatrix}\begin{Bmatrix}1 & \frac{1}{2} & \frac{1}{2}\\ 1 & S' & \frac{1}{2}\end{Bmatrix}$$

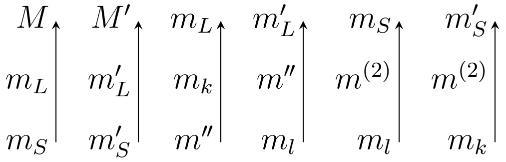

(A.26)

And on the last step we change the order of the first two entries on the first, second and fourth arrows using Eq. (A.5), and see that the remaining six arrows fall into the pattern of the Eq. (A.12) giving the final expression:

$$
\begin{aligned}
P_{kl} &= -36kp\sum_{L''}\tilde{Q}_{L''}\sqrt{\frac{\bar{L}''}{\bar{L}'}}C^{0,0,0}_{L,1,L''}C^{0,0,0}_{L'',1,L'} \\
&\quad \begin{Bmatrix} 1 & \frac{1}{2} & \frac{1}{2} \\ 1 & S & \frac{1}{2} \end{Bmatrix}\begin{Bmatrix} 1 & \frac{1}{2} & \frac{1}{2} \\ 1 & S' & \frac{1}{2} \end{Bmatrix}
\left.\begin{array}{c} M \\ m_L \\ m_S \end{array}\right\uparrow
\left.\begin{array}{c} M' \\ m'_L \\ m'_S \end{array}\right\uparrow
\left.\begin{array}{c} m_L \\ m_k \\ m'' \end{array}\right\uparrow
\left.\begin{array}{c} m'_L \\ m'' \\ m_l \end{array}\right\uparrow
\left.\begin{array}{c} m_S \\ m^{(2)} \\ m_l \end{array}\right\uparrow
\left.\begin{array}{c} m'_S \\ m^{(2)} \\ m_k \end{array}\right\uparrow \\
&= -36kp\sum_{L''}(-1)^{S+L-J}(-1)^{S'+L'-J'}(-1)^{L''+1-L'}\tilde{Q}_{L''}\sqrt{\frac{\bar{L}''}{\bar{L}'}}C^{0,0,0}_{L,1,L''}C^{0,0,0}_{L'',1,L'} \\
&\quad \begin{Bmatrix} 1 & \frac{1}{2} & \frac{1}{2} \\ 1 & S & \frac{1}{2} \end{Bmatrix}\begin{Bmatrix} 1 & \frac{1}{2} & \frac{1}{2} \\ 1 & S' & \frac{1}{2} \end{Bmatrix}
\left.\begin{array}{c} M \\ m_S \\ m_L \end{array}\right\uparrow
\left.\begin{array}{c} M' \\ m'_S \\ m'_L \end{array}\right\uparrow
\left.\begin{array}{c} m_L \\ m_k \\ m'' \end{array}\right\uparrow
\left.\begin{array}{c} m'_L \\ m_l \\ m'' \end{array}\right\uparrow
\left.\begin{array}{c} m_S \\ m^{(2)} \\ m_l \end{array}\right\uparrow
\left.\begin{array}{c} m'_S \\ m^{(2)} \\ m_k \end{array}\right\uparrow \\
&= 36kp\sum_{L''}(-1)^{S+S'+L+L''-J-J'}\tilde{Q}_{L''}\sqrt{\frac{\bar{L}''}{\bar{L}'}}C^{0,0,0}_{L,1,L''}C^{0,0,0}_{L'',1,L'} \\
&\quad \begin{Bmatrix} 1 & \frac{1}{2} & \frac{1}{2} \\ 1 & S & \frac{1}{2} \end{Bmatrix}\begin{Bmatrix} 1 & \frac{1}{2} & \frac{1}{2} \\ 1 & S' & \frac{1}{2} \end{Bmatrix}
\end{aligned}
$$

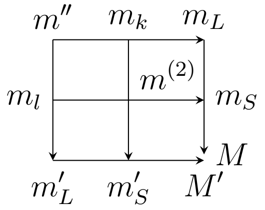

$$
\begin{aligned}
&= 36kp\sum_{L''}(-1)^{S+S'+L+L''-2J}\tilde{Q}_{L''}\sqrt{\bar{L}''\bar{L}\bar{S}\bar{S}'}C^{0,0,0}_{L,1,L''}C^{0,0,0}_{L'',1,L'} \\
&\quad \begin{Bmatrix} 1 & \frac{1}{2} & \frac{1}{2} \\ 1 & S & \frac{1}{2} \end{Bmatrix}\begin{Bmatrix} 1 & \frac{1}{2} & \frac{1}{2} \\ 1 & S' & \frac{1}{2} \end{Bmatrix}\begin{Bmatrix} L'' & 1 & L \\ 1 & \frac{1}{2} & S \\ L' & S' & J \end{Bmatrix}\delta_{J,J'}\delta_{M,M'}
\end{aligned}
\tag{A.27}
$$

which coincides with Eq. (A.29), from which some parts are suppressed because they are common in all the terms. The Kronecker deltas in the final answer confirm that the operators we had preserve the total angular momentum and its projection. We see that in the final expression we have none of the magnetic quantum numbers, those are “integrated over” and the answers depends only on the angular momenta.

A.1 Two-body P-wave contributions to nd scattering, one-loop diagram: Projections

Here I give the results of projecting all the terms in Eq. (3.24), which are calculated using the techniques described in this Appendix. Once these answers are combined with the orbital angular-momentum projections the answer needs to be summed over L''. In general in all the answers that I give in this Appendix, all the angular momenta that are not S, S', L, L' and J are to be summed over.

A.1.1 Deuteron to Deuteron Projections Spin

δ_{kl} -term:

$$= 36\delta_{SS'}\delta_{LL'}\begin{Bmatrix}1 & \frac{1}{2} & \frac{1}{2}\\ 1 & S' & \frac{1}{2}\end{Bmatrix}\begin{Bmatrix}1 & \frac{1}{2} & \frac{1}{2}\\ 1 & S & \frac{1}{2}\end{Bmatrix} \tag{A.28}$$

$k_k p_l$ -term:

$$= 36(-1)^{S+S'+L+L''-2J}C^{000}_{L1L''}C^{000}_{L''1L'}(\bar{L}\bar{L}''\bar{S}\bar{S}')^{\frac{1}{2}}\begin{Bmatrix}1 & \frac{1}{2} & \frac{1}{2}\\ 1 & S' & \frac{1}{2}\end{Bmatrix}\begin{Bmatrix}1 & \frac{1}{2} & \frac{1}{2}\\ 1 & S & \frac{1}{2}\end{Bmatrix}\begin{Bmatrix}L'' & 1 & L'\\ 1 & \frac{1}{2} & S'\\ L & S & J\end{Bmatrix} \tag{A.29}$$

$k_l p_k$ -term:

$$= 36(-1)^{S+S'+L+L''-2J}C^{000}_{L1L''}C^{000}_{L''1L'}(\bar{L}\bar{L}''\bar{S}\bar{S}')^{\frac{1}{2}}\begin{Bmatrix}1 & \frac{1}{2} & \frac{1}{2}\\ 1 & S' & \frac{1}{2}\end{Bmatrix}\begin{Bmatrix}1 & \frac{1}{2} & \frac{1}{2}\\ 1 & S & \frac{1}{2}\end{Bmatrix}\begin{Bmatrix}\frac{1}{2} & 1 & S'\\ L' & J & L''\end{Bmatrix}\begin{Bmatrix}L & 1 & L''\\ \frac{1}{2} & J & S\end{Bmatrix} \tag{A.30}$$

$k_l k_k$ -term:

$$= 36(-1)^{\frac{3}{2}+2S'+L+L''-J} C^{000}_{11L''} C^{000}_{LL''L'} (\bar{L}\bar{L}''\bar{S}\bar{S}')^{\frac{1}{2}} \begin{Bmatrix}1 & \frac{1}{2} & \frac{1}{2} \\ 1 & S' & \frac{1}{2}\end{Bmatrix} \begin{Bmatrix}1 & \frac{1}{2} & \frac{1}{2} \\ 1 & S & \frac{1}{2}\end{Bmatrix} \begin{Bmatrix}L'' & 1 & 1 \\ \frac{1}{2} & S & S'\end{Bmatrix} \begin{Bmatrix}S' & L'' & S \\ L & J & L'\end{Bmatrix} \tag{A.31}$$

$^1P_1$-term:

$$= 3\delta_{S\frac{1}{2}}\delta_{S'\frac{1}{2}}\delta_{LL'} \tag{A.32}$$

A.1.2 Singlet to Deuteron Projections Spin

δ_{kl} -term:

$$= 6\sqrt{3}\delta_{S'\frac{1}{2}}\delta_{LL'} \begin{Bmatrix}1 & \frac{1}{2} & \frac{1}{2} \\ 1 & S' & \frac{1}{2}\end{Bmatrix} \tag{A.33}$$

$k_k p_l$ -term:

$$= 6\sqrt{3}(-1)^{\frac{1}{2}+S'+L+L''-2J} C^{000}_{L1L''} C^{000}_{L''1L'} (\bar{L}\bar{L}''\bar{S}\bar{S}')^{\frac{1}{2}} \begin{Bmatrix}1 & \frac{1}{2} & \frac{1}{2} \\ 1 & S' & \frac{1}{2}\end{Bmatrix} \begin{Bmatrix}L'' & 1 & L' \\ 1 & \frac{1}{2} & S' \\ L & \frac{1}{2} & J\end{Bmatrix} \tag{A.34}$$

$k_l p_k$ -term:

$$= 6\sqrt{3}(-1)^{\frac{1}{2}+S'+L+L''-2J} C^{000}_{L1L''} C^{000}_{L''1L'} (\bar{L}\bar{L}''\bar{S}\bar{S}')^{\frac{1}{2}} \begin{Bmatrix}1 & \frac{1}{2} & \frac{1}{2} \\ 1 & S' & \frac{1}{2}\end{Bmatrix} \begin{Bmatrix}\frac{1}{2} & 1 & S' \\ L' & J & L''\end{Bmatrix} \begin{Bmatrix}L & 1 & L'' \\ \frac{1}{2} & J & \frac{1}{2}\end{Bmatrix} \tag{A.35}$$

$k_l k_k$ -term:

$$= 6\sqrt{3}(-1)^{\frac{3}{2}+2S'+L+L''-J} C^{000}_{11L''} C^{000}_{LL''L'} (\bar{L}\bar{L}''\bar{S}\bar{S}')^{\frac{1}{2}} \begin{Bmatrix}1 & \frac{1}{2} & \frac{1}{2} \\ 1 & S' & \frac{1}{2}\end{Bmatrix} \begin{Bmatrix}L'' & 1 & 1 \\ \frac{1}{2} & \frac{1}{2} & S'\end{Bmatrix} \begin{Bmatrix}S' & L'' & \frac{1}{2} \\ L & J & L'\end{Bmatrix} \tag{A.36}$$

$^1P_1$-term:

$$= \sqrt{3}\delta_{S'\frac{1}{2}}\delta_{LL'} \tag{A.37}$$

A.1.3 Deuteron to Singlet Projections Spin

δ_{kl} -term:

$$= 6\sqrt{3}\delta_{S\frac{1}{2}}\delta_{LL'} \begin{Bmatrix} 1 & \frac{1}{2} & \frac{1}{2} \\ 1 & S & \frac{1}{2} \end{Bmatrix} \tag{A.38}$$

$k_k p_l$ -term:

$$= 6\sqrt{3}(-1)^{\frac{1}{2}+S+L+L''-2J} C^{000}_{L1L''} C^{000}_{L''1L'} (\bar{L}\bar{L}''\bar{S}\bar{S}')^{\frac{1}{2}} \begin{Bmatrix} 1 & \frac{1}{2} & \frac{1}{2} \\ 1 & S & \frac{1}{2} \end{Bmatrix} \begin{Bmatrix} L'' & 1 & L' \\ 1 & \frac{1}{2} & \frac{1}{2} \\ L & S & J \end{Bmatrix} \tag{A.39}$$

$k_l p_k$ -term:

$$= 6\sqrt{3}(-1)^{\frac{1}{2}+S+L+L''-2J} C^{000}_{L1L''} C^{000}_{L''1L'} (\bar{L}\bar{L}''\bar{S}\bar{S}')^{\frac{1}{2}} \begin{Bmatrix} 1 & \frac{1}{2} & \frac{1}{2} \\ 1 & S & \frac{1}{2} \end{Bmatrix} \begin{Bmatrix} \frac{1}{2} & 1 & \frac{1}{2} \\ L' & J & L'' \end{Bmatrix} \begin{Bmatrix} L & 1 & L'' \\ \frac{1}{2} & J & S \end{Bmatrix} \tag{A.40}$$

$k_l k_k$ -term:

$$= 6\sqrt{3}(-1)^{\frac{1}{2}+L+L''-J} C^{000}_{11L''} C^{000}_{LL''L'} (\bar{L}\bar{L}''\bar{S}\bar{S}')^{\frac{1}{2}} \begin{Bmatrix} 1 & \frac{1}{2} & \frac{1}{2} \\ 1 & S & \frac{1}{2} \end{Bmatrix} \begin{Bmatrix} L'' & 1 & 1 \\ \frac{1}{2} & S & \frac{1}{2} \end{Bmatrix} \begin{Bmatrix} S' & L'' & S \\ L & J & L' \end{Bmatrix} \tag{A.41}$$

${}^1P_1$-term:

$$= \sqrt{3}\delta_{S\frac{1}{2}}\delta_{LL'} \tag{A.42}$$

A.1.4 Singlet to Singlet Projections Spin

δ_{kl} -term:

$$= 3\delta_{LL'} \tag{A.43}$$

$k_k p_l$ -term:

$$= 3(-1)^{1+L+L''-2J} C^{000}_{L1L''} C^{000}_{L''1L'} (\bar{L}\bar{L}''\bar{S}\bar{S}')^{\frac{1}{2}} \begin{Bmatrix} L'' & 1 & L' \\ 1 & \frac{1}{2} & \frac{1}{2} \\ L & \frac{1}{2} & J \end{Bmatrix} \tag{A.44}$$

$k_l p_k$ -term:

$$= 3(-1)^{1+L+L''-2J} C^{000}_{L1L''} C^{000}_{L''1L'} (\bar{L}\bar{L}''\bar{S}\bar{S}')^{\frac{1}{2}} \begin{Bmatrix} \frac{1}{2} & 1 & \frac{1}{2} \\ L' & J & L'' \end{Bmatrix} \begin{Bmatrix} L & 1 & L'' \\ \frac{1}{2} & J & \frac{1}{2} \end{Bmatrix} \tag{A.45}$$

$k_l k_k$ -term:

$$= 3(-1)^{\frac{1}{2}+L+L''-J} C^{000}_{11L''} C^{000}_{LL''L'} (\bar{L}\bar{L}''\bar{S}\bar{S}')^{\frac{1}{2}} \begin{Bmatrix} L'' & 1 & 1 \\ \frac{1}{2} & \frac{1}{2} & \frac{1}{2} \end{Bmatrix} \begin{Bmatrix} S' & L'' & \frac{1}{2} \\ L & J & L' \end{Bmatrix} \tag{A.46}$$

${}^1P_1$-term:

$$= \delta_{LL'} \tag{A.47}$$

A.1.5 Isospin Projections

Deuteron to Deuteron 3^P_J-terms: 3

Deuteron to Deuteron 1^P_1-terms: 1

Singlet to Deuteron 3^P_J-terms: $-\sqrt{3}$

Singlet to Deuteron 1^P_1-terms: $\sqrt{3}$

Deuteron to Singlet 3^P_J-terms: $-\sqrt{3}$

Deuteron to Singlet 1^P_1-terms: $\sqrt{3}$

Singlet to Singlet 3^P_J-terms: 1

Singlet to Singlet 1^P_1-terms: 3

A.2 Magnetic photon exchange contributions to *nd* scattering, one-loop vertex-photon diagram: Projections

Here I give the results of projecting all the terms in the diagram in Fig. A.1. The Lagrangian that describes the photon vertices are given in Appendix C.

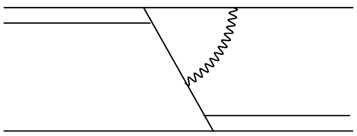

Figure A.1: Magnetic photon exchange on the vertex.

A.2.1 Deuteron to Deuteron Projections Spin

δ_{kl} -term:

$$= 36\delta_{SS'}\delta_{LL'}\begin{Bmatrix}1 & \frac{1}{2} & \frac{1}{2}\\ 1 & S & \frac{1}{2}\end{Bmatrix}\begin{Bmatrix}1 & \frac{1}{2} & \frac{1}{2}\\ 1 & \frac{1}{2} & \frac{1}{2}\end{Bmatrix} \tag{A.48}$$

$k_k p_l$ -term:

$$\begin{aligned}&= 36(-1)^{1+L+S-S'+L''+2J_4-2J}C^{000}_{L1L''}C^{000}_{L''1L'}\bar{J}_4\bar{J}_6(\bar{L}\bar{L}''\bar{S}\bar{S}')^{\frac{1}{2}}\\ &\times\begin{Bmatrix}1 & \frac{1}{2} & \frac{1}{2}\\ 1 & J_4 & \frac{1}{2}\end{Bmatrix}\begin{Bmatrix}1 & \frac{1}{2} & \frac{1}{2}\\ 1 & S & J_4\end{Bmatrix}\begin{Bmatrix}1 & \frac{1}{2} & \frac{1}{2}\\ 1 & J_6 & S'\end{Bmatrix}\begin{Bmatrix}1 & \frac{1}{2} & J_4\\ 1 & S & J_6\end{Bmatrix}\begin{Bmatrix}L & 1 & L''\\ J_6 & J & S\end{Bmatrix}\begin{Bmatrix}L'' & 1 & L'\\ S' & J & J_6\end{Bmatrix}\end{aligned} \tag{A.49}$$

$k_l p_k$ -term:

$$\begin{aligned}&= 36(-1)^{1-L+L''-S+S'+2J_4+2J_6}C^{000}_{L1L''}C^{000}_{L''1L'}\bar{J}_4\bar{J}_6(\bar{L}\bar{L}''\bar{S}\bar{S}')^{\frac{1}{2}}\\ &\times\begin{Bmatrix}1 & \frac{1}{2} & \frac{1}{2}\\ 1 & J_4 & \frac{1}{2}\end{Bmatrix}\begin{Bmatrix}1 & \frac{1}{2} & \frac{1}{2}\\ 1 & S & J_4\end{Bmatrix}\begin{Bmatrix}1 & \frac{1}{2} & \frac{1}{2}\\ 1 & J_6 & S'\end{Bmatrix}\begin{Bmatrix}1 & \frac{1}{2} & J_4\\ 1 & S & J_6\end{Bmatrix}\begin{Bmatrix}J_6 & 1 & S'\\ 1 & L'' & L'\\ S & L & J\end{Bmatrix}\end{aligned} \tag{A.50}$$

$k_l k_k$ -term:

$$= 36(-1)^{1+2S'+S-J} C^{000}_{11L''} C^{000}_{LL''L'} \bar{J}_4 (\bar{L}\bar{L}''\bar{S}\bar{S}')^{\frac{1}{2}}$$

$$\times \quad \begin{Bmatrix} 1 & \frac{1}{2} & \frac{1}{2} \\ 1 & J_4 & \frac{1}{2} \end{Bmatrix} \begin{Bmatrix} 1 & \frac{1}{2} & \frac{1}{2} \\ 1 & S & J_4 \end{Bmatrix} \begin{Bmatrix} 1 & 1 & L'' \\ \frac{1}{2} & J_4 & \frac{1}{2} \end{Bmatrix} \begin{Bmatrix} 1 & \frac{1}{2} & S' \\ L'' & S & J_4 \end{Bmatrix} \begin{Bmatrix} S' & L'' & S \\ L & J & L' \end{Bmatrix} \tag{A.51}$$

A.2.2 Singlet to Deuteron Projections Spin

δ_{kl} -term:

$$= 3\delta_{S'\frac{1}{2}} \delta_{S\frac{1}{2}} \delta_{LL'} \tag{A.52}$$

$k_k p_l$ -term:

$$= 6\sqrt{6}(-1)^{\frac{3}{2}+3S'+L+L''} C^{000}_{L1L''} C^{000}_{L''1L'} \bar{J}_4 (\bar{L}\bar{L}''\bar{S}')^{\frac{1}{2}} \begin{Bmatrix} 1 & \frac{1}{2} & \frac{1}{2} \\ 1 & J_4 & \frac{1}{2} \end{Bmatrix} \begin{Bmatrix} 1 & \frac{1}{2} & \frac{1}{2} \\ 1 & J_4 & S' \end{Bmatrix} \begin{Bmatrix} L'' & 1 & L \\ \frac{1}{2} & J & J_4 \end{Bmatrix} \begin{Bmatrix} L'' & 1 & L' \\ S' & J & J_4 \end{Bmatrix} \tag{A.53}$$

$k_l p_k$ -term:

$$= 12\sqrt{3}(-1)^{\frac{1}{2}+S'-L+L''} C^{000}_{L1L''} C^{000}_{L''1L'} \bar{J}_4 (\bar{L}\bar{L}'')^{\frac{1}{2}} \begin{Bmatrix} 1 & \frac{1}{2} & \frac{1}{2} \\ 1 & J_4 & \frac{1}{2} \end{Bmatrix} \begin{Bmatrix} 1 & \frac{1}{2} & \frac{1}{2} \\ 1 & J_4 & S' \end{Bmatrix} \begin{Bmatrix} J_4 & 1 & S' \\ 1 & L'' & L' \\ \frac{1}{2} & L & J \end{Bmatrix} \tag{A.54}$$

$k_l k_k$ -term:

$$= 6\sqrt{6}(-1)^{1+L+J_4-J} C^{000}_{11L''} C^{000}_{LL''L'} \bar{J}_4 (\bar{L}\bar{L}''\bar{S}')^{\frac{1}{2}} \begin{Bmatrix} 1 & \frac{1}{2} & \frac{1}{2} \\ 1 & J_4 & \frac{1}{2} \end{Bmatrix} \begin{Bmatrix} 1 & \frac{1}{2} & \frac{1}{2} \\ 1 & J_4 & S' \end{Bmatrix} \begin{Bmatrix} 1 & 1 & L'' \\ S' & \frac{1}{2} & J_4 \end{Bmatrix} \begin{Bmatrix} L & L'' & L' \\ S' & J & \frac{1}{2} \end{Bmatrix} \tag{A.55}$$

A.2.3 Deuteron to Singlet Projections Spin

δ_{kl} -term:

$$= 6\sqrt{3}\delta_{S\frac{1}{2}}\delta_{LL'}\begin{Bmatrix}1 & \frac{1}{2} & \frac{1}{2}\\ 1 & \frac{1}{2} & \frac{1}{2}\end{Bmatrix} \tag{A.56}$$

$k_k p_l$ -term:

$$= 6\sqrt{3}(-1)^{\frac{1}{2}+S+L+L''-2J}C^{000}_{L1L''}C^{000}_{L''1L'}(\bar{L}\bar{L}''\bar{S}\bar{S}')^{\frac{1}{2}}\begin{Bmatrix}1 & \frac{1}{2} & \frac{1}{2}\\ 1 & S & \frac{1}{2}\end{Bmatrix}\begin{Bmatrix}\frac{1}{2} & 1 & \frac{1}{2}\\ L' & J & L''\end{Bmatrix}\begin{Bmatrix}L & 1 & L''\\ \frac{1}{2} & J & S\end{Bmatrix} \tag{A.57}$$

$k_l p_k$ -term:

$$= 6\sqrt{3}(-1)^{\frac{1}{2}+S+L+L''-2J}C^{000}_{L1L''}C^{000}_{L''1L'}(\bar{L}\bar{L}''\bar{S}\bar{S}')^{\frac{1}{2}}\begin{Bmatrix}1 & \frac{1}{2} & \frac{1}{2}\\ 1 & S & \frac{1}{2}\end{Bmatrix}\begin{Bmatrix}L'' & 1 & L'\\ 1 & \frac{1}{2} & \frac{1}{2}\\ L & S & J\end{Bmatrix} \tag{A.58}$$

$k_l k_k$ -term:

$$= 6\sqrt{3}(-1)^{\frac{1}{2}+L+L''-J}C^{000}_{11L''}C^{000}_{LL''L'}(\bar{L}\bar{L}''\bar{S}\bar{S}')^{\frac{1}{2}}\begin{Bmatrix}1 & \frac{1}{2} & \frac{1}{2}\\ 1 & S & \frac{1}{2}\end{Bmatrix}\begin{Bmatrix}L'' & 1 & 1\\ \frac{1}{2} & S & \frac{1}{2}\end{Bmatrix}\begin{Bmatrix}S' & L'' & S\\ L & J & L'\end{Bmatrix} \tag{A.59}$$

A.2.4 Singlet to Singlet Projections Spin

δ_{kl} -term:

$$= 3\delta_{LL'} \tag{A.60}$$

$k_k p_l$ -term:

$$= 3(-1)^{1+L+L''-2J}C^{000}_{L1L''}C^{000}_{L''1L'}(\bar{L}\bar{L}''\bar{S}\bar{S}')^{\frac{1}{2}}\begin{Bmatrix}L'' & 1 & L'\\ 1 & \frac{1}{2} & \frac{1}{2}\\ L & \frac{1}{2} & J\end{Bmatrix} \tag{A.61}$$

$k_l p_k$ -term:

$$= 3(-1)^{1+L+L''-2J} C^{000}_{L1L''} C^{000}_{L''1L'} (\bar{L}\bar{L}''\bar{S}\bar{S}')^{\frac{1}{2}} \begin{Bmatrix} \frac{1}{2} & 1 & \frac{1}{2} \\ L' & J & L'' \end{Bmatrix} \begin{Bmatrix} L & 1 & L'' \\ \frac{1}{2} & J & \frac{1}{2} \end{Bmatrix} \tag{A.62}$$

$k_l k_k$ -term:

$$= 3(-1)^{\frac{1}{2}+L+L''-J} C^{000}_{11L''} C^{000}_{LL''L'} (\bar{L}\bar{L}''\bar{S}\bar{S}')^{\frac{1}{2}} \begin{Bmatrix} L'' & 1 & 1 \\ \frac{1}{2} & \frac{1}{2} & \frac{1}{2} \end{Bmatrix} \begin{Bmatrix} S' & L'' & \frac{1}{2} \\ L & J & L' \end{Bmatrix} \tag{A.63}$$

A.2.5 Isospin Projections

Deuteron to Deuteron: $\kappa_0^2 - \kappa_1^2$

Singlet to Deuteron: $\sqrt{3}\kappa_0^2 + \frac{1}{\sqrt{3}}\kappa_1^2 - \frac{4}{\sqrt{3}}\kappa_0\kappa_1$

Deuteron to Singlet: $\sqrt{3}(\kappa_0^2 - \kappa_1^2)$

Singlet to Singlet: $-\kappa_0^2 - \frac{1}{3}\kappa_1^2 + \frac{4}{3}\kappa_0\kappa_1$

A.3 Magnetic photon exchange contributions to *nd* scattering, one-loop bubble diagram: Projections

Here I give the results of projecting all the terms in the diagram in Fig. A.2. The Lagrangian that describes the photon vertices are given in Appendix C.

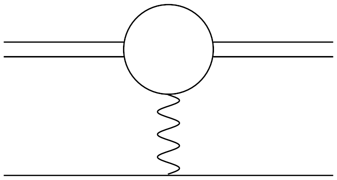

FIGURE A.2: Magnetic photon exchange on the bubble.

A.3.1 Deuteron to Deuteron Projections Spin

δ_{kl} -term:

$$= 12(-1)^{S}\delta_{SS'}\delta_{LL'}\begin{Bmatrix} \frac{1}{2} & 1 & \frac{1}{2} \\ 1 & S & 1 \end{Bmatrix} \tag{A.64}$$

$k_k p_l$ -term:

$$\begin{aligned} &= 12(-1)^{1+2S'+L'-L-J+J_1} C^{000}_{L1L''} C^{000}_{L''1L'} \bar{J}_1 (\bar{L}\bar{L}''\bar{S}\bar{S}')^{\frac{1}{2}} \\ \times \quad & \begin{Bmatrix} L' & 1 & L'' \\ \frac{1}{2} & J_1 & \frac{1}{2} \end{Bmatrix} \begin{Bmatrix} 1 & \frac{1}{2} & S' \\ L' & J & J_1 \end{Bmatrix} \begin{Bmatrix} 1 & \frac{1}{2} & S \\ 1 & L'' & L \\ 1 & J_1 & J \end{Bmatrix} \end{aligned} \tag{A.65}$$

$k_l p_k$ -term:

$$\begin{aligned} &= 12(-1)^{\frac{1}{2}+S'+L'-L-J-J_1} C^{000}_{L1L''} C^{000}_{L''1L'} \bar{J}_1 (\bar{L}\bar{L}''\bar{S}\bar{S}')^{\frac{1}{2}} \\ \times \quad & \begin{Bmatrix} L'' & 1 & L' \\ 1 & J_1 & 1 \end{Bmatrix} \begin{Bmatrix} \frac{1}{2} & 1 & S' \\ L' & J & J_1 \end{Bmatrix} \begin{Bmatrix} \frac{1}{2} & 1 & S \\ 1 & L'' & L \\ \frac{1}{2} & J_1 & J \end{Bmatrix} \end{aligned} \tag{A.66}$$

$k_l k_k$ -term:

$$\begin{aligned} &= 12(-1)^{\frac{1}{2}+2S'+S+L+L'+2J_1} C^{000}_{11L''} C^{000}_{LL''L'} \bar{J}_1 (\bar{L}''\bar{L}'\bar{S}\bar{S}')^{\frac{1}{2}} \\ \times \quad & \begin{Bmatrix} L'' & 1 & 1 \\ \frac{1}{2} & J_1 & \frac{1}{2} \end{Bmatrix} \begin{Bmatrix} 1 & 1 & 1 \\ \frac{1}{2} & S & J_1 \end{Bmatrix} \begin{Bmatrix} 1 & \frac{1}{2} & S' \\ L'' & S & J_1 \end{Bmatrix} \begin{Bmatrix} S' & L'' & S \\ L & J & L' \end{Bmatrix} \end{aligned} \tag{A.67}$$

A.3.2 Singlet to Deuteron Projections Spin

δ_{kl} -term:

$$= 2\sqrt{3}\delta_{S'\frac{1}{2}}\delta_{LL'} \tag{A.68}$$

$k_k p_l$ -term:

$$= 2\sqrt{6}(-1)C^{000}_{L1L''}C^{000}_{L''1L'}(\bar{L}\bar{L}''\bar{S}')^{\frac{1}{2}}\begin{Bmatrix} \frac{1}{2} & 1 & S' \\ 1 & L'' & L' \\ S & L & J \end{Bmatrix} \tag{A.69}$$

$k_l p_k$ -term:

$$= 2\sqrt{6}(-1)^{S'+L+L''-2J}C^{000}_{L1L''}C^{000}_{L''1L'}(\bar{L}\bar{L}''\bar{S}')^{\frac{1}{2}}\begin{Bmatrix} L' & 1 & L'' \\ \frac{1}{2} & J & S' \end{Bmatrix}\begin{Bmatrix} L & 1 & L'' \\ \frac{1}{2} & J & \frac{1}{2} \end{Bmatrix} \tag{A.70}$$

$k_l k_k$ -term:

$$= 2\sqrt{6}(-1)^{1+S+2S'+L+L''-J}C^{000}_{11L''}C^{000}_{LL''L'}(\bar{L}\bar{L}''\bar{S}')^{\frac{1}{2}}\begin{Bmatrix} L'' & 1 & 1 \\ \frac{1}{2} & \frac{1}{2} & S' \end{Bmatrix}\begin{Bmatrix} S' & L'' & \frac{1}{2} \\ L & J & L' \end{Bmatrix} \tag{A.71}$$

A.3.3 Deuteron to Singlet Projections Spin

δ_{kl} -term:

$$= 2\sqrt{3}\delta_{S\frac{1}{2}}\delta_{LL'} \tag{A.72}$$

$k_k p_l$ -term:

$$= 2\sqrt{6}(-1)^{\frac{1}{2}+S+L+L''-2J}C^{000}_{L1L''}C^{000}_{L''1L'}(\bar{L}'\bar{L}''\bar{S})^{\frac{1}{2}}\begin{Bmatrix} L'' & 1 & L' \\ \frac{1}{2} & J & \frac{1}{2} \end{Bmatrix}\begin{Bmatrix} L & 1 & L'' \\ \frac{1}{2} & J & S \end{Bmatrix} \tag{A.73}$$

$k_l p_k$ -term:

$$= 2\sqrt{6}(-1)^{\frac{1}{2}-S-L+L''}C^{000}_{L1L''}C^{000}_{L''1L'}(\bar{L}\bar{L}''\bar{S})^{\frac{1}{2}}\begin{Bmatrix} \frac{1}{2} & 1 & \frac{1}{2} \\ 1 & L'' & L' \\ S & L & J \end{Bmatrix} \tag{A.74}$$

$k_l k_k$ -term:

$$= 2\sqrt{6}(-1)^{\frac{3}{2}+S} C^{000}_{11L''} C^{000}_{LL''L'} (\bar{L}\bar{L}''\bar{S})^{\frac{1}{2}} \begin{Bmatrix} 1 & 1 & L'' \\ \frac{1}{2} & S & \frac{1}{2} \end{Bmatrix} \begin{Bmatrix} L & L'' & L' \\ \frac{1}{2} & J & S \end{Bmatrix} \tag{A.75}$$

A.3.4 Singlet to Singlet Projections Spin

0

A.3.5 Isospin Projections

Deuteron to Deuteron: $2(\kappa_0^2 - \kappa_0\kappa_1)$

Singlet to Deuteron: $\frac{2}{\sqrt{3}}\kappa_1^2 - \frac{2}{\sqrt{3}}\kappa_0\kappa_1$

Deuteron to Singlet: $\frac{2}{\sqrt{3}}\kappa_1^2 - \frac{2}{\sqrt{3}}\kappa_0\kappa_1$

Singlet to Singlet: $2\kappa_0^2 - \frac{4}{3}\kappa_1^2 - \frac{2}{3}\kappa_0\kappa_1$

A.4 Magnetic photon exchange contributions to *nd* scattering, one-loop non-planar diagram: Projections

Here I give the results of projecting all the terms in the diagram in Fig. A.3. The Lagrangian that describes the photon vertices are given in Appendix C.

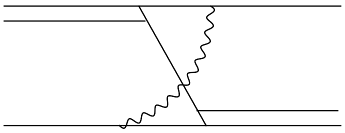

FIGURE A.3: Magnetic photon exchange non-planar diagram.

A.4.1 Deuteron to Deuteron Projections Spin

δ_{kl} -term:

$$= -36\delta_{SS'}\delta_{LL'}\begin{Bmatrix} \frac{1}{2} & \frac{1}{2} & 1 \\ \frac{1}{2} & 1 & \frac{1}{2} \\ 1 & \frac{1}{2} & S \end{Bmatrix} \tag{A.76}$$

$k_k p_l$ -term:

$$\begin{aligned} &= 36(-1)^{L''-L-S-S'} C^{000}_{L1L''} C^{000}_{L''1L'} \bar{J}_1 (\bar{L}'\bar{L}''\bar{S}\bar{S}')^{\frac{1}{2}} \\ &\times \begin{Bmatrix} 1 & \frac{1}{2} & \frac{1}{2} \\ 1 & J_1 & \frac{1}{2} \end{Bmatrix} \begin{Bmatrix} 1 & \frac{1}{2} & \frac{1}{2} \\ 1 & S & J_1 \end{Bmatrix} \begin{Bmatrix} 1 & \frac{1}{2} & \frac{1}{2} \\ 1 & S' & J_1 \end{Bmatrix} \begin{Bmatrix} J_1 & 1 & S' \\ 1 & L'' & L' \\ S & L & J \end{Bmatrix} \end{aligned} \tag{A.77}$$

$k_l p_k$ -term:

$$\begin{aligned} &= 36(-1)^{2J_1+L+L'+L''+S-J} C^{000}_{L1L''} C^{000}_{L''1L'} \bar{J}_1 (\bar{L}'\bar{L}''\bar{S}\bar{S}')^{\frac{1}{2}} \\ &\times \begin{Bmatrix} 1 & \frac{1}{2} & \frac{1}{2} \\ 1 & J_1 & \frac{1}{2} \end{Bmatrix} \begin{Bmatrix} 1 & \frac{1}{2} & \frac{1}{2} \\ 1 & S & J_1 \end{Bmatrix} \begin{Bmatrix} 1 & \frac{1}{2} & \frac{1}{2} \\ 1 & S' & J_1 \end{Bmatrix} \begin{Bmatrix} L & 1 & L'' \\ J_1 & J & S \end{Bmatrix} \begin{Bmatrix} L' & 1 & L'' \\ J_1 & J & S' \end{Bmatrix} \end{aligned} \tag{A.78}$$

$k_l k_k$ -term:

$$\begin{aligned} &= 36(-1)^{J_1+L+L''+2S'} C^{000}_{11L''} C^{000}_{LL''L'} \bar{J}_1 (\bar{L}'\bar{L}''\bar{S}\bar{S}')^{\frac{1}{2}} \\ &\times \begin{Bmatrix} 1 & \frac{1}{2} & \frac{1}{2} \\ 1 & J_1 & \frac{1}{2} \end{Bmatrix} \begin{Bmatrix} 1 & \frac{1}{2} & \frac{1}{2} \\ 1 & S & J_1 \end{Bmatrix} \begin{Bmatrix} 1 & \frac{1}{2} & \frac{1}{2} \\ 1 & S' & J_1 \end{Bmatrix} \begin{Bmatrix} J_1 & 1 & S' \\ L'' & S & 1 \end{Bmatrix} \begin{Bmatrix} L & L'' & L' \\ S' & J & S \end{Bmatrix} \end{aligned} \tag{A.79}$$

A.4.2 Singlet to Deuteron Projections Spin

δ_{kl} -term:

$$= 6\sqrt{3}\delta_{S'\frac{1}{2}}\delta_{LL'}\begin{Bmatrix} 1 & \frac{1}{2} & \frac{1}{2} \\ 1 & S' & \frac{1}{2} \end{Bmatrix} \tag{A.80}$$

$k_k p_l$ -term:

$$= 6\sqrt{3}(-1)^{\frac{1}{2}+S'+L+L''-2J} C^{000}_{L1L''} C^{000}_{L''1L'} (\bar{L}\bar{L}''\bar{S}\bar{S}')^{\frac{1}{2}} \begin{Bmatrix} 1 & \frac{1}{2} & \frac{1}{2} \\ 1 & S' & \frac{1}{2} \end{Bmatrix} \begin{Bmatrix} L'' & 1 & L' \\ 1 & \frac{1}{2} & S' \\ L & \frac{1}{2} & J \end{Bmatrix} \tag{A.81}$$

$k_l p_k$ -term:

$$= 6\sqrt{3}(-1)^{\frac{1}{2}+S'+L+L''-2J} C^{000}_{L1L''} C^{000}_{L''1L'} (\bar{L}\bar{L}''\bar{S}\bar{S}')^{\frac{1}{2}} \begin{Bmatrix} 1 & \frac{1}{2} & \frac{1}{2} \\ 1 & S' & \frac{1}{2} \end{Bmatrix} \begin{Bmatrix} \frac{1}{2} & 1 & S' \\ L' & J & L'' \end{Bmatrix} \begin{Bmatrix} L & 1 & L'' \\ \frac{1}{2} & J & \frac{1}{2} \end{Bmatrix} \tag{A.82}$$

$k_l k_k$ -term:

$$= 6\sqrt{3}(-1)^{\frac{3}{2}+2S'+L+L''-J} C^{000}_{11L''} C^{000}_{LL''L'} (\bar{L}\bar{L}''\bar{S}\bar{S}')^{\frac{1}{2}} \begin{Bmatrix} 1 & \frac{1}{2} & \frac{1}{2} \\ 1 & S' & \frac{1}{2} \end{Bmatrix} \begin{Bmatrix} L'' & 1 & 1 \\ \frac{1}{2} & \frac{1}{2} & S' \end{Bmatrix} \begin{Bmatrix} S' & L'' & \frac{1}{2} \\ L & J & L' \end{Bmatrix} \tag{A.83}$$

A.4.3 Deuteron to Singlet Projections Spin

δ_{kl} -term:

$$= 6\sqrt{3}\delta_{S\frac{1}{2}}\delta_{LL'} \begin{Bmatrix} 1 & \frac{1}{2} & \frac{1}{2} \\ 1 & S & \frac{1}{2} \end{Bmatrix} \tag{A.84}$$

$k_k p_l$ -term:

$$= 6\sqrt{3}(-1)^{\frac{1}{2}+S+L+L''-2J} C^{000}_{L1L''} C^{000}_{L''1L'} (\bar{L}\bar{L}''\bar{S}\bar{S}')^{\frac{1}{2}} \begin{Bmatrix} 1 & \frac{1}{2} & \frac{1}{2} \\ 1 & S & \frac{1}{2} \end{Bmatrix} \begin{Bmatrix} L'' & 1 & L' \\ 1 & \frac{1}{2} & \frac{1}{2} \\ L & S & J \end{Bmatrix} \tag{A.85}$$

$k_l p_k$ -term:

$$= 6\sqrt{3}(-1)^{\frac{1}{2}+S+L+L''-2J} C^{000}_{L1L''} C^{000}_{L''1L'} (\bar{L}\bar{L}''\bar{S}\bar{S}')^{\frac{1}{2}} \begin{Bmatrix} 1 & \frac{1}{2} & \frac{1}{2} \\ 1 & S & \frac{1}{2} \end{Bmatrix} \begin{Bmatrix} \frac{1}{2} & 1 & \frac{1}{2} \\ L' & J & L'' \end{Bmatrix} \begin{Bmatrix} L & 1 & L'' \\ \frac{1}{2} & J & S \end{Bmatrix} \tag{A.86}$$

$k_l k_k$ -term:

$$= 6\sqrt{3}(-1)^{\frac{1}{2}+L+L''-J} C^{000}_{11L''} C^{000}_{LL''L'} (\bar{L}\bar{L}''\bar{S}\bar{S}')^{\frac{1}{2}} \begin{Bmatrix} 1 & \frac{1}{2} & \frac{1}{2} \\ 1 & S & \frac{1}{2} \end{Bmatrix} \begin{Bmatrix} L'' & 1 & 1 \\ \frac{1}{2} & S & \frac{1}{2} \end{Bmatrix} \begin{Bmatrix} S' & L'' & S \\ L & J & L' \end{Bmatrix} \tag{A.87}$$

A.4.4 Singlet to Singlet Projections Spin

δ_{kl} -term:

$$= 3\delta_{LL'} \tag{A.88}$$

$k_k p_l$ -term:

$$= 3(-1)^{1+L+L''-2J} C^{000}_{L1L''} C^{000}_{L''1L'} (\bar{L}\bar{L}''\bar{S}\bar{S}')^{\frac{1}{2}} \begin{Bmatrix} L'' & 1 & L' \\ 1 & \frac{1}{2} & \frac{1}{2} \\ L & \frac{1}{2} & J \end{Bmatrix} \tag{A.89}$$

$k_l p_k$ -term:

$$= 3(-1)^{1+L+L''-2J} C^{000}_{L1L''} C^{000}_{L''1L'} (\bar{L}\bar{L}''\bar{S}\bar{S}')^{\frac{1}{2}} \begin{Bmatrix} \frac{1}{2} & 1 & \frac{1}{2} \\ L' & J & L'' \end{Bmatrix} \begin{Bmatrix} L & 1 & L'' \\ \frac{1}{2} & J & \frac{1}{2} \end{Bmatrix} \tag{A.90}$$

$k_l k_k$ -term:

$$= 3(-1)^{\frac{1}{2}+L+L''-J} C^{000}_{11L''} C^{000}_{LL''L'} (\bar{L}\bar{L}''\bar{S}\bar{S}')^{\frac{1}{2}} \begin{Bmatrix} L'' & 1 & 1 \\ \frac{1}{2} & \frac{1}{2} & \frac{1}{2} \end{Bmatrix} \begin{Bmatrix} S' & L'' & \frac{1}{2} \\ L & J & L' \end{Bmatrix} \tag{A.91}$$

A.4.5 Isospin Projections

Deuteron to Deuteron: $(\kappa_0 - \kappa_1)^2$

Singlet to Deuteron: $\sqrt{3}\kappa_0^2 - \frac{1}{\sqrt{3}}\kappa_1^2 - \frac{2}{\sqrt{3}}\kappa_0\kappa_1$

Deuteron to Singlet: $\sqrt{3}\kappa_0^2 - \frac{1}{\sqrt{3}}\kappa_1^2 - \frac{2}{\sqrt{3}}\kappa_0\kappa_1$

Singlet to Singlet: $-\kappa_0^2 + \frac{5}{3}\kappa_1^2 - \frac{2}{3}\kappa_0\kappa_1$

Appendix B

Integral equations

B.1 Analytical methods

In this section I will formulate some important facts about a class of integral equations and give some proofs or proof sketches of these facts [99, 100]. I will also give some discussion of the numerical methods used. The following form for linear integral equations is called Fredholm integral equation of the second kind:

$$y(p) = f(p) + \int_a^b K(p,q)y(q)dq \tag{B.1}$$

where $f(p)$ and $K(p,q)$ are known functions and this is an equation for the unknown function $y(p)$. $K(p,q)$ is called the kernel of the equation. All the functions and the integral are defined on a finite interval (a,b). The theory of this integral equation is very similar to the theory of linear algebraic equations. To understand the analogy and to derive theorems about this equations let's break the interval (a,b) into n pieces of equal length and approximate the integral by a sum. Denoting:

$$\Delta q = \frac{b-a}{n} \tag{B.2}$$

$$p_i = a + i\frac{b-a}{n} \tag{B.3}$$

$$q_j = a + j\frac{b-a}{n} \tag{B.4}$$

we find from the original equation the following equations:

$$y(p_i) = f(p_i) + \sum_j K(p_i, q_j)y(q_j)\Delta q, \quad 0 \leqslant i \leqslant n \tag{B.5}$$

With further notations: $y(p_i) = y_i$, $f(p_i) = f_i$ and $K(p_i, q_j)\Delta q = K_{ij}$ we arrive at a system of linear algebraic equations:

$$y_i = f_i + \sum_j K_{ij}y_j, \quad 0 \leqslant i, j \leqslant n \tag{B.6}$$

which can be put into the following form:

$$\sum_j (\delta_{ij} - K_{ij})y_j = f_i \tag{B.7}$$

Now the analogy between the theory of linear integral equations and the theory of linear algebraic equations becomes obvious. The theorems about linear algebraic equations serve as a motivation to formulate analogous theorems about integral equations. All the theorems about linear algebraic equations involve the concept of matrices and determinants, hence our purpose will be to formulate these theorems without using determinants so that they can be generalized to integral equations.

First of all we know that if the determinant of the matrix $(\delta_{ij} - K_{ij})$ is non-zero then this system of equations has a unique solution for arbitrary numbers f_i. But if this determinant is zero then our system of linear equations has at least one non-trivial solution if $f_i = 0$ for all i. So we can formulate the following "determinant-free" statements:

Statement 1:

Either a system of linear algebraic equations has a unique solution for arbitrary inhomogeneous parts or the corresponding homogeneous system of equations has at least one non-trivial solution.

Statement 2: If for a given system of algebraic equations the first part of statement 1 is true then the first part of the statement 1 is also true for the transposed system of equations.

Using the quantum mechanical notation for vectors the system of linear equations can be put in the following form:

$$M |y\rangle = |f\rangle \tag{B.8}$$

where M is the matrix given by $(\delta_{ij} - K_{ij})$.

Now let's assume that the second part of the statement 1 is true for this system of equations, hence it is also true for the transposed system of equations. In this case one can ask the question: for which values of f_i does the system of equations still have a solution? To answer this question let's denote a solution of the transposed homogeneous equation by $|z\rangle$. Then the following is true:

$$M^T |z\rangle = \langle z| M = 0 \tag{B.9}$$

so we can contract the equation (B.8) with the dual vector $\langle z|$:

$$\langle z| M |y\rangle = \langle z|f\rangle \tag{B.10}$$

but the left hand side of this equation is zero by the definition of $\langle z|$, so we have:

$$\langle z|f\rangle = 0 \tag{B.11}$$

So we derived that a necessary condition for an inhomogeneous system of linear algebraic equations that satisfies the second part of the statement 1 to have a solution is that the vector f be perpendicular to all of the solutions of the transposed homogeneous system of equations. With linear algebra it can be shown that this is also a sufficient condition, so we have the third statement:

Statement 3:

Given a system of inhomogeneous linear algebraic equations, for which the second part of the statement 1 is true, it will have a solution if and only if $\sum_i f_i z_i = 0$ for all the solutions z_i of the transposed homogeneous of the original system of the equations.

Note that in this case the solution to the inhomogeneous system of equations is not unique because adding any solution of the homogeneous system of equations to a solution of the inhomogeneous system of equations we can find new solutions.

Having these three statements in hand we can try to formulate corresponding theorems for integral equations:

Theorem 1: Given a Fredholm integral equation of the second kind it will either have a unique solution for any inhomogeneous part, or the corresponding homogeneous equation has at least one solution.

Theorem 2: For a given Fredholm integral equation of the second kind for which the first part of the statement 1 is true, the first part of the statement will also be true for the transposed equation.

Theorem 3: For a given Fredholm integral equation of the second kind for which the second part of the statement 1 is true, it will have a solution if and only if

$$\int f(q)z(q)dq = 0 \tag{B.12}$$

for any solution of the transposed homogeneous integral equation $z(q)$.

These theorems are called Fredholm theorems and are true for a large class of functions $f(p)$ and $K(q,p)$. Next I will prove these theorems for certain cases. Before doing that, I want to mention that in practice integral equations are numerically solved using the machinery described here. Even the Fadeev equations for *nd* scattering with infinite cutoff are solved by picking a very large cutoff (cutoff is very large if it is much larger than the characteristic energy scales of the scattering problem), then discretizing the integration interval, arriving at a system of linear algebraic equations, which can be solved numerically. In this process one usually hopes that increasing the cutoff and the number of mesh points will make the numerical solution converge, approaching to the actual solution. This happens, for example, for the quartet channel *nd* scattering amplitude. Sometimes the numerical solution does not show any sign of convergence though; it keeps oscillating as the cutoff increases. This happens, for example, for the LO doublet channel nd scattering and the LO three-boson system without three-body forces. This usually means that the renormalization of the theory is not done correctly and one needs to include more conterterms in the Lagrangian to make the scattering amplitude converge.

A very important class of integral equations arises when one considers so-called separable kernels which are of the form:

$$K(p,q) = \sum_{i=1}^{m} a_i(p) b_i(q). \tag{B.13}$$

Without loss of generality we can assume that all $a_i(p)$ are linearly independent and that all $b_i(q)$ are linearly independent. Substituting this into the equation we can see that the dependence of the function $y(p)$ on the variable p can be pulled out of the integral and determined easily:

$$y(p) = f(p) + \sum_{i=1}^{m} a_i(p) \int b_i(q) y(q) dq. \tag{B.14}$$

Denoting $\int b_i(q) y(q) dq = C_i$ we have:

$$y(p) = f(p) + \sum_{i=1}^{m} C_i a_i(p). \tag{B.15}$$

We have determined the dependence of $y(p)$ on p up to some undetermined constants C_i. To determine these constants we substitute this solution back into the equation finding:

$$f(p) + \sum_{i=1}^{m} C_i a_i(p) = f(p) + \sum_{i=1}^{m} a_i(p) \int b_i(q) [f(q) + \sum_{j=1}^{m} C_j a_j(q)] dq. \tag{B.16}$$

Canceling $f(p)$ from both sides and using the fact that $a_i(p)$ are linearly independent we find:

$$C_i = \int b_i(q) f(q) dq + \sum_{j=1}^{m} \int b_i(q) a_j(q) dq C_j \tag{B.17}$$

for any $0 \leqslant i \leqslant m$. Making the notations: $\int b_i(q)f(q)dq = f_i$ and $\int b_i(q)a_j(q)dq = K_{ij}$ we can put the last equation in the following form:

$$\sum_{j=1}^{m}(\delta_{ij} - K_{ij})C_j = f_i \tag{B.18}$$

for any $0 \leqslant i \leqslant m$. This is a system of linear algebraic equations for the unknown constants C_i. So we have proven that for this class of integral equation the solution can be actually reduced to the solution of an ordinary system of linear algebraic equations. It is easy to see that to any solution of the integral equation corresponds a unique solution to this system of linear algebraic equations and vise versa. Using this correspondence between the solutions of the integral equation and the solutions of the system of linear algebraic equations the Fredholm theorems can be proven easily for this class of integral equations.

Next let's consider integral equations which have "small" kernels and prove that for this class of equations the first part of the theorem 1 is always true, with smallness to be defined later. Before doing that let's introduce the following notation:

$$[K_2 \circ K_1](p,q) = \int K_2(p,s)K_1(s,q)ds. \tag{B.19}$$

It can be shown that if the two functions $K_1(p,q)$ and $K_2(p,q)$ are uniformly continuous then $[K_2 \circ K_1](p,q)$ is uniformly continuous also:

$$\begin{aligned} & |[K_2 \circ K_1](p_1,q_1) - [K_2 \circ K_1](p_2,q_2)| \\ = \ & |\int K_2(p_1,s)K_1(s,q_1)ds - \int K_2(p_2,s)K_1(s,q_2)ds| \\ \leqslant \ & |\int K_2(p_1,s)[K_1(s,q_1) - K_1(s,q_2)]ds| + |\int [K_2(p_1,s) - K_2(p_2,s)]K_1(s,q_2)ds.| \end{aligned} \tag{B.20}$$

Denoting the upper limit of the functions $K_1(p,q)$ and $K_2(p,q)$ by M, and the length of integration interval by L, we see that for any ϵ there is a δ such that for any $|p_1 - p_2| < \delta$

and $|q_1 - q_2| < \delta$:

$$|K_1(s, q_1) - K_1(s, q_2)| < \frac{\epsilon}{2ML} \tag{B.21}$$

and

$$|K_2(p_1, s) - K_2(p_2, s)| < \frac{\epsilon}{2ML}. \tag{B.22}$$

Substituting these inequalities into previous inequality we find that $|[K_2 \circ K_1](p_1, q_1) - [K_2 \circ K_1](p_2, q_2)| < \epsilon$, which proves the uniform continuity of the function $[K_2 \circ K_1](p, q)$.

Now let's take an integral equation of the following form:

$$y(p) = f(p) + \lambda \int K(p, q) y(q) dq, \tag{B.23}$$

with $K(p, q)$ and $f(p)$ uniformly continuous and λ some small parameter. A natural way of finding an approximate solution to the equation would be to do an interpolation. At the first step we would take $y(p) = f(p)$, then we would substitute this back into the same equation to find $y(p) = f(p) + \lambda \int K(p, q) f(q) dq$ etc., and we would hope that this sequence of functions eventually converges. Another way of finding the same formal solution would be do write the function $y(p)$ as series in powers of λ:

$$y(p) = y_0(p) + \lambda y_1(p) + \lambda^2 y_2(p) + ..., \tag{B.24}$$

then substitute this into the equation and match the coefficients of the powers of λ. After matching we find for the functions $y_k(p)$:

$$\begin{aligned} y_0(p) &= f(p) \\ y_{k+1}(p) &= \int K(p, q) y_k(q) dq, \quad k = 0, 1, 2, ... \end{aligned} \tag{B.25}$$

Doing the iterations it is easy to see:

$$y_k(p) = \int K^{(k)}(p, q) f(q) dq, \quad k = 1, 2, ... \tag{B.26}$$

where using the notation introduced above:

$$K^{(n)}(p,q) = K \circ K \circ \text{...n times...} \circ K \tag{B.27}$$

Using what we have proved earlier it can be shown that all the functions $K^{(k)}(p,q)$ and $y_k(p)$ are uniformly continuous. Denote the upper limit of the function $|K(p,q)|$ by M: $|K(p,q)| < M$, and the length of the integration interval by L. Using the definition of $K^{(k)}(p,q)$ we find:

$$K^{(k)}(p,q) \leqslant M^k L^{k-1} \tag{B.28}$$

As $f(p)$ is uniformly continuous too, we also have an upper limit for this function: $|f(p)| < F$. Using the definition of $y_k(p)$ we find an estimate:

$$|y_k(p)| \leqslant M^k L^k F. \tag{B.29}$$

Substituting this last equation into the equation (B.24) we find that this series will be uniformly convergent for all λ in the circle:

$$|\lambda| < \frac{1}{ML} \tag{B.30}$$

So as far as λ is in this circle the function $y(p)$ defined by the series (B.24) will be uniformly continuous and will satisfy the integral equation. To show that this solution is unique let's take two solutions $y_1(p)$ and $y_2(p)$ to our equation. Substituting these functions into the equation and subtracting from each other we find:

$$y_2(p) - y_1(p) = \lambda \int K(p,q)[y_2(q) - y_1(q)]dq \tag{B.31}$$

Denoting the upper limit of $|y_2(p) - y_1(p)|$ by Y we find:

$$Y \leqslant |\lambda| MLY = cY, \tag{B.32}$$

where $c = |\lambda| ML$. Now using $|\lambda| < \frac{1}{ML}$ we also have that $c \leqslant 1$. This can be consistent with the inequality (B.32) only if $Y = 0$. Hence the series solution that we find for the integral equation is unique.

So we have proven the Fredholm theorems for two kinds of kernels. More general case of uniformly continuous kernels is proven by noting that any uniformly continuous function $K(p, q)$ defined on a finite square can be approximated by a polynomial in powers of q and coefficients that are only functions of p and we already know how to deal with this kind of kernels. Then the difference of $K(p, q)$ and this approximating polynomial can be made arbitrarily small, which is also something that we have already covered.

B.2 Numerical methods

In practice the analytical methods introduced in the previous section of this appendix B.1 are not very useful for the equations that we encounter in the EFT$_{\not\pi}$, because the kernels of the integral equations are not separable. Instead we break the integration intervals into smaller intervals and numerically solve the system of linear algebraic equations obtained as described in section B.1. For definiteness let's consider the LO quartet channel equation again (see Eq. (B.33)).

$$t_0^l(k,p) = -\frac{y_t^2 M_N}{pk} Q_l\left(\frac{p^2+k^2-M_N E}{pk}\right)$$
$$- \frac{2}{\pi}\int_0^\Lambda dq q^2 t_0^l(k,q) \frac{1}{\sqrt{\frac{3q^2}{4} - M_N E - i\epsilon} - \gamma_t} \frac{1}{pq} Q_l\left(\frac{p^2+q^2-M_N E - i\epsilon}{pq}\right). \tag{B.33}$$

We can see that the integrand of the integral term in Eq. (B.33) has singularities along the real axis. Because of these singularities we need to increase the number of mesh points to make the solution to eventually converge numerically. Alternatively we could change the integration contour into the complex q plane. In doing so we need to make sure the new integration contour satisfies some conditions. Firstly it has to start and end at $q = 0$ and $q = \Lambda$, and secondly, in the region of the complex q plane separated by the new contour and the real axis our integrand has to have no singularities. Then by applying Cauchy's integral theorem we wouldn't have changed the value of the integral. We can put both of the variables q and p on this contour before solving the equation. Then after having the solution function on this contour we can substitute it into the same equation, but this time choosing p on the real axis, and we would get the solution on the real axis. The advantage of this approach is that if the new contour is chosen such that the integrand has no singularities on it, then we would need fewer mesh points to get a converging solution. This method of solving Faddeev equations was introduced by J.H. Hetherington and L.H. Schick [69]. The kernel in Eq. (B.33) has two sources of singularities. The first one is the deuteron propagator, which gives the singularity on the real axis. The second one is the function $Q_l\left(\frac{p^2+q^2-M_N E-i\epsilon}{pq}\right)$, which can give branch cuts on the complex plane which are not the real axis. Therefore the new contour has to be chosen appropriately, such that it avoids all of the singularities. This is done by investigating the analytical properties of the kernel of the integral equation [101]. For the equations we solve we choose the contour given in Fig. B.1 with $\phi = \tan^{-1}(\frac{2k}{\gamma_t})$ and the reference [101] shows that there are no singularities on this contour.

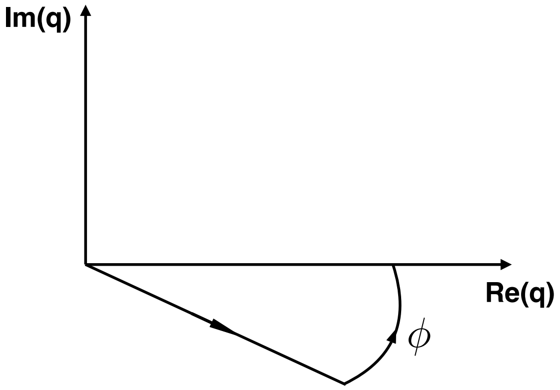

FIGURE B.1: The integration contour in the complex q plane.

Appendix C

Relevant integrals

C.1 Two-body P-wave contributions to nd scattering, one-loop diagram

The integrals that come up calculating the one-loop diagram with the two-body P-wave interactions are given in Eq. (C.1), Eq. (C.2) and Eq. (C.3). Here I will derive these integrals and give a couple general results.

$$
\begin{aligned}
I_{kl}(\vec{k},\vec{p},a^2,b^2) &= \int \frac{d^3q}{(2\pi)^3}\frac{1}{(\vec{q}-\frac{\vec{k}}{2})^2+a^2}\frac{1}{(\vec{q}-\frac{\vec{p}}{2})^2+b^2}\vec{q}_k\vec{q}_l \\
= &\quad \frac{4\pi}{3(2\pi)^3}\Lambda\delta_{kl} \\
- &\quad \frac{\pi^2}{4(2\pi)^3}\delta_{kl}\left\{a+b-\frac{4(a^2-b^2)^2}{(a+b)(\vec{k}-\vec{p})^2}+8\frac{\tan^{-1}(\alpha)}{|\vec{k}-\vec{p}|}\frac{(a^2-b^2)^2+(a^2+b^2)\frac{(\vec{k}-\vec{p})^2}{2}+\frac{(\vec{k}-\vec{p})^4}{16}}{(\vec{k}-\vec{p})^2}\right\} \\
- &\quad \frac{\pi^2}{4(2\pi)^3}k_kk_l\left\{\frac{12(a^2-b^2)^2}{(a+b)(\vec{k}-\vec{p})^4}+\frac{5a-3b}{(\vec{k}-\vec{p})^2}-8\frac{\tan^{-1}(\alpha)}{|\vec{k}-\vec{p}|}\frac{3(a^2-b^2)^2+(3a^2-b^2)\frac{(\vec{k}-\vec{p})^2}{2}+\frac{3(\vec{k}-\vec{p})^4}{16}}{(\vec{k}-\vec{p})^4}\right\} \\
- &\quad \frac{\pi^2}{4(2\pi)^3}p_kp_l\left\{\frac{12(b^2-a^2)^2}{(a+b)(\vec{k}-\vec{p})^4}+\frac{5b-3a}{(\vec{k}-\vec{p})^2}-8\frac{\tan^{-1}(\alpha)}{|\vec{k}-\vec{p}|}\frac{3(a^2-b^2)^2+(3b^2-a^2)\frac{(\vec{k}-\vec{p})^2}{2}+\frac{3(\vec{k}-\vec{p})^4}{16}}{(\vec{k}-\vec{p})^4}\right\} \\
+ &\quad \frac{\pi^2}{4(2\pi)^3}(k_kp_l+k_lp_k) \\
\times &\quad \left\{\frac{12(a^2-b^2)^2}{(a+b)(\vec{k}-\vec{p})^4}+\frac{a+b}{(\vec{k}-\vec{p})^2}-8\frac{\tan^{-1}(\alpha)}{|\vec{k}-\vec{p}|}\frac{3(a^2-b^2)^2+(a^2+b^2)\frac{(\vec{k}-\vec{p})^2}{2}-\frac{(\vec{k}-\vec{p})^4}{16}}{(\vec{k}-\vec{p})^4}\right\}
\end{aligned}
\tag{C.1}
$$

and:

$$
\begin{aligned}
I_l(\vec{k},\vec{p},a^2,b^2) &= \int \frac{d^3q}{(2\pi)^3}\frac{1}{(\vec{q}-\frac{\vec{k}}{2})^2+a^2}\frac{1}{(\vec{q}-\frac{\vec{p}}{2})^2+b^2}\vec{q}_l \\
= &\quad \frac{\pi}{(2\pi)^2}k_l\left\{\frac{b-a}{(\vec{k}-\vec{p})^2}+2\frac{\tan^{-1}(\alpha)}{|\vec{k}-\vec{p}|}\frac{(a^2-b^2)+\frac{(\vec{k}-\vec{p})^2}{4}}{(\vec{k}-\vec{p})^2}\right\} \\
+ &\quad \frac{\pi}{(2\pi)^2}p_l\left\{\frac{a-b}{(\vec{k}-\vec{p})^2}+2\frac{\tan^{-1}(\alpha)}{|\vec{k}-\vec{p}|}\frac{(b^2-a^2)+\frac{(\vec{k}-\vec{p})^2}{4}}{(\vec{k}-\vec{p})^2}\right\}
\end{aligned}
\tag{C.2}
$$

and:

$$I(\vec{k},\vec{p},a^2,b^2) = \int \frac{d^3q}{(2\pi)^3}\frac{1}{(\vec{q}-\frac{\vec{k}}{2})^2+a^2}\frac{1}{(\vec{q}-\frac{\vec{p}}{2})^2+b^2} = \frac{\pi^2}{(2\pi)^3}4\frac{\tan^{-1}(\alpha)}{|\vec{k}-\vec{p}|} \tag{C.3}$$

where

$$\alpha = \frac{|\vec{k}-\vec{p}|}{2(a+b)} \tag{C.4}$$

The integral given in (C.2) can be expressed in terms of (C.3), and integral given in (C.1) can be expressed in terms of (C.2) and (C.3) [102, 103]. To prove this let's take (C.1) and express it in terms of (C.2) and (C.3), the case of (C.2) will be analogous and simpler. Notice that in (C.1) we can change the integration variable $\vec{q} \to \vec{q} - \frac{\vec{p}}{2}$ to find it expressed in terms of (C.2) and (C.3) with appropriate parameters and the following integral: (after redefining $\frac{\vec{k}-\vec{p}}{2}$)

$$\int \frac{d^3q}{(2\pi)^3}\frac{1}{(\vec{q}-\frac{\vec{k}}{2})^2+a^2}\frac{1}{\vec{q}^{\,2}+b^2}\vec{q}_k\vec{q}_l \tag{C.5}$$

Now notice that the answer of this integral has to be of the following form:

$$I_{kl}(\vec{k},\vec{p},a^2,b^2) = A\delta_{kl} + Bk_kk_l \tag{C.6}$$

Where A and B are just rotational scalars. To find A and B we can contract both sides of the last equation with δ_{kl} and k_kk_l. This will give us the following two equations respectively:

$$\int \frac{d^3q}{(2\pi)^3}\frac{1}{(\vec{q}-\frac{\vec{k}}{2})^2+a^2}\frac{1}{\vec{q}^{\,2}+b^2}\vec{q}^{\,2} = 3A + B\vec{k}^2 \tag{C.7}$$

$$\int \frac{d^3q}{(2\pi)^3}\frac{1}{(\vec{q}-\frac{\vec{k}}{2})^2+a^2}\frac{1}{\vec{q}^{\,2}+b^2}(\vec{q}\cdot\vec{k})^2 = A\vec{k}^2 + B\vec{k}^4 \tag{C.8}$$

These equations give a system of linear algebraic equations for the constants A and B, but we first need to calculate the integrals in the left hand sides of these equations.

Let's first see how the calculation goes for the left hand side of the first equation. Adding and subtracting b^2 to the numerator the integral breaks into two:

$$\int \frac{d^3q}{(2\pi)^3} \frac{1}{(\vec{q}-\frac{\vec{k}}{2})^2+a^2} \frac{1}{\vec{q}^{\,2}+b^2} \vec{q}^{\,2} = \int \frac{d^3q}{(2\pi)^3} \frac{1}{(\vec{q}-\frac{\vec{k}}{2})^2+a^2} - b^2 \int \frac{d^3q}{(2\pi)^3} \frac{1}{(\vec{q}-\frac{\vec{k}}{2})^2+a^2} \frac{1}{\vec{q}^{\,2}+b^2} \tag{C.9}$$

The second integral here can be recognized as (C.3) and the first one can be calculated either directly or by replacing the integration variable to $\vec{q} \rightarrow \vec{q} - \frac{\vec{p}}{2}$ to give:

$$\int \frac{d^3q}{(2\pi)^3} \frac{1}{(\vec{q}-\frac{\vec{k}}{2})^2+a^2} = \frac{1}{2\pi^2}(\Lambda - \frac{a\pi}{2}) \tag{C.10}$$

where Λ is the cutoff for $|\vec{q}|$. Here and in what follows after we neglect all the positive powers of $\frac{1}{\Lambda}$.

Now lets turn to the calculation of the left hand side of the second equation in our system of equations for A and B. Here we can do the following substitution:

$$\vec{q}\cdot\vec{k} = -((\vec{q}-\frac{\vec{k}}{2})^2+a^2) + (\vec{q}^{\,2}+b^2) + \frac{k^2}{4} + a^2 - b^2 \tag{C.11}$$

After the substitution we find:

$$\begin{aligned} & \int \frac{d^3q}{(2\pi)^3} \frac{1}{(\vec{q}-\frac{\vec{k}}{2})^2+a^2} \frac{1}{\vec{q}^{\,2}+b^2} (\vec{q}\cdot\vec{k})^2 \\ = & \; -\int \frac{d^3q}{(2\pi)^3} \frac{1}{\vec{q}^{\,2}+b^2} \vec{q}\cdot\vec{k} + \int \frac{d^3q}{(2\pi)^3} \frac{1}{(\vec{q}-\frac{\vec{k}}{2})^2+a^2} \vec{q}\cdot\vec{k} \\ + & \; (\frac{k^2}{4}+a^2-b^2) \int \frac{d^3q}{(2\pi)^3} \frac{1}{(\vec{q}-\frac{\vec{k}}{2})^2+a^2} \frac{1}{\vec{q}^{\,2}+b^2} \vec{q}\cdot\vec{k} \end{aligned} \tag{C.12}$$

The first integral in this equation is obviously equal to zero, because of symmetry considerations. In the third integral we do the same substitution ($\vec{q}\cdot\vec{k} = -((\vec{q}-\frac{\vec{k}}{2})^2+a^2)+(\vec{q}^{\,2}+b^2)+\frac{\vec{k}^2}{4}+a^2-b^2$) to find:

$$\begin{aligned} &\int \frac{d^3q}{(2\pi)^3}\frac{1}{(\vec{q}-\frac{\vec{k}}{2})^2+a^2}\frac{1}{\vec{q}^{\,2}+b^2}\vec{q}\cdot\vec{k} \\ = &-\int \frac{d^3q}{(2\pi)^3}\frac{1}{\vec{q}^{\,2}+b^2}+\int \frac{d^3q}{(2\pi)^3}\frac{1}{(\vec{q}-\frac{\vec{k}}{2})^2+a^2} \\ + &\left(\frac{k^2}{4}+a^2-b^2\right)\int \frac{d^3q}{(2\pi)^3}\frac{1}{(\vec{q}-\frac{\vec{k}}{2})^2+a^2}\frac{1}{\vec{q}^{\,2}+b^2} \end{aligned} \tag{C.13}$$

Here we know the first two integrals and the third one is again given by (C.3).

The trickiest integral is the middle term in (C.12). The naive change of integration variable $\vec{q} \to \vec{q}-\frac{\vec{k}}{2}$ gives the result $\frac{k^2}{(2\pi)^2}(\Lambda - \frac{a\pi}{2})$, which has the correct finite piece but incorrect infinite piece. The problem is that after the shift of the integration variable the integrand looks rotationally symmetric, but as the limits of the integration are changed also, this symmetry is just illusionary. This means that the change of variables is of course allowed, but one has to be careful about changing the limits of integration too. For example after the mentioned change of variables the integral breaks into two parts one of which seem to be the same as the first terms in (C.12) and hence it should be zero, but it is in fact a different integral and is not equal to zero. Instead of changing the integration variables, I calculated this integral directly integrating first over ϕ then θ then q, and I got the following result:

$$\int \frac{d^3q}{(2\pi)^3}\frac{1}{(\vec{q}-\frac{\vec{k}}{2})^2+a^2}\vec{q}\cdot\vec{k} = \frac{1}{6\pi^2}k^2\Lambda - \frac{ak^2}{8\pi} \tag{C.14}$$

So putting everything together we are able to solve the system of equations (C.7) and (C.8) for the constants A and B and from there it is easy to get to the answer of the integral in (C.1).

There is a simpler way to calculate the integral in (C.14), then the direct integration over the angles and the magnitude. To describe this I will need to use a lemma proven in what follows.

The discussion here is based on the following lemma.

Lemma: Suppose there is a function of one variable $f(x)$ that is analytic near infinity and integrable on any given interval on the real axes. Construct the following two functions of Λ:

$$\int_{-\Lambda}^{\Lambda} f(x)dx \tag{C.15}$$

and

$$\int_{-\Lambda+a}^{\Lambda+a} f(x)dx \tag{C.16}$$

where Λ and $a < \Lambda$ are arbitrary positive numbers such that $f(x)$ is analytic outside of a circle with radius smaller than $\Lambda - a$. Then the difference of the two functions (C.15) and (C.16) is an analytic function of Λ near infinity and its series does not contain the $\Lambda-$free term.

Basically this lemma is just stating that after the shift of the integration limits the constant part of the integral does not change and only the non-zero powers of the infinity change. Note that the integral in (C.16) is the same as $\int_{-\Lambda}^{\Lambda} f(x+a)dx$, so we can rephrase the statement in the lemma saying that the $\Lambda-$free term in the series of the function $\int_{-\Lambda}^{\Lambda}(f(x) - f(x-a))dx$ is zero. The generalization of this lemma will state that the $\Lambda-$free term of the series of the function $\int(f(\vec{q}) - f(\vec{q}-\vec{k}))d^3q$ is zero, where the integration is done over a three dimensional ball of radius Λ. This generalized version can be used to calculate the infinite part of the integral (C.14) without any change of variables, then to calculate the finite part of it after changing the variables $\vec{q} \to \vec{q} - \frac{\vec{k}}{2}$, but not changing the limits of integration, as we know that the finite part is the same before and after the change of variables.

Proof of Lemma: Let's do the following calculation:

$$\begin{aligned}
& \int_{-\Lambda}^{\Lambda} f(x)dx - \int_{-\Lambda+a}^{\Lambda+a} f(x)dx \\
= & \int_{-\Lambda}^{-\Lambda+a} f(x)dx + \int_{-\Lambda+a}^{\Lambda} f(x)dx - \int_{-\Lambda+a}^{\Lambda} f(x)dx - \int_{\Lambda}^{\Lambda+a} f(x)dx \\
= & \int_{-\Lambda}^{-\Lambda+a} f(x)dx - \int_{\Lambda}^{\Lambda+a} f(x)dx
\end{aligned} \tag{C.17}$$

In both of those integrals the integration variable x is such that $|x| > \Lambda - a$, hence $f(x)$ is analytic and can be written as:

$$f(x) = \sum_{n=-\infty}^{\infty} a_n x^n \tag{C.18}$$

At this point we can see that the first statement in the lemma is a statement from complex analysis: any integral of an analytic function in the region of its analyticity is an analytic function.

Substituting this into the equation (C.17) we get:

$$
\begin{aligned}
& \int_{-\Lambda}^{\Lambda} f(x)dx - \int_{-\Lambda+a}^{\Lambda+a} f(x)dx \\
= \quad & \int_{-\Lambda}^{-\Lambda+a} \sum_{n=-\infty}^{\infty} a_n x^n dx - \int_{\Lambda}^{\Lambda+a} \sum_{n=-\infty}^{\infty} a_n x^n dx \\
= \quad & a_{-1} \int_{-\Lambda}^{-\Lambda+a} \frac{1}{x} dx - a_{-1} \int_{\Lambda}^{\Lambda+a} \frac{1}{x} dx \\
+ \quad & \sum_{n\neq -1} a_n \int_{-\Lambda}^{-\Lambda+a} x^n dx - \sum_{n\neq -1} a_n \int_{\Lambda}^{\Lambda+a} x^n dx
\end{aligned}
\tag{C.19}
$$

The first line of this equation, after doing the integration can be simplified into $\log\big(1 - \frac{2a}{\Lambda+a}\big)$, which goes to zero as $\Lambda \to \infty$ and hence contains only negative powers of Λ and the constant term is zero. The second line can be written as:

$$
\begin{aligned}
& \sum_{n\neq -1} a_n \int_{-\Lambda}^{-\Lambda+a} x^n dx - \sum_{n\neq -1} a_n \int_{\Lambda}^{\Lambda+a} x^n dx \\
= \quad & \sum_{n<-1} a_n \int_{-\Lambda}^{-\Lambda+a} x^n dx - \sum_{n<-1} a_n \int_{\Lambda}^{\Lambda+a} x^n dx \\
+ \quad & \sum_{n>-1} a_n \int_{-\Lambda}^{-\Lambda+a} x^n dx - \sum_{n>-1} a_n \int_{\Lambda}^{\Lambda+a} x^n dx
\end{aligned}
\tag{C.20}
$$

and after doing the integration:

$$
\begin{aligned}
& \sum_{n\neq -1} a_n \int_{-\Lambda}^{-\Lambda+a} x^n dx - \sum_{n\neq -1} a_n \int_{\Lambda}^{\Lambda+a} x^n dx \\
= \; & \sum_{n<-1} \frac{a_n}{n+1}((-\Lambda+a)^{n+1} - (-\Lambda)^{n+1} - (\Lambda+a)^{n+1} + \Lambda^{n+1}) \\
+ \; & \sum_{n>-1} \frac{a_n}{n+1}((-\Lambda+a)^{n+1} - (-\Lambda)^{n+1} - (\Lambda+a)^{n+1} + \Lambda^{n+1})
\end{aligned}
\tag{C.21}
$$

All the summands in the sum of the first line of the last equation go to zero as Λ → ∞ and hence, with the same argument as in the first line of the equation (C.19), this line contains only negative powers of Λ and the constant term is zero. In the second line we can open the brackets and it becomes obvious that for any given n the constant term in the first term cancels the constant term in the third term.

A much easier way to prove the much stronger version of the second statement of the lemma is to notice that the difference function is an odd function of Λ, hence when put into series in powers of Λ it will only have odd powers. This proves that only the odd powers of Λ change and all the even powers do not. □

The applications of this lemma go beyond the calculation of the integral (C.14), for example many of the steps of the calculation of the integrals given in (C.3), (C.2) and (C.1) are justified by this. More generally in Feynman parameter technique a change of the integration variable always occurs, which in principal may lead to an alteration of the answer and it is not always well explained why it does not. Also in dimensional regularization it is always considered that the same kind of change of variables is always allowed and this lemma can serve as a justification for that, because in dimensional regularization the dimension of the space is rendered such that the integrals always converge, hence they only have the finite part, which according to the lemma does not change.

The generalization of the lemma to the higher dimensional integrals needs to be verified in the future.

The integral (C.3) can be calculated using position space techniques [104, 105]. The idea is to use Fourier transformations. First note that:

$$\int d^3x \frac{e^{-a|\vec{x}|}}{|\vec{x}|} e^{i(\vec{q}+\frac{\vec{k}}{2})\cdot\vec{x}} = \frac{4\pi i}{a^2 + (\vec{q}+\frac{\vec{k}}{2})^2} \tag{C.22}$$

using this the integral (C.3) can be written as:

$$\begin{aligned} I(\vec{k},\vec{p},a^2,b^2) &= \int \frac{d^3q}{(2\pi)^3} \frac{1}{(\vec{q}-\frac{\vec{k}}{2})^2 + a^2} \frac{1}{(\vec{q}-\frac{\vec{p}}{2})^2 + b^2} \\ = \quad & -\frac{1}{(4\pi)^2} \int \frac{d^3q}{(2\pi)^3} \int d^3x \frac{e^{-a|\vec{x}|}}{|\vec{x}|} e^{i(\vec{q}-\frac{\vec{k}}{2})\cdot\vec{x}} \int d^3y \frac{e^{-b|\vec{y}|}}{|\vec{y}|} e^{i(\vec{q}-\frac{\vec{p}}{2})\cdot\vec{y}} \end{aligned} \tag{C.23}$$

Where $\vec{x}$ and $\vec{y}$ are three dimensional spatial vectors. Doing the $\vec{q}$ integration first we find a delta function of the vector $\vec{x}+\vec{y}$, which then can be used to do the $\vec{y}$ integration. After that the $\vec{x}$ integration becomes trivial giving the result in (C.3).

C.2 Magnetic photon exchange diagrams

In the *nd* elastic scattering process there is only one electrically charged particle, the proton, so we don't have Coulomb interaction diagrams, but the neutrons and the proton can interact through their magnetic moments. These interactions are given by the Lagrangian in Eq. (C.24) [106]:

$$\mathcal{L}_B = \frac{e}{2M_N} N^\dagger(\kappa_0 + \kappa_1\tau_3)\vec{\sigma}\cdot\vec{B}N \tag{C.24}$$

where κ_0 and κ_1 are the magnetic moments of the neutron and the proton, and $\vec{B}$ is given by the vector potential $\vec{B} = \vec{\nabla} \times \vec{A}$. The diagrams that contribute to *nd* scattering and involve this interaction vertex are of higher order than N^{3}LO, so they are not included in our calculations. Some of the lowest order diagrams that involve this interaction contribute at N^{5}LO and are given in Fig. C.1.

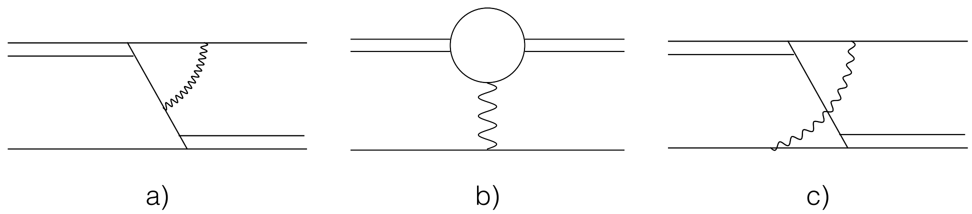

FIGURE C.1: Magnetic photon exchange contributions.

To see that these diagrams contribute at N^{5}LO let's use the rules described in Section 3.4: the diagrams have two dNN vertices together scaling as $\sim y_t^2 \sim \frac{1}{M}$, three nucleon propagators $\sim \frac{M^3}{Q^6}$, one photon propagator $\sim \frac{1}{Q^2}$, a non-relativistic loop integration $\sim \frac{Q^5}{M}$, and two photon vertices $\sim \alpha(\frac{Q}{M})^2$, where α is the fine structure constant and it can be approximated as $\alpha \sim 0.01$. Putting all of these together we get for the magnetic-photon diagrams' scaling: $\sim \alpha\frac{1}{MQ}$. As we work at energy scales where the power counting parameter is about $\frac{Q}{M} \sim 0.3$ we can estimate the scaling of the fine structure constant as $\alpha \sim (\frac{Q}{M})^4$. Substituting this we find for the scaling of the diagrams: $\sim (\frac{Q}{M})^5\frac{1}{Q^2}$. Recalling that the LO contributions scale as $\sim \frac{1}{Q^2}$, we see that the magnetic-moment diagrams contribute at N^{5}LO.

As I already mentioned we have not included the contributions from these diagrams in our calculation of the N^{3}LO nd scattering amplitude, but we have calculated them and they can be useful in the future, for the higher order calculations of this amplitude. Here I will just mention that the spin-isospin projections of these diagrams is done by using all the techniques described in Appendix A and they pose no extra complications. The integration part of the first two diagrams a) and b) is done using the integrals Eqs.(C.3), (C.2) and (C.1) given in the first section of this appendix. The only new complication that we encounter comes from the loop-integration part of the diagram c). A new type of integral needs to be calculated which is given by:

$$I_c(\vec{k},\vec{p},a^2,b^2) = \int \frac{d^3q}{(2\pi)^3}\frac{1}{q^2}\frac{1}{(\vec{q}-\frac{\vec{k}}{2})^2+a^2}\frac{1}{(\vec{q}-\frac{\vec{p}}{2})^2+b^2}. \tag{C.25}$$

Note that the only difference between this integral and the one in Eq. (C.3) is the extra denominator $\frac{1}{q^2}$ that come from the photon propagator. The integral in Eq. (C.3) can be calculated using position space techniques, as described earlier, or it can also be done using Feynman parametrization. Neither of these approaches works for Eq. (C.25). Using the position space techniques, after using the delta function that comes from integrating over $\vec{q}$ we get two more integrals left as opposed to one when doing Eq. (C.3) and it doesn't seem to show any way to proceed. Using Feynman parametrization we get two parameters as opposed to one when doing Eq. (C.3), the integration over the first parameter is fairly simple, but it gives expressions involving square roots and arctan functions. After that we have one more parameter left in the integral, and it shows no hope of being integrable in a closed form. So a new approach is necessary if we want to find a closed form for this integral. I found a simple change of integration variable that simplifies it considerably and expresses it in terms of Eq. (C.3). Defining a new vector:

$$\vec{l} = \frac{\hat{q}}{|\vec{q}|} \tag{C.26}$$

we can change the integration over $\vec{q}$ to an integration over $\vec{l}$ finding:

$$I_c(\vec{k},\vec{p},a^2,b^2) = \int \frac{d^3q}{(2\pi)^3}\frac{1}{q^2}\frac{1}{(\vec{q}-\frac{\vec{k}}{2})^2+a^2}\frac{1}{(\vec{q}-\frac{\vec{p}}{2})^2+b^2}$$

$$= \frac{1}{\kappa_1^2\kappa_2^2}\int \frac{d^3l}{(2\pi)^3}\frac{1}{(\vec{l}-\frac{\vec{k}}{2\kappa_1^2})^2+\frac{a^2}{\kappa_1^4}}\frac{1}{(\vec{l}-\frac{\vec{p}}{2\kappa_2^2})^2+\frac{b^2}{\kappa_2^4}}, \tag{C.27}$$

where

$$\kappa_1^2 = a^2 + \frac{k^2}{2} \tag{C.28}$$

and

$$\kappa_2^2 = b^2 + \frac{p^2}{2}. \tag{C.29}$$

The last line of Eq. (C.27) is just the integral Eq. (C.3), so we get the final answer:

$$I_c(\vec{k},\vec{p},a^2,b^2) = \frac{1}{\kappa_1^2\kappa_2^2} I\left(\frac{\vec{k}}{2\kappa_1^2},\frac{\vec{p}}{2\kappa_2^2},\frac{a^2}{\kappa_1^4},\frac{b^2}{\kappa_2^4}\right) = \frac{1}{2\pi\kappa_1^2\kappa_2^2}\frac{1}{|\frac{\vec{k}}{\kappa_1^2}-\frac{\vec{p}}{\kappa_2^2}|}\tan^{-1}\left(\frac{|\frac{\vec{k}}{\kappa_1^2}-\frac{\vec{p}}{\kappa_2^2}|}{2(\frac{a}{\kappa_1^2}+\frac{b}{\kappa_2^2})}\right). \tag{C.30}$$

Bibliography

[1] Michael E Peskin and Daniel V Schroeder. *An Introduction to Quantum Field Theory; 1995 ed.* Westview, Boulder, CO, 1995. URL `https://cds.cern.ch/record/257493`. Includes exercises.

[2] Steven Weinberg. *The quantum theory of fields. Vol. 2: Modern applications.* Cambridge University Press, 2013. ISBN 9781139632478, 9780521670548, 9780521550024.

[3] Kenneth G. Wilson. Quantum Chromodynamics on a Lattice. In *Cargese Summer Institute: New Developments in Quantum Field Theory and Statistical Mechanics Cargese, France, July 12-31, 1976*, page 0143, 1977.

[4] Hideki Yukawa. On the Interaction of Elementary Particles I. *Proc. Phys. Math. Soc. Jap.*, 17:48–57, 1935. doi: 10.1143/PTPS.1.1. [Prog. Theor. Phys. Suppl.1,1(1935)].

[5] V. G. J. Stoks, R. A. M. Klomp, C. P. F. Terheggen, and J. J. de Swart. Construction of high quality N N potential models. *Phys. Rev.*, C49:2950–2962, 1994. doi: 10.1103/PhysRevC.49.2950.

[6] Roderick V. Reid, Jr. Local phenomenological nucleon-nucleon potentials. *Annals Phys.*, 50:411–448, 1968. doi: 10.1016/0003-4916(68)90126-7.

[7] M. M Nagels, T. A. Rijken, and J. J De Swart. N n Potential from Regge Pole Theory. pages 17–18, 1978.

[8] R. B. Wiringa, V. G. J. Stoks, and R. Schiavilla. Accurate nucleon-nucleon potential with charge-independence breaking. *Phys. Rev. C*, 51:38–51, Jan 1995. doi: 10.1103/PhysRevC.51.38. URL `https://link.aps.org/doi/10.1103/PhysRevC.51.38`.

[9] Silas R. Beane, Paulo F. Bedaque, Wick C. Haxton, Daniel R. Phillips, and Martin J. Savage. From hadrons to nuclei: Crossing the border. 2000. doi: 10.1142/9789812810458_0011.

[10] David B. Kaplan, Martin J. Savage, and Mark B. Wise. Two nucleon systems from effective field theory. *Nucl. Phys.*, B534:329–355, 1998. doi: 10.1016/S0550-3213(98)00440-4.

[11] Paulo F. Bedaque and Harald W. Griesshammer. Quartet S wave neutron deuteron scattering in effective field theory. *Nucl. Phys.*, A671:357–379, 2000. doi: 10.1016/S0375-9474(99)00691-0.

[12] Harald W. Griesshammer. Improved convergence in the three-nucleon system at very low energies. *Nucl. Phys.*, A744:192–226, 2004. doi: 10.1016/j.nuclphysa.2004.08.012.

[13] Daniel R. Phillips, Gautam Rupak, and Martin J. Savage. Improving the convergence of N N effective field theory. *Phys. Lett.*, B473:209–218, 2000. doi: 10.1016/S0370-2693(99)01496-3.

[14] Jared Vanasse. Three-body systems in pionless effective field theory. *Int. J. Mod. Phys.*, E25(05):1641002, 2016. doi: 10.1142/S0218301316410020.

[15] Paulo F. Bedaque, H. W. Hammer, and U. van Kolck. Effective theory of the triton. *Nucl. Phys.*, A676:357–370, 2000. doi: 10.1016/S0375-9474(00)00205-0.

[16] Chen Ji and Daniel R. Phillips. Effective Field Theory Analysis of Three-Boson Systems at Next-To-Next-To-Leading Order. *Few Body Syst.*, 54:2317–2355, 2013. doi: 10.1007/s00601-013-0710-5.

[17] Harald W. Griesshammer. Naive dimensional analysis for three-body forces without pions. *Nucl. Phys.*, A760:110–138, 2005. doi: 10.1016/j.nuclphysa.2005.05.202.

[18] Jared Vanasse. Fully Perturbative Calculation of *nd* Scattering to Next-to-next-to-leading-order. *Phys. Rev.*, C88(4):044001, 2013. doi: 10.1103/PhysRevC.88.044001.

[19] Steven Weinberg. Phenomenological Lagrangians. *Physica*, A96:327–340, 1979. doi: 10.1016/0378-4371(79)90223-1.

[20] V. Bernard, Norbert Kaiser, and Ulf-G. Meissner. Chiral dynamics in nucleons and nuclei. *Int. J. Mod. Phys.*, E4:193–346, 1995. doi: 10.1142/S0218301395000092.

[21] Steven Weinberg. Nuclear forces from chiral Lagrangians. *Phys. Lett.*, B251:288–292, 1990. doi: 10.1016/0370-2693(90)90938-3.

[22] U. van Kolck. Few nucleon forces from chiral Lagrangians. *Phys. Rev.*, C49:2932–2941, 1994. doi: 10.1103/PhysRevC.49.2932.

[23] R. Machleidt and D. R. Entem. Chiral effective field theory and nuclear forces. *Phys. Rept.*, 503:1–75, 2011. doi: 10.1016/j.physrep.2011.02.001.

[24] A. Nogga, R. G. E. Timmermans, and U. van Kolck. Renormalization of one-pion exchange and power counting. *Phys. Rev.*, C72:054006, 2005. doi: 10.1103/PhysRevC.72.054006.

[25] Deepshikha Choudhury, Andreas Nogga, and Daniel R. Phillips. Investigating neutron polarizabilities through Compton scattering on He-3. *Phys. Rev. Lett.*, 98:232303, 2007. doi: 10.1103/PhysRevLett.98.232303.

[26] Deepshikha Shukla, Andreas Nogga, and Daniel R. Phillips. Analyzing the Effects of Neutron Polarizabilities in Elastic Compton Scattering off He-3. *Nucl. Phys.*, A819: 98–134, 2009. doi: 10.1016/j.nuclphysa.2009.01.003.

[27] Harald W. Griesshammer, Judith A. McGovern, and Daniel R. Phillips. Nucleon Polarisabilities at and Beyond Physical Pion Masses. *Eur. Phys. J.*, A52(5):139, 2016. doi: 10.1140/epja/i2016-16139-5.

[28] Vladimir Pascalutsa and Daniel R. Phillips. Effective theory of the delta(1232) in Compton scattering off the nucleon. *Phys. Rev.*, C67:055202, 2003. doi: 10.1103/PhysRevC.67.055202.

[29] S. R. Beane, M. Malheiro, Daniel R. Phillips, and U. van Kolck. Compton scattering on the deuteron in baryon chiral perturbation theory. *Nucl. Phys.*, A656:367–399, 1999. doi: 10.1016/S0375-9474(99)00312-7.

[30] Robert P. Hildebrandt, Harald W. Griesshammer, Thomas R. Hemmert, and Barbara Pasquini. Signatures of chiral dynamics in low-energy compton scattering off the nucleon. *Eur. Phys. J.*, A20:293–315, 2004. doi: 10.1140/epja/i2003-10144-9.

[31] S.R. Beane, M. Malheiro, J.A. McGovern, D.R. Phillips, and U. van Kolck. Compton scattering on the proton, neutron, and deuteron in chiral perturbation theory to o(q4). *Nuclear Physics A*, 747(2):311 – 361, 2005. ISSN 0375-9474. doi: http://dx.doi.org/10.1016/j.nuclphysa.2004.09.068. URL `http://www.sciencedirect.com/science/article/pii/S0375947404010279`.

[32] Nathan Isgur and Mark B. Wise. Weak decays of heavy mesons in the static quark approximation. *Physics Letters B*, 232(1):113 – 117, 1989. ISSN 0370-2693. doi: http://dx.doi.org/10.1016/0370-2693(89)90566-2. URL `http://www.sciencedirect.com/science/article/pii/0370269389905662`.

[33] Howard Georgi. An effective field theory for heavy quarks at low energies. *Physics Letters B*, 240(3):447 – 450, 1990. ISSN 0370-2693. doi: http://dx.doi.org/10.1016/0370-2693(90)91128-X. URL `http://www.sciencedirect.com/science/article/pii/037026939091128X`.

[34] Mark B. Wise. Chiral perturbation theory for hadrons containing a heavy quark. *Phys. Rev. D*, 45:R2188–R2191, Apr 1992. doi: 10.1103/PhysRevD.45.R2188. URL `https://link.aps.org/doi/10.1103/PhysRevD.45.R2188`.

[35] Mark B. Wise. Combining chiral and heavy quark symmetry. In *Particle physics at the Fermi scale. Proceedings, CCAST (World Laboratory) Symposium/Workshop, Beijing, P.R. China, May 27 - June 4, 1993*, pages 71–114, 1993.

[36] Adam F. Falk. Hadrons of arbitrary spin in the heavy quark effective theory. *Nucl. Phys.*, B378:79–94, 1992. doi: 10.1016/0550-3213(92)90004-U.

[37] Fulvia De Fazio. Radiative transitions of heavy quarkonium states. *Phys. Rev.*, D79: 054015, 2009. doi: 10.1103/PhysRevD.83.099901,10.1103/PhysRevD.79.054015. [Erratum: Phys. Rev.D83,099901(2011)].

[38] S. Fleming, M. Kusunoki, T. Mehen, and U. van Kolck. Pion interactions in the $X(3872)$. *Phys. Rev.*, D76:034006, 2007. doi: 10.1103/PhysRevD.76.034006.

[39] S. K. Choi et al. Observation of a narrow charmonium - like state in exclusive B+- —> K+- pi+ pi- J / psi decays. *Phys. Rev. Lett.*, 91:262001, 2003. doi: 10.1103/PhysRevLett.91.262001.

[40] D. Acosta et al. Observation of the narrow state $X(3872) \to J/\psi\pi^+\pi^-$ in $\bar{p}p$ collisions at $\sqrt{s} = 1.96$ TeV. *Phys. Rev. Lett.*, 93:072001, 2004. doi: 10.1103/PhysRevLett.93.072001.

[41] V. M. Abazov et al. Observation and properties of the $X(3872)$ decaying to $J/\psi\pi^+\pi^-$ in $p\bar{p}$ collisions at $\sqrt{s} = 1.96$ TeV. *Phys. Rev. Lett.*, 93:162002, 2004. doi: 10.1103/PhysRevLett.93.162002.

[42] Bernard Aubert et al. Study of the $B \to J/\psi K^-\pi^+\pi^-$ decay and measurement of the $B \to X(3872)K^-$ branching fraction. *Phys. Rev.*, D71:071103, 2005. doi: 10.1103/PhysRevD.71.071103.

[43] R. Aaij et al. Observation of $X(3872)$ production in pp collisions at $\sqrt{s} = 7$ TeV. *Eur. Phys. J.*, C72:1972, 2012. doi: 10.1140/epjc/s10052-012-1972-7.

[44] Arman Margaryan and Roxanne P. Springer. Using the decay $\psi(4160) \to X(3872)\gamma$ to probe the molecular content of the X(3872). *Phys. Rev.*, D88(1):014017, 2013. doi: 10.1103/PhysRevD.88.014017.

[45] Thomas Mehen and Roxanne Springer. Radiative Decays $X(3872) \to \psi(2S)\gamma$ and $\psi(4040) \to X(3872)\gamma$ in Effective Field Theory. *Phys. Rev.*, D83:094009, 2011. doi: 10.1103/PhysRevD.83.094009.

[46] Christian W. Bauer, Sean Fleming, and Michael E. Luke. Summing Sudakov logarithms in B —> X(s gamma) in effective field theory. *Phys. Rev.*, D63:014006, 2000. doi: 10.1103/PhysRevD.63.014006.

[47] Adam K. Leibovich, Zoltan Ligeti, and Mark B. Wise. Comment on quark masses in SCET. *Phys. Lett.*, B564:231–234, 2003. doi: 10.1016/S0370-2693(03)00565-3.

[48] Paulo F. Bedaque and Ubirajara van Kolck. Effective field theory for few nucleon systems. *Ann. Rev. Nucl. Part. Sci.*, 52:339–396, 2002. doi: 10.1146/annurev.nucl.52.050102.090637.

[49] V. G. J. Stoks, R. A. M. Klomp, M. C. M. Rentmeester, and J. J. de Swart. Partial wave analaysis of all nucleon-nucleon scattering data below 350-MeV. *Phys. Rev.*, C48: 792–815, 1993. doi: 10.1103/PhysRevC.48.792.

[50] L. D. Faddeev. Scattering theory for a three particle system. *Sov. Phys. JETP*, 12: 1014–1019, 1961. [Zh. Eksp. Teor. Fiz.39,1459(1960)].

[51] W. Tornow, P. W. Lisowski, R. C. Byrd, and R. L. Walter. The analyzing power A ? (?) for the elastic scattering of 12 MeV neutrons from deuterons. *Nucl. Phys.*, A296: 23–49, 1978. doi: 10.1016/0375-9474(78)90411-6.

[52] W. Tornow, C. R. Howell, R. C. Byrd, R. S. Pedroni, and R. L. Walter. Analyzing Power Measurements for (H-2 (npol, n) H-2) Scattering at 10 MeV Compared to Few-Nucleon Calculations and Data for (H-2 (ppol, p) H-2) Scattering. *Phys. Rev. Lett.*, 49:312–315, 1982. doi: 10.1103/PhysRevLett.49.312.

[53] W. Tornow, R. C. Byrd, C. R. Howell, R. S. Pedroni, and R. L. Walter. Measurements of analyzing power for H-2 (n—>, n) H-2 scattering at 14.1 MeV and comparisons to H-2 (p—>, p) H-2. *Phys. Rev.*, C27:2439–2442, 1983. doi: 10.1103/PhysRevC.27.2439.

[54] C. R. Howell, W. Tornow, K. Murphy, H. G. Pfützner, M. L. Roberts, Anli Li, P. D. Felsher, R. L. Walter, I. Šlaus, P. A. Treado, and Y. Koike. Comparisons of vector analyzing-power data and calculations for neutron-deuteron elastic scattering from 10 to 14 mev. *Few-Body Systems*, 2(1):19–32, 1987. ISSN 1432-5411. doi: 10.1007/BF01078989. URL `http://dx.doi.org/10.1007/BF01078989`.

[55] D. R. Entem, R. Machleidt, and H. Witala. Chiral NN model and A(y) puzzle. *Phys. Rev.*, C65:064005, 2002. doi: 10.1103/PhysRevC.65.064005.

[56] A. Kievsky, S. Rosati, W. Tornow, and M. Viviani. Critical comparison of experimental data and theoretical predictions for nucleon deuteron scattering below the breakup threshold. *Nucl. Phys. A*, 607:402–424, 1996. doi: 10.1016/0375-9474(96)00240-0.

[57] J. E. McAninch, L. O. Lamm, and W. Haeberli. Analyzing power in neutron-deuteron elastic scattering at Elabn=3 MeV. *Phys. Rev.*, C50:589–601, 1994. doi: 10.1103/PhysRevC.50.589.

[58] H. Witała, W. Glöckle, and T. Cornelius. Rigorous faddeev calculations for elastic neutron-deuteron scattering around 8 mev c.m. energy. *Nuclear Physics A*, 491(2):157 – 172, 1989. ISSN 0375-9474. doi: http://dx.doi.org/10.1016/0375-9474(89)90696-9. URL `http://www.sciencedirect.com/science/article/pii/0375947489906969`.

[59] D. Huber and James Lewis Friar. The A_y puzzle and the nuclear force. *Phys. Rev.*, C58:674–685, 1998. doi: 10.1103/PhysRevC.58.674.

[60] E. Epelbaum, H. Kamada, A. Nogga, H. Witała, W. Glöckle, and Ulf-G. Meißner. Three- and four-nucleon systems from chiral effective field theory. *Phys. Rev. Lett.*, 86: 4787–4790, May 2001. doi: 10.1103/PhysRevLett.86.4787. URL `https://link.aps.org/doi/10.1103/PhysRevLett.86.4787`.

[61] A. Kievsky, M. Viviani, and S. Rosati. Cross section, polarization observables, and phase-shift parameters in p-d and n-d elastic scattering. *Phys. Rev. C*, 52:R15–R19, Jul 1995. doi: 10.1103/PhysRevC.52.R15. URL `https://link.aps.org/doi/10.1103/PhysRevC.52.R15`.

[62] A. Kievsky. *Variational Calculations for Continuum States in Few-Nucleon Systems*, pages 405–409. Springer Vienna, Vienna, 1996. ISBN 978-3-7091-9453-9. doi: 10.1007/978-3-7091-9453-9_59. URL `http://dx.doi.org/10.1007/978-3-7091-9453-9_59`.

[63] R Blankenbecler, M.L Goldberger, N.N Khuri, and S.B Treiman. Mandelstam representation for potential scattering. *Annals of Physics*, 10(1):62 – 93, 1960. ISSN 0003-4916. doi: http://dx.doi.org/10.1016/0003-4916(60)90016-6. URL `http://www.sciencedirect.com/science/article/pii/0003491660900166`.

[64] John M. Blatt and J. David Jackson. On the interpretation of neutron-proton scattering data by the schwinger variational method. *Phys. Rev.*, 76:18–37, Jul 1949. doi: 10.1103/PhysRev.76.18. URL `https://link.aps.org/doi/10.1103/PhysRev.76.18`.

[65] David B. Kaplan, Martin J. Savage, and Mark B. Wise. A New expansion for nucleon-nucleon interactions. *Phys. Lett.*, B424:390–396, 1998. doi: 10.1016/S0370-2693(98)00210-X.

[66] Jared Vanasse, David A. Egolf, John Kerin, Sebastian König, and Roxanne P. Springer. ^{3}He and *pd* Scattering to Next-to-Leading Order in Pionless Effective Field Theory. *Phys. Rev.*, C89(6):064003, 2014. doi: 10.1103/PhysRevC.89.064003.

[67] Jared Vanasse. Triton charge radius to next-to-next-to-leading order in pionless effective field theory. *Phys. Rev.*, C95(2):024002, 2017. doi: 10.1103/PhysRevC.95.024002.

[68] G.V.Skornyakov and K.A.Ter-Martirosian. *Sov. Phys.JETP*, 4, 1957.

[69] J. H. Hetherington and L. H. Schick. Exact multiple-scattering analysis of low-energy elastic $K^- - d$ scattering with separable potentials. *Phys. Rev.*, 137:B935–B948, Feb 1965. doi: 10.1103/PhysRev.137.B935. URL `https://link.aps.org/doi/10.1103/PhysRev.137.B935`.

[70] Paulo F. Bedaque, H. W. Hammer, and U. van Kolck. The Three boson system with short range interactions. *Nucl. Phys.*, A646:444–466, 1999. doi: 10.1016/S0375-9474(98)00650-2.

[71] PhD dissertation: Ji, C. Universality and Beyond: Effective Field Theory for Three-Body Physics in Cold Atoms and Halo Nuclei, 2012. URL `https://etd.ohiolink.edu/ap/10?0::NO:10:P10_ACCESSION_NUM:ohiou1343316877`.

[72] Paulo F. Bedaque, H. W. Hammer, and U. van Kolck. Renormalization of the three-body system with short range interactions. *Phys. Rev. Lett.*, 82:463–467, 1999. doi: 10.1103/PhysRevLett.82.463.

[73] H. W. Hammer and Thomas Mehen. A Renormalized equation for the three-body system with short range interactions. *Nucl. Phys.*, A690:535–546, 2001. doi: 10.1016/S0375-9474(00)00710-7.

[74] Sean Fleming, Thomas Mehen, and Iain W. Stewart. The N N scattering 3S1 - 3D1 mixing angle at NNLO. *Phys. Rev.*, C61:044005, 2000. doi: 10.1103/PhysRevC.61.044005.

[75] Jiunn-Wei Chen and Martin J. Savage. n p —> d gamma for big bang nucleosynthesis. *Phys. Rev.*, C60:065205, 1999. doi: 10.1103/PhysRevC.60.065205.

[76] Arman Margaryan, Roxanne P. Springer, and Jared Vanasse. *nd* scattering and the A_y puzzle to next-to-next-to-next-to-leading order. *Phys. Rev.*, C93(5):054001, 2016. doi: 10.1103/PhysRevC.93.054001.

[77] International Symposium on Polarization Phenomena in Nuclear Reactions, H. H. Barschall, and W. Haeberli. *Polarization phenomena in nuclear reactions; proceedings. Edited by H. H. Barschall and W. Haeberli.* University of Wisconsin Press Madison, 1971. ISBN 0299058905.

[78] Gerald G. Ohlsen. Polarization transfer and spin correlation experiments in nuclear physics. *Rept. Prog. Phys.*, 35:717–801, 1972. doi: 10.1088/0034-4885/35/2/305.

[79] W. Glöckle. *The quantum mechanical few-body problem.* Texts and monographs in physics. Springer-Verlag, 1983. ISBN 9783540125877. URL `https://books.google.com/books?id=0yGCAAAAIAAJ`.

[80] Kenji Fukukawa and Yoshikazu Fujiwara. Effective-Range Expansion of the Neutron-Deuteron Scattering Studied by a Quark-Model Nonlocal Gaussian Potential. *Prog. Theor. Phys.*, 125:957–978, 2011. doi: 10.1143/PTP.125.957.

[81] P. Schwarz, H.O. Klages, P. Doll, B. Haesner, J. Wilczynski, B. Zeitnitz, and J. Kecskemeti. Elastic neutron-deuteron scattering in the energy range from 2.5 mev to 30 mev. *Nuclear Physics A*, 398(1):1 – 18, 1983. ISSN 0375-9474. doi: http://dx.doi.org/10.1016/0375-9474(83)90645-0. URL `http://www.sciencedirect.com/science/article/pii/0375947483906450`.

[82] EM Neidel, W Tornow, DE González Trotter, CR Howell, AS Crowell, RA Macri, RL Walter, GJ Weisel, J Esterline, H Witała, et al. A new twist to the long-standing three-nucleon analyzing power puzzle. *Physics Letters B*, 552(1):29–34, 2003.

[83] S. Shimizu, K. Sagara, H. Nakamura, K. Maeda, T. Miwa, N. Nishimori, S. Ueno, T. Nakashima, and S. Morinobu. Analyzing powers of p+d scattering below the deuteron breakup threshold. *Phys. Rev.*, C52:1193–1202, 1995. doi: 10.1103/PhysRevC.52.1193.

[84] L. Platter. An Effective theory for the four-body system. *AIP Conf. Proc.*, 768: 185–187, 2005. doi: 10.1063/1.1932907. [,185(2004)].

[85] L. Platter, H. W. Hammer, and Ulf-G. Meissner. The Four boson system with short range interactions. *Phys. Rev.*, A70:052101, 2004. doi: 10.1103/PhysRevA.70.052101.

[86] L. Platter, H. W. Hammer, and Ulf-G. Meissner. On the correlation between the binding energies of the triton and the alpha-particle. *Phys. Lett.*, B607:254–258, 2005. doi: 10.1016/j.physletb.2004.12.068.

[87] A. Nogga, H. Kamada, and Walter Gloeckle. Modern nuclear force predictions for the alpha particle. *Phys. Rev. Lett.*, 85:944–947, 2000. doi: 10.1103/PhysRevLett.85.944.

[88] E. Epelbaum, H. Kamada, A. Nogga, H. Witala, Walter Gloeckle, and Ulf-G. Meissner. The Three nucleon and four nucleon systems from chiral effective field theory. *Phys. Rev. Lett.*, 86:4787–4790, 2001. doi: 10.1103/PhysRevLett.86.4787.

[89] H. W. Hammer, C. Ji, and D. R. Phillips. Effective field theory description of halo nuclei. 2017.

[90] Evgeny Epelbaum, Hans-Werner Hammer, and Ulf-G. Meissner. Modern Theory of Nuclear Forces. *Rev. Mod. Phys.*, 81:1773–1825, 2009. doi: 10.1103/RevModPhys.81.1773.

[91] C. A. Bertulani, H. W. Hammer, and U. Van Kolck. Effective field theory for halo nuclei. *Nucl. Phys.*, A712:37–58, 2002. doi: 10.1016/S0375-9474(02)01270-8.

[92] P. F. Bedaque, H. W. Hammer, and U. van Kolck. Narrow resonances in effective field theory. *Phys. Lett.*, B569:159–167, 2003. doi: 10.1016/j.physletb.2003.07.049.

[93] Jared Vanasse. Charge and Matter Form Factors of Two-Neutron Halo Nuclei in Halo Effective Field Theory at Next-to-leading-order. *Phys. Rev.*, C95(2):024318, 2017. doi: 10.1103/PhysRevC.95.024318.

[94] Lakma Fernando, Renato Higa, and Gautam Rupak. Resonance Contribution to Radiative Neutron Capture on Lithium-7. *Eur. Phys. J.*, A48:24, 2012. doi: 10.1140/epja/i2012-12024-7.

[95] Daniel R. Phillips. One- and two-neutron halos in effective field theory. *Few Body Syst.*, 55:931–934, 2014. doi: 10.1007/s00601-013-0769-z.

[96] PhD dissertation: Vanasse, Jared James. Parity Violation in Neutron Deuteron Scattering in Pionless Effective Field Theory, 2012.

[97] George L. Strobel. Construction of invariants from Clebsch-Gordan coefficients. *Nucl. Phys.*, A96:229–237, 1967. doi: 10.1016/0375-9474(67)90707-5.

[98] Jun John Sakurai. *Modern quantum mechanics; rev. ed.* Addison-Wesley, Reading, MA, 1994. URL `https://cds.cern.ch/record/1167961`.

[99] Ivan Georgievich Petrovskii. *Lectures on the theory of integral equations.* Courier Corporation, 1996.

[100] Harry. Hochstadt. *Integral equations / Harry Hochstadt.* Wiley New York ; Sydney, 1973. ISBN 047140165.

[101] D. D. Brayshaw. Off- and on-shell analyticity of three-particle scattering amplitudes. *Phys. Rev.*, 176:1855–1870, Dec 1968. doi: 10.1103/PhysRev.176.1855. URL `https://link.aps.org/doi/10.1103/PhysRev.176.1855`.

[102] G. Passarino and M. J. G. Veltman. One Loop Corrections for e+ e- Annihilation Into mu+ mu- in the Weinberg Model. *Nucl. Phys.*, B160:151–207, 1979. doi: 10.1016/0550-3213(79)90234-7.

[103] R. Keith Ellis, Zoltan Kunszt, Kirill Melnikov, and Giulia Zanderighi. One-loop calculations in quantum field theory: from Feynman diagrams to unitarity cuts. *Phys. Rept.*, 518:141–250, 2012. doi: 10.1016/j.physrep.2012.01.008.

[104] Martin J. Savage and Roxanne P. Springer. The Anapole form-factor of the deuteron. *Nucl. Phys.*, A686:413–428, 2001. doi: 10.1016/S0375-9474(00)00568-6.

[105] Michael Binger. Multiloop diagrams in nonrelativistic field theories and the deuteron quadrupole moment. 1999.

[106] Jiunn-Wei Chen, Gautam Rupak, and Martin J. Savage. Nucleon-nucleon effective field theory without pions. *Nucl. Phys.*, A653:386–412, 1999. doi: 10.1016/S0375-9474(99)00298-5.

Biography

My name is Arman Margaryan. I was born on January 9, 1990 in Yerevan, Armenia. I graduated with my bachelor's degree in Physics and Pedagogics from the department of physics in Yerevan State University in June, 2010. I graduated with my PhD degree in Physics from the department of physics in Duke University on June 21, 2017. My PhD dissertation is about the calculation of the transverse asymmetry in a neutron-deuteron elastic scattering process in pionless effective field theory and was based on a publication in *Phys. Rev.*, C [76]. The first project at Duke Physics that I have completed with my academic advisor Roxanne Springer was about the structure of the particle $X(3872)$. That work was published in *Phys. Rev.*, D [44]. The third project that I have completed while in PhD school was about the Compton scattering from ^{3}He. I worked on this project under the supervision of Harald W. Griehammer in The George Washington University, Washington DC and Daniel R. Phillips in Ohio University, Athens, Ohio. Publication of that work is expected in the near future.